Development of an *in vitro* model by CRISPR-Cas9 for the study of metastatic-promoting properties of mutated TP53 and RB1 in triple-negative breast cancer

by

Chanajai (Kady) Tishyadhigama

B.Sc. (Hons.), Simon Fraser University, 2017

Thesis Submitted in Partial Fulfillment of the
Requirements for the Degree of
Master of Science

in the
Master of Science Program
Faculty of Health Sciences

SIMON FRASER UNIVERSITY
Fall 2022

Declaration of Committee

Name:	**Chanajai Tishyadhigama**
Degree:	**Master of Science**
Title:	**Development of an *in vitro* model by CRISPR-Cas9 for the study of metastatic-promoting properties of mutated *TP53* and *RB1* in triple-negative breast cancer**
Committee:	**Chair:** **Jean-Christophe Bélisle-Pipon** Assistant Professor, Health Sciences
	Timothy Beischlag Supervisor Professor, Health Sciences
	Mark Brockman Committee Member Professor, Health Sciences
	Ian Tietjen Committee Member Adjunct Professor, Health Sciences
	Nada Lallous Committee Member Assistant Professor, Medicine University of British Columbia
	Timothy Audas Examiner Associate Professor, Molecular Biology and Biochemistry

Abstract

Cancer is a complex disease, requiring specific treatments for each type. Triple-negative breast cancer (TNBC) is the most aggressive form of human breast cancer; however, it lacks specialized treatments, leaving patients with poor prognoses. The underlying molecular mechanisms responsible for the aggressive traits of TNBC remain elusive; however, one crucial clue is that *TP53* and *RB1*, important tumour suppressor genes, are commonly mutated together in TNBC patients. Evidence suggests mutations of these genes could collectively promote metastasis. To better understand the effects *TP53* and *RB1* mutations have on metastatic characteristics of TNBC, we generated a cell line model by successfully knocking out *TP53* and *RB1* from a TNBC cell line, utilizing CRISPR-Cas9. Validation assays monitoring cell cycle phase distribution, metastasis-promoting gene expression, and cell migration revealed the intricacy of developing a TNBC cell line model and that further modifications are essential. Once established, the model could prove essential for identifying TNBC therapeutic targets.

Keywords: Triple Negative Breast Cancer; *TP53*; *RB1*; Metastasis; Cell line model; CRISPR-Cas9

Acknowledgements

I would like to thank Dr. Timothy Beischlag for taking me on as a graduate student and training me to become a better research scientist. I would also like to thank all the committee members: Dr. Mark Brockman, Dr. Ian Tietjen, and Dr. Nada Lallous for their support throughout my graduate career. My journey here has been up and down, and I would not be able to get through the challenging time without the support from my peers: Dr. Shabnam Massah, Dr. Andressa Coope, Robert Payer, Raymond Lo, Nathan Gock, Maude Comtois-Cabana, Emily Barr, Quiana Ang, Brockman-Brumme Lab's members, Choy Lab's members, and Audas Lab's members. I would also like to thank Dr. Timothy Audas for being my thesis examiner. Lastly, I would like to thank my partner, Daniel Knowles, and my family for believing in me and providing mental support throughout my degree.

Table of Contents

List of Tables

List of Figures

List of Acronyms

Amp	Ampicillin
ANGPT2	Angiopoietin 2
ANGPTL4	Angiopoietin Like 4
AR	Androgen Receptor
ARNT	Aryl hydrocarbon Receptor Nuclear Translocator
BAX	Bcl2-Associated X
Bcl2	B-cell Lymphoma 2
BM	Basement Membrane
BRM	BRAHMA
c-Abl	Abelson tyrosine kinase
Cas9	CRISPR-associated protein 9
CCL5	C-C motif chemokine Ligand 5
CCR5	C-C motif chemokine Receptor 5
Cdk	Cyclin-Dependent Kinase
CDKN1A	Cyclin-Dependent Kinase Inhibitor 1A
cDNA	Complementary DNA
COX-2	Cyclooxygenase-2
CRISPR	Clustered Regularly Interspaced Short Palindromic Repeat
CSF1	Colony-Stimulating Factor 1
CSRP2	Cysteine and Glycine Rich Protein 2
CTC	Circulating Tumour Cell
CTL	Cytotoxic T Lymphocyte
CXCL10	C-X-C motif chemokine Ligand 10
CXCL12	C-X-C motif chemokine Ligand 12
CXCL16	C-X-C motif chemokine Ligand 16
CXCL5	C-X-C motif chemokine Ligand 5
CXCL8	C-X-C motif chemokine Ligand 8
CXCR4	C-X-C motif chemokine Receptor 4
CXCR6	C-X-C motif chemokine Receptor 6

DAISY	Data mining synthetic lethality identification pipeline
DKO	Double Knockout
DMEM	Dulbecco-s Modified Eagle Medium
DMSO	Dimethyl Sulfoxide
DNA	Deoxyribonucleic Acid
dNTP	Deoxynucleoside triphosphate
DSB	Double Stranded Break
E2F	E2F transcription factor family
EC	Endothelial Cell
ECM	Extracellular Matrix
EDTA	Ethylenediamine tetraacetic acid
EGFR	Epidermal Growth Factor Receptor
EMT	Epithelial-Mesenchymal Transition
ERα	Estrogen Receptor Alpha
ETS	Erythroblast Transformation Specific
FBS	Fetal Bovine Serum
FGF10	Fibroblast Growth Factor 10
FHS	Faculty of Health Sciences
GLUT1	Glucose Transporter 1
gRNA	Guide RNA
HDAC	Histone Deacetylase
HeLa	Henrietta Lacks
HER2	Human Epidermal growth factor Receptor 2
HIF1α	Hypoxia-Inducible Factor 1α
HIF1β	Hypoxia-Inducible Factor 1β
HRP	Horseradish Peroxidase
IDC	Invasive Ductal Carcinoma
ILC	Invasive Lobular Carcinoma
ITGA3	Integrin Alpha-3
kDa	Kilodalton
KO	Knockout

LNCaP	Lymph Node Carcinoma of the Prostate
LOH	Loss of Heterozygosity
MCF-7	Michigan Cancer Foundation-7
MDA-MB-231	M.D. Anderson-Metastatic Breast 231
MDM2	Mouse Double Minute-2
MDR1	Multi-Drug Resistance-1
miR	MicroRNA
mmHg	Millimetre of Mercury
MMP	Matrix Metalloproteinase
MMP-2	Matrix Metalloproteinase-2
MMP-9	Matrix Metalloproteinase-9
mRNA	Messenger RNA
MSC	Mesenchymal Stem Cell
Myc	Myc proto-oncogene
Neo	Neomycin
NFIB	Nuclear Factor 1 B-type
p107	Retinoblastoma-like protein1
p130	Retinoblastoma-like protein 2
p21	Cyclin-dependent kinase inhibitor 1A protein
p53	Tumour Protein P53
p63	Tumour Protein p63
PAM	Protospacer Adjacent Motif
PBS	Phosphate-Buffered Saline
PD-1	Programmed Cell Death Protein 1
PD-L1	Programmed Death-Ligand 1
Pen	Penicillin
PLOD2	Procollagen-Lysine, 2-Oxogutarate 5-dioxygenase
pO_2	Partial Pressure of Oxygen
PR	Progesterone Receptor
PTGS2	Prostaglandin-endoperoxide synthase 2
PTP1B	Protein Tyrosine Phosphatase 1B

PTPN1	Protein Tyrosine Phosphatase Non-receptor type 1
RB	Retinoblastoma protein
RB1	RB transcriptional corepressor 1
RIPA	Radio-Immunoprecipitation Assay
RNA	Ribonucleic Acid
RT	Reverse Transcriptase
S1P	Sphingosine-1 Phosphate
S1P3	Sphingosine-1 Phosphate receptor 3
SCLC	Small Cell Lung Cancer
SDS-PAGE	Sodium Dodecyl-Sulfate Polyacrylamide Gel Electrophoresis
SFU	Simon Fraser University
sgRNA	Single Guide RNA
shRNA	Short Hairpin RNA
siRNA	Small Interfering RNA
SK1	Sphingosine Kinase
SLC2A1	Solute Carrier Family 2 Member 1
Strep	Streptomycin
SV40	Simian Virus 40
SWI/SNF	Switch/Sucrose Non-Fermentable
TAD	Transactivation Domain
TAM	Tumour-Associated Macrophage
TBS	Tris-Buffered Saline
TBS-T	Tris-Buffered Saline – Tween
TCGA	The Cancer Genome Atlas
TGF-α	Transforming Growth Factor α
TGF-β	Transforming Growth Factor β
TNBC	Triple-Negative Breast Cancer
TP53	Tumour Protein p53
TRIP230	Thyroid receptor-Retinoblastoma Interacting Protein
VEGF	Vascular Endothelial Growth Factor
VEGFA	Vascular Endothelial Growth Factor A

WT	Wildtype
ZEB1	Zinc finger E-box Binding homeobox-1
ZEB2	Zinc finger E-box Binding homeobox-2
β -ME	β-mercaptoethanol
β-tub	β-tubulin

Chapter 1.

Introduction

What Is Cancer? Cancer is commonly characterized as an aberrant proliferation of cells that often results in abnormal function of the affected tissue or organ. Cancer can occur in various body tissues ranging from the non-vital ones such as colon, breast, and ovaries, to the most vital such as the brain, lungs, and liver, with certain types being more common than others[1]. Cancer can be inherited genetically or induced by environmental factors, leading to mutations in genes that drive tumourigenesis. In late stages, cancer cells can acquire the ability to infiltrate neighbouring blood or lymph vessels, and eventually metastasize to other organs, the main cause of cancer-related deaths. Despite a tremendous amount of research investigating the characteristics of cancers, for instance, tumourigenesis pathways, tumour microenvironment, or tumour metastatic mechanisms, that potentially lead to the development of therapeutics, cancer remains one of the top 10 causes of death, worldwide. One of the reasons for such high mortality is, undoubtedly, the complexity and diversity of these diseases; each cancer type is unique, based on the particular tissues and mutations involved. Certain types of cancer are classified further into subtypes which require their own specific treatments. Therefore, to fully understand the characteristics and complications of each cancer subtype, an investigative model that closely mimics specific types of cancer cells and is compatible with various experimental approaches is crucial.

1.1. Breast Cancer

Breast cancer is the most commonly diagnosed cancer among females, in Canada and globally[2,3]. Histologically, breast carcinoma is divided into multiple subtypes based on its specific morphological and cytological patterns[4]. While there are many histological breast carcinoma subtypes, invasive lobular carcinoma (ILC) and invasive ductal carcinoma (IDC) are the two main subtypes, with IDC being the most common subtype. ILC initiates at breast lobules where milk is produced, whereas IDC originates at the milk duct. Due to the physical location of breast lobules, ILC is much more difficult to detect by a mammogram[5], causing patients to remain undiagnosed until later stages of cancer development. Despite the late diagnosis, ILC patients exhibit a significantly

better survival rate than IDC patients[6]. This phenomenon could be explained by the molecular differences among the breast cancer subtypes.

1.1.1. Molecular Subtypes of Breast Cancer

Breast cancer is highly heterogeneous and requires different strategies for efficient treatment, depending on the subtype. Generally, its progression is driven by an over-expression of at least one of the following endocrine or growth factor receptors: estrogen receptor (ERα), progesterone receptor (PR)[7], and human epidermal growth factor receptor 2 (HER2)[8]. In normal breast epithelium, these receptors function to regulate growth and differentiation[9,10]. Overexpression of these receptors leads to uncontrolled, aberrant growth of tumour cells. Based on the expression status of these receptors, breast cancer is classified by immunohistochemistry into four major subtypes: luminal A, luminal B, HER2-enriched, and basal-like[11]. Both luminal A and B subtypes exhibit the overexpression of either ERα or PR but may or may not over-express HER2[12]. The expression status of these hormone receptors may appear similar; however, luminal B proliferates at a quicker rate than luminal A[13]. Both of these subtypes often show a better prognosis and are more common in ILC than other, more aggressive molecular subtypes[14]. They can be treated by hormonal therapy, which represses hormone production or inhibits hormones from binding to their corresponding receptor[12]. The HER2-enriched subtype however, lacks ERα and PR expression but shows an elevation in HER2 expression[15]. This subtype is more aggressive than luminal A and B; patients often experience a worse prognosis and develop a higher risk of relapse[11]. Nonetheless, it can also be treated by targeted therapy, suppressing the kinase function of HER2[16]. On the other hand, the basal-like subtype, usually referred to as triple-negative breast cancer (TNBC), displays the most aggressive traits, clinically, but its specific treatments remain underdeveloped[17].

1.1.2. Triple Negative Breast Cancer (TNBC)

TNBC is classified by immunohistochemical data as breast cancer that lacks the expression of ERα, PR, and HER2[18]. Approximately 17% of patients diagnosed with breast cancer have TNBC[18]. The terms TNBC and basal-like breast cancer are sometimes used interchangeably. However, basal-like breast cancer also expresses genes that are characteristic of myoepithelial breast cells[19]. Not all TNBC cases are

classified as basal-like; TNBC can also be classified as claudin-low breast cancer[20]. The claudin-low subtype has mesenchymal and stemness characteristics, which are traits of metastatic cancer cells[20]. This subtype has low expression of claudin and occludin proteins, which are important tight junction proteins, facilitating cell-cell adhesion[20]. Due to the lack of ERα, PR, and HER2 expression, hormone therapy or HER2-targeted therapy are not an option for TNBC patients, instead, the main treatment approach for TNBC is chemotherapy[21]. Moreover, studies show TNBC patients express a higher likelihood of metastasis and death within five years, compared to non-TNBC patients[22]. Surprisingly, those rates were only higher in the first three years after diagnosis, suggesting TNBC has an early aggressive nature[22]. Furthermore, TNBC patients have a higher risk of developing brain and lung metastasis[19], which drastically increases the likelihood of death. Thus, the development of specific therapeutics for TNBC, especially therapies that suppress metastasis, needs to be a top priority of clinical breast cancer research.

1.1.2.1. Molecular Subtypes of TNBC

The heterogeneity of breast cancer further divides triple-negative breast cancer into six different molecular subtypes[23]. The six subtypes are basal-like 1 and 2, immunomodulatory, mesenchymal, mesenchymal stem-like, and luminal androgen receptor. Each subtype has unique characteristics to support tumour growth and progression. Basal-like 1 and 2 subtypes have enriched expression of genes associated with cell division, DNA damage response, and growth factor signaling pathways, allowing them to rapidly grow and divide[24] (**Table 1.1**). The immunomodulatory subtype, on the other hand, often overexpresses genes involved in immune signal transduction pathways[25] (**Table 1.1**). Mesenchymal and mesenchymal stem-like subtypes are among the most aggressive types as they have an enhanced expression of genes involved in cell motility, extracellular matrices (ECM) rearrangement, cell differentiation pathways, and epithelial-mesenchymal transition (EMT)[25] (**Table 1.1**), all of which promote cancer metastases. Lastly, the luminal androgen receptor subtype has high levels of expression of androgen receptor (AR) and genes involved in steroid synthesis[26] (**Table 1.1**). Interestingly, this subtype shows a similar gene-expression profile to the HER2-enriched breast cancer subtype, while the other subtypes express a profile more similar to the basal-like subtype[23].

Table 1.1. Six TNBC molecular subtypes

TNBC Subtypes	Molecular Characteristics
Basal-like 1	↑ expression of genes associated with cell division and DNA repair
Basal-like 2	↑ expression of genes associated with growth factor signaling pathway
Immunomodulatory	↑ expression of genes associated with immune signal transduction pathways
Mesenchymal	↑ expression of genes associated with cell motility, ECM rearrangement, MET
Mesenchymal stem-like	↑ expression of genes associated with mesenchymal stem-cell
Luminal AR	↑ expression of AR and genes associated with steroids synthesis

Note: ↑ indicates an enhancement

1.1.2.2. TP53 and RB1 are frequently mutated together in TNBC

Despite the differences in the molecular traits, TNBC patients often express mutations in *tumour protein p53* (*TP53*) and *RB transcriptional corepressor 1* (*RB1*) genes, which correlates with poor prognosis[27–29]. These are well characterized tumour suppressor genes which encode for Tumour Protein P53 (p53) and Retinoblastoma protein (RB), respectively. These proteins play an important role in regulating cell-cycle, DNA repair, and apoptosis (programmed cell death)[30,31]. Malfunctioning of these genes can potentially lead to disastrous, uncontrollable cell growth.

In a high-throughput RNA sequencing study by Shah *et al*., approximately 53% of the primary TNBC samples had mutations in *TP53* and 7.7% had mutations in *RB1*[32]. Out of those 53% with mutations in *TP53*, 14% also showed mutations in *RB1*[32] (**Figure 1.1**). Unsurprisingly, tumours with deficiency in both *TP53* and *RB1* display high rates of aneuploidy and abnormalities of chromosomes which include chromosomal changes, translocations, and the loss of chromosomal fragments[33]. This level of severity of abnormalities in chromosomes can lead to downstream modifications in cell growth and further drive replication of 'abnormal' cells. Similarly, another study utilizing genome and transcriptome sequencing revealed *TP53* mutations and/or loss of heterozygosity in 64% of the TNBC tumour samples[28]. The most frequent mutation occurred in the DNA-binding region of p53, which may perturb its DNA-binding ability. In this study, *RB1* was also found to be mutated in 21% of TNBC tumour samples[28]. One of the detected mutations occurs within the conserved pocket domain, resulting in a malfunctioning RB protein. Ultimately, using larger data sets obtained from cBioPortal and The Cancer Genome Atlas (TCGA), Jones *et al*. found that 40% of TNBC samples show concurrent *TP53* and *RB1* mutations[29] (**Figure 1.1**). Interestingly, mutations in both these genes together

occur more frequently in TNBC, compared to the other breast cancer subtypes[29], suggesting their potential concomitant role in driving the progression of TNBC.

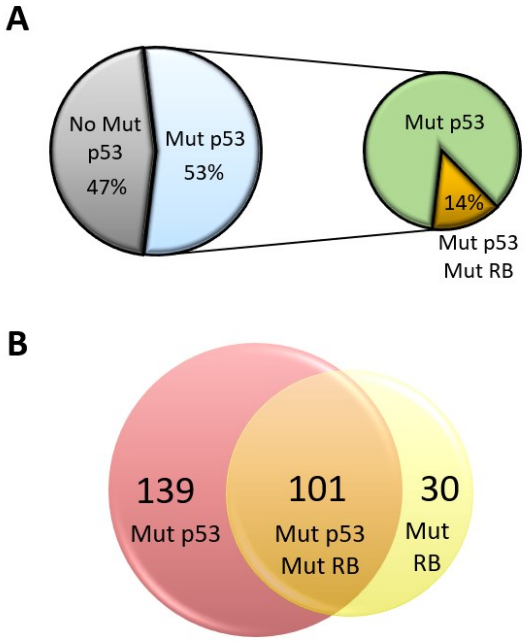

Figure 1.1. p53 and RB are commonly mutated together in TNBC patients.
RNA sequencing analysis by Shah *et al*. (**A**) revealed that 53% of TNBC primary samples have p53 mutations[32]. 14% out of those samples also have RB mutations[32]. An analysis by Jones *et al.*, using the TNBC data from cBioPortal and The Cancer Genome Atlas (**B**), showed that 40% of the samples have both p53 and RB mutations[29].

Not only do *TP53* mutations occur in the primary TNBC tumours, *TP53* mutations have been found in circulating tumour cells (CTCs) of metastatic TNBC patients[34,35] and are conserved between primary and metastatic tumours[36]. Using next-generation sequencing, Madic *et al*. revealed that 26 out of 31 metastatic TNBC patients had a *TP53*-mutated tumour and *TP53* mutations were also found in the circulating tumour DNA of 84% of those patients[35]. Likewise, another study by Bingham *et al.* revealed *RB1* mutations in CTCs as well as metastatic tumours of TNBC patients[37]. Moreover, the increasing number of circulating tumour cells also correlates with a shortening of the time of disease progression and decrease in overall survival of patients[35]. The above evidence strongly suggests a potential role of mutated *TP53* and *RB1* in promoting aggressive metastatic TNBC.

1.2. Tumour Protein P53 (p53)

TP53 is a tumour suppressor gene which encodes for p53 protein, “the Guardian of the Genome”. p53 functions as a transcription factor to prevent tumourigenesis by regulating cell cycle arrest, DNA repair, and apoptosis[30]. Its function is induced by DNA damage detected during the cell cycle. In response to DNA damage, p53 becomes phosphorylated[38] and upregulates cyclin-dependent kinase inhibitor 1A protein (p21) expression, which induces G1/S cell cycle arrest by upregulating RB activity to stall the cell cycle from transitioning into the S phase, when synthesis and replication of DNA occurs[39] (**Figure 1.2**). p53 can also bind to transcription-replication repair factors to transactivate genes which are responsible for DNA repair[40,41]. For cases in which DNA damage is not repaired, p53 promotes the expression of B-cell lymphoma 2 (Bcl2) and Bcl2-Associated X (BAX) proteins to induce apoptosis[42] (**Figure 1.2**). Overall, these functions of p53 allow the elimination of abnormal cells, preventing their accumulation and progression to tumour formation. p53 is tightly regulated by mouse double minute-2 (MDM2) (also known as E3 ubiquitin-protein ligase) via a p53-MDM2 negative feedback loop[30] (**Figure 1.2**). When DNA is damaged, MDM2 is expressed through transcriptional activation facilitated by p53; however, MDM2 function is inhibited. Once DNA is repaired, MDM2 is activated and targets p53 for ubiquitination by binding to its N-terminus, inducing p53 degradation[43]. Interestingly, *MDM2* gene expression is amplified in human breast cancer, inhibiting p53 tumour suppressor function[44].

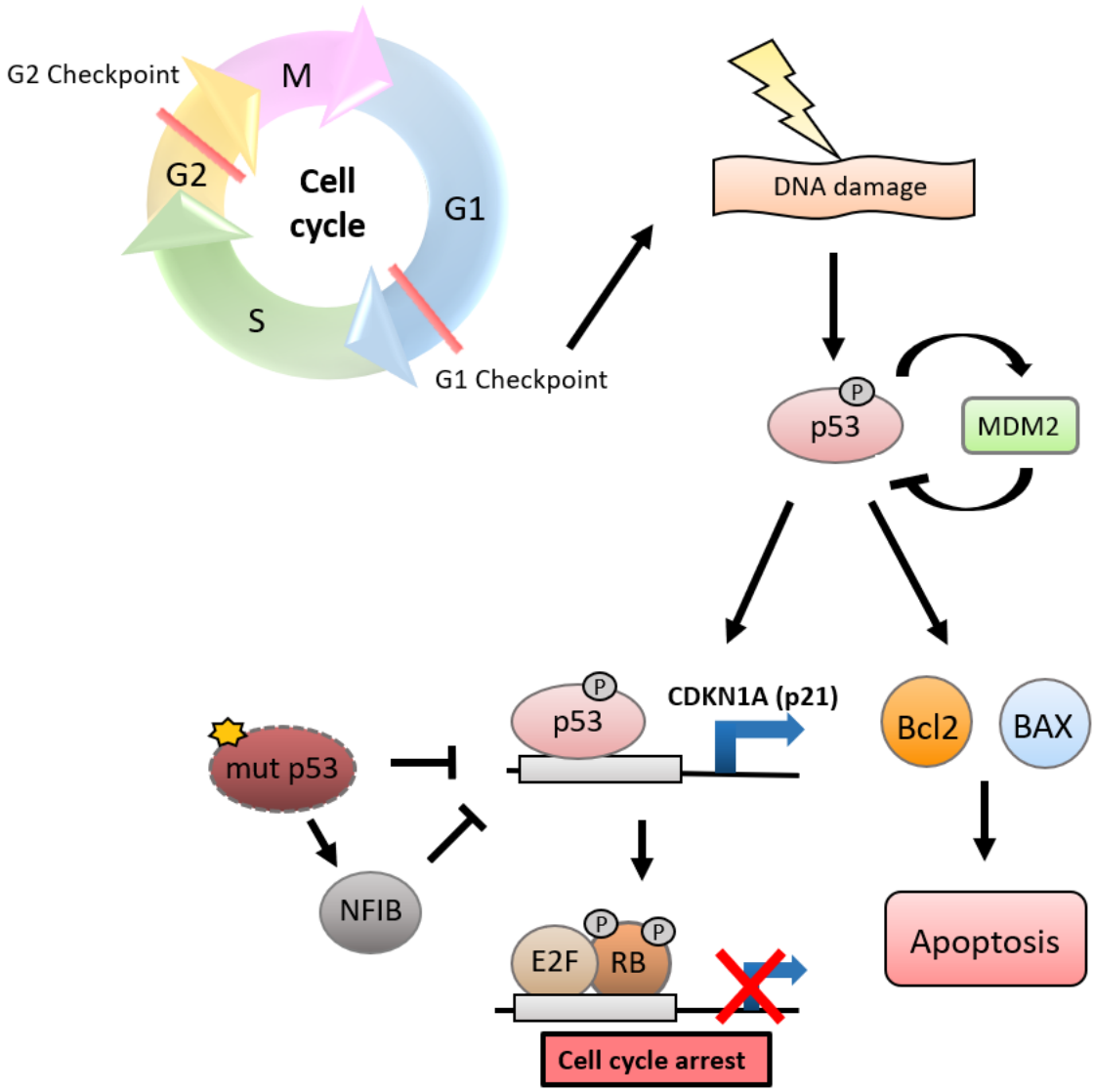

Figure 1.2. p53 regulates apoptosis and cell cycle progression.
At the G1 checkpoint of the cell cycle, phosphorylation (P) of p53 is induced by DNA damage. p53 activates CDKN1A transcription which enhances G1/S cycle arrest via E2F transcriptional activity inhibition by phosphorylated RB. On the other hand, mutant p53 inhibits CDKN1A transcription either directly or through NFIB activation. p53 enhances Bcl2 and BAX expression to induce apoptosis. p53 is negatively regulated by MDM2.

1.2.1. Mutations in *TP53* lead to malfunctioning p53 proteins

Mutations in *TP53* can arise from both germline and somatic mutations. Children or young adults who carry germline *TP53* mutations inherited from their family are more susceptible to developing Li-Fraumeni syndrome, a disease characterized by the formation of multiple primary tumours, including breast carcinomas[45]. Li-Fraumeni syndrome is caused by mutations of *TP53* in both alleles; thus, people with a germline

TP53 mutation only require a somatic mutation in the other allele to develop the syndrome[45]. Exposure to environmental factors such as carcinogens, including ultraviolet radiation and tobacco smoke, can induce DNA alterations which lead to somatic mutations in *TP53*[46].

Mutations in *TP53* often result in p53 losing its tumour suppressor function. The six main domains of p53 are: the transactivation domain I (amino acid residues 1 – 42), the transactivation domain II (amino acid residues 43 – 63), proline-rich domain (amino acid residues 64 – 93), DNA-binding domain (amino acid residues 94 – 291), the homo-oligomerization domain (amino acid residues 324 – 355), and the C-terminal phosphorylation domain (amino acid residues 356 – 393)[47] (**Figure 1.3**). A linker segment tethers the DNA-binding domain and the homo-oligomerization domain[47] (**Figure 1.3**). To perform its gene transactivation function, p53 forms a homo-tetramer on DNA strands. Thus, mutations that affect p53 oligomerization or DNA-binding will likely diminish wild-type p53 functions. Mutations in *TP53* are often missense mutations, which are point mutations that convert one amino acid residue to another. Known mutational hotspots include R175H, G245S, R248Q/W, and R273H/C[48,49] (**Figure 1.3**). These mutations in the DNA-binding domain directly perturb the DNA-binding ability of p53 as they abolish arginine residues, a positively charged amino acid that interacts with the negatively charged phosphate groups of the DNA backbone. On the other hand, replacing glycine, a small amino acid lacking a side chain, with serine, containing a hydroxyl group, could potentially affect the folding of the DNA binding domain of p53, disrupting its DNA binding ability. Aside from disrupting the DNA-binding region, mutations can also affect the structural stability of p53 by creating large water accessible crevices within the protein[50]. This will result in the exposure of hydrophobic residues to the aqueous surroundings, leading to thermodynamic instability. Mutations can also prevent tetramerization of p53, inhibiting its gene transactivation function[50]. Overall, mutations in p53 that directly affect its DNA-binding ability, protein stability, or ability to form a homo-tetramer often lead to a loss of its wild-type function as a tumour suppressor protein.

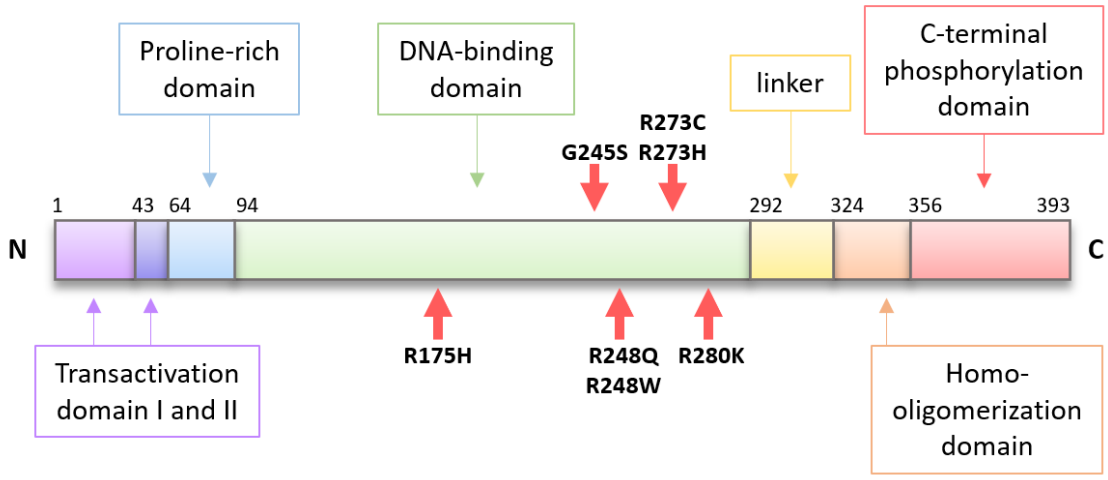

Figure 1.3. p53 domain architecture.
p53 consists of six main domains: Transactivation domain I (aa. 1 – 42), Transactivation domain II (aa. 43 – 63), Proline-rice domain (aa. 64 – 93), DNA-binding domain (aa. 94 – 291), linker (aa. 292 – 323), Homo-oligomerization domain (aa. 324 – 355), and C-terminal phosphorylation domain (aa. 356 – 393). Seven hot spot mutations are shown in the DNA-binding domain. (aa. = amino acid)

1.2.2. Can *TP53* be an oncogene and promote tumour metastasis?

Despite p53 being well-known as a tumour suppressor protein, *TP53* was initially thought to be a proto-oncogene, a gene which generally functions in cell growth, but promotes tumourigenesis once mutated. p53 was first discovered in 1979 as a protein that interacts with simian virus 40 (SV40) large tumour (T) antigen[51]. In SV40-transformed mouse cell lines where the virus DNA was integrated into the mouse cell lines' genome, Lane and Crawford observed that the T antigen expressed from SV40 DNA formed a complex with two proteins from the host cells, one of which was a 53 kDa (kilodalton) protein[51]. This protein was much more prevalent in the transformed cells compared to the normal, healthy cells[52]. Shortly after, molecular cloning of the 53 kDa protein was performed to allow researchers to better understand its function[53]. Several experiments revealed that p53 could promote tumourigenesis and cell immortality[54–56]. Interestingly, p53 from normal cells and p53 from virus-induced tumour cells reacted differently to various conformational-specific monoclonal antibodies[57], suggesting they are potentially two different proteins. Moreover, virus-induced tumour cells also showed genomic re-arrangements which led to either an inactivation of wildtype (WT) p53 or an expression of mutant p53[58,59]. Soon after, researchers realized that the p53 they used in the previously mentioned experiments, which implicated p53 as a tumour promoting

protein, was the mutant form. The p53 protein from normal cells was not able to transform normal, healthy cells to cancer cells; rather, it suppressed the process[60,61]. Thus, it was concluded that the WT p53 exhibits a tumour suppressor function but acquires the ability to promote tumourigenesis once mutated.

As demonstrated during the discovery process of p53, mutant p53 acquires the ability to promote tumour formation and progression. In addition to losing tumour suppressor functions, mutant p53 can exhibit 'new' molecular functions. For instance, mutations can alter binding sites on p53, affecting its ability to interact with other proteins. Mutant p53 can forge new interactions with different transcriptional factors and enhance or repress gene transcription, or it can interact with other proteins, enhancing or inhibiting their functions[62–65]. For instance, p53 D281G but not the WT p53 can bind to erythroblast transformation specific (ETS) transcription factor to upregulate *multi-drug resistance-1* (*MDR1*) gene expression, which is responsible for alterations in drug transport[63] (**Figure 1.4**). This enhances the ability of tumours to become more resistant to chemotherapy and thus, continue to proliferate and potentially mutate to more aggressive progenitors.

Another mechanism by which mutant p53 enhances tumour progression is down-regulating MicroRNA (miR)-223, miR-205, miR-130b, and miR-27a[66–69]. miRs are short fragments of RNA which post-transcriptionally regulate gene expression by interacting with complementary mRNA sequences to prevent their translation. The direct target of miR-223, miR-205, and miR130b is zinc finger E-box binding homeobox-1 (ZEB1)[68,70–72]; whereas, the direct target of miR-27a is epidermal growth factor receptor (EGFR)[69]. With a reduction in these miRs, epithelial-mesenchymal transition (EMT) and invasion are promoted via increased ZEB1[66,68] and EGFR-induced tumourigenesis[69]. ZEB1 represses the expression of E-cadherin, a junction protein and an epithelial cell marker, allowing cells to transition into mesenchymal cells by loss of adhesion to neighbouring cells[73]. In line with this, patients with more miR-130b appear to have better survival rates[68].

Mutations in p53 can further exert their ability to promote tumour progression by inhibiting the expression of other tumour suppressor proteins. As discussed briefly, WT p53 induces expression of p21 when cell cycle arrest is needed[30]. p53 R280K, another common p53 mutation, induces a conformational alteration in the region that interacts with the promoter site of *CDKN1A*, the gene that encodes p21[47] (**Figure 1.4**). This

mutation could therefore result in decreased expression of p21. Consequently, cell cycle regulation function of RB would be decreased as well, preventing G1/S cell cycle arrest and therefore, promoting cell proliferation. As this mutation of p53 is dominant negative, the presence of a WT p53 allele will not restore the WT function[74]. Similarly, a transcription factor nuclear factor 1 B-type (NFIB) interacts with the *Cyclin-Dependent Kinase Inhibitor 1A* (*CDKN1A*) promoter to down-regulate p21 expression[75] (**Figure 1.4**). Interestingly, an increase in expression of NFIB is found in *TP53*-mutated TNBC, which suggests the involvement of mutant p53 in elevating NFIB expression[75] (**Figure 1.4**). Though overexpression of NFIB has not been found to promote TNBC metastasis, it is highly associated with the elevated replication of mesenchymal stem cells (MSCs) in *TP53*- and *RB1*-mutated small cell lung cancer (SCLC)[76]. In TNB carcinomas, MSCs have been shown to promote lung colonization by secreting the C-C motif chemokine ligand 5 (CCL5) which enhances cell motility and invasiveness[77]. As a consequence, mouse xenograft experiments revealed that the presence of CCL5 significantly facilitated the extravasation of intravenously injected human TNBC cells into the lung[77].

Another tumour suppressor that mutant p53 targets is tumour protein p63 (p63). p63 is a transcription factor in the p53 family[78]. Through whole genome analysis, p63 has been shown to regulate hundreds of genes which include other transcription factors and adhesion molecules[78]. Its particular role in suppressing tumour progression is through maintenance of epithelial homeostasis[79]. Under WT conditions, p63 can form a complex with p53 to suppress EMT through transcriptional regulation. However, studies have found that when p63 forms a complex with mutant p53 (R172H and R175H) in tumours, its ability to suppress EMT is inhibited[80,81] (**Figure 1.4**). WT p53 may be able to compete and forms a functioning p53/p63 complex; nevertheless, the overall repression of EMT via p63 would still be reduced even with only one mutant p53 allele.

Mutant p53 also upregulates C-X-C-motif chemokine expression by increasing the promoter activity, while the WT p53 represses the expression[82]. CXC-chemokines that are found to have elevated expression level in cells with mutant p53 (R175H, H179L, R273H, D281G) includes CXCL5, CXCL8, and CXCL12 (**Figure 1.4**), all of which induce cell metastasis through various mechanisms[82]. CXCL5 and CXCL8 both induce angiogenesis[83], while CXCL12 is involved in EMT[84] (**Figure 1.4**). As a result, wound healing and Boyden chamber migration assays revealed that breast cancer cells with mutant p53 migrate significantly more than cells with WT p53[82]. However, knocking

down CXCL5 from cells expressing mutant p53 decreased cell migration, suggesting that mutant p53 promotes cell migration though increasing the expression of CXCL5[82].

Lastly, mutant p53 can promote metastasis by upregulating the expression of genes responsible for angiogenesis and extracellular matrix (ECM) modification. WT p53 typically inhibits angiogenesis[85], which is a process essential for tumour progression. Mutant p53, conversely, can lose the ability to do so, resulting in significantly higher expression levels of vascular endothelial growth factor (VEGF) in patients with mutant p53 breast tumours[85] (**Figure 1.4**). An experiment using a breast cancer cell line with a knocked-in mutant p53 (R273H) showed an increase in epidermal growth factor receptor (EGFR), which promotes cell growth, and integrins on the cell surface[86] (**Figure 1.4**). Integrins allow tumour cells to form a meshwork with the ECM, inducing ECM modification and, therefore, removing a physical barrier for cell migration[87]. Overall, there is considerable evidence that mutant p53 promotes tumour progression and metastases in TNBC through various mechanisms and pathways.

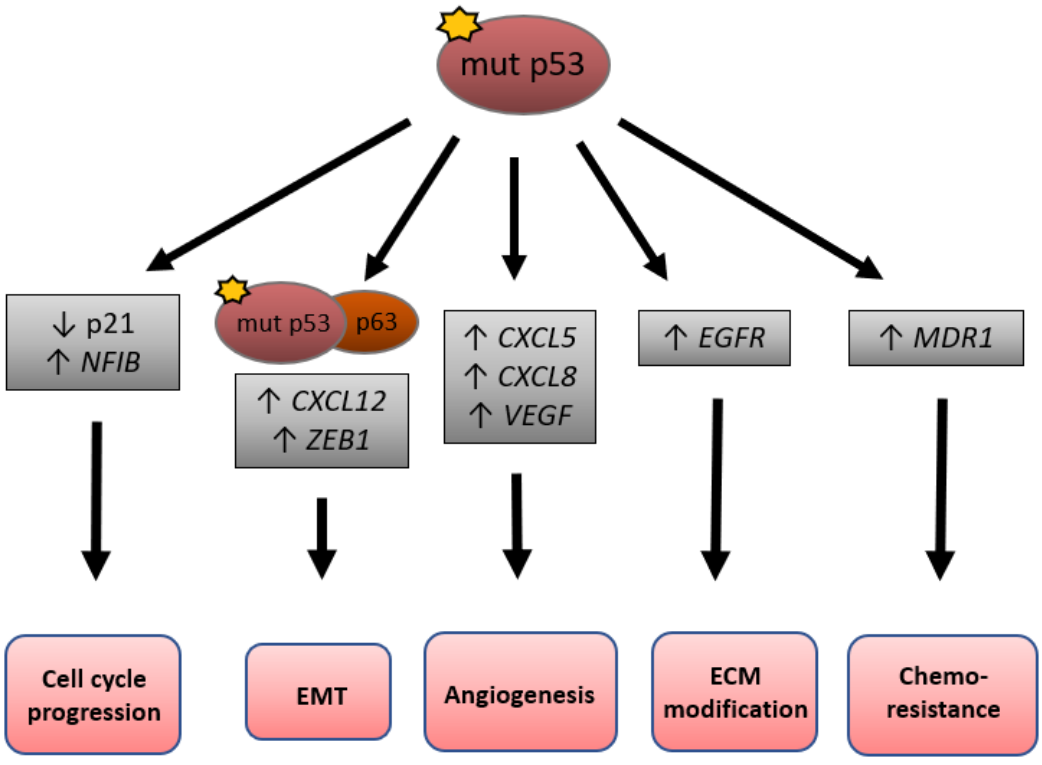

Figure 1.4. Mutant p53 promotes tumour progression through various mechanisms.
By modifying protein expression or forming a complex with p63, mutant p53 enhances tumour cell cycle progression, epithelial-mesenchymal transition (EMT), angiogenesis, extracellular matrix (ECM) modification, and chemoresistance.

1.3. Retinoblastoma Protein (RB)

Retinoblastoma gene (*RB1*) is another important tumour suppressor gene which encodes for retinoblastoma protein (RB). RB controls cell-cycle regulation by binding to members of the E2F transcription factor family (E2F) to halt cell cycle progression[31] (**Figure 1.5**). During the early G1 phase of the cell cycle, cyclin D/cyclin-dependent kinase (Cdk)4,6 phosphorylate RB to activate its function[88] (**Figure 1.5**). Phosphorylated RB inhibits E2F activity by forming a complex with the transactivation domain of E2F and blocking gene transcription[89,90] (**Figure 1.5**). During the late G1 phase, RB becomes hyperphosphorylated by cyclin A, E/Cdk2, releasing E2F to allow gene transcription and progression of the cell cycle to the S phase[91,92], when DNA replication occurs (**Figure 1.5**). If DNA damage is detected, p21, which is positively regulated by p53, will inhibit Cdk2, allowing RB to continue blocking E2F transcription activity[30] (**Figure 1.5**). RB also represses gene transcription downstream of E2F by recruiting histone deacetylase (HDAC), an enzyme responsible for DNA-chromatin packaging, to E2F-regulated gene promoter sites[93]. A removal of acetyl groups facilitates the condensation of chromatin, resulting in transcriptional repression. There is a hypothesis that RB-E2F may be further involved in chromatin modification by forming a complex with a chromatin remodeling complex switch/sucrose non-fermentable (SWI/SNF)[94]. RB simultaneously binds to BRAHMA (BRM), a core subunit of the SWI/SNF complex[95], and E2F to inhibit E2F activity and fully arrest the cell cycle at the G1 phase[94]. However, the ability of RB to modify chromatin complexes and modulate transcription of genes primarily regulated by other transcription factors has not been addressed. Overall, RB typically functions downstream of p53 to prevent replication of abnormal cells.

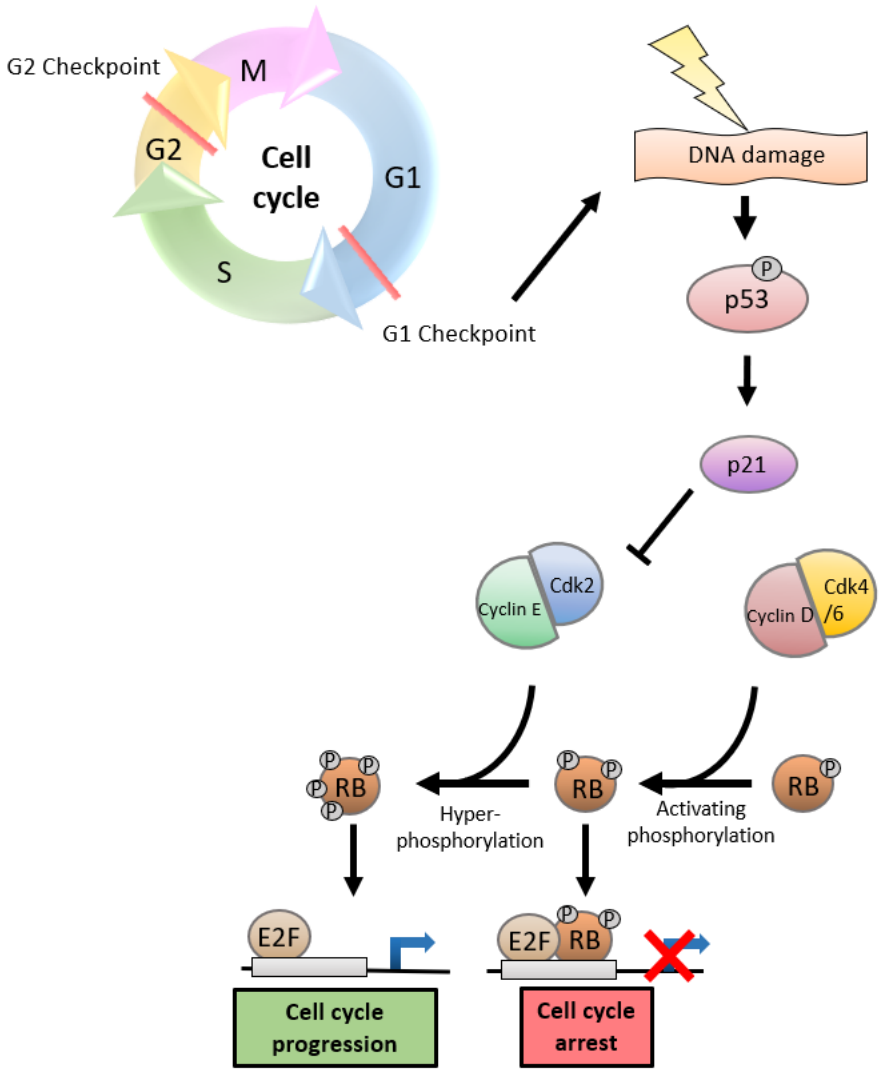

Figure 1.5. RB regulates cell cycle progression downstream of p53.
At the G1 checkpoint of the cell cycle, phosphorylation (P) of p53 is induced by DNA damage. Subsequently, p53 activates the expression of p21, which negatively regulates RB function. Cyclin D/Cdk4/6 activates E2F-inhibition activity of RB by phosphorylating (P) RB. The inhibition of E2F transcriptional activity induces G1/S cell cycle arrest. Cyclin E/Cdk2, which is negatively regulated by p21, hyper-phosphorylates RB, releasing E2F from inhibitory interaction with RB to allow cell cycle progression.

1.3.1. Mutation of *RB1* leads to loss of RB function

Mutations in *RB1* commonly lead to a loss of function in RB protein, which is found in many types of cancer, including osteosarcomas, small cell lung carcinomas, prostate carcinomas, and breast carcinomas[96–99]. In order to acquire loss of function in cells, *RB1* needs to be mutated in both alleles[100]. This is known as the two-hit hypothesis[100]. The first mutation is often genetically inherited[100]. With the presence of

only one WT allele, RB function is reduced, though it is sufficient for cells to produce WT phenotypes[100]. The second mutation, or a somatic mutation, is introduced by exposure to environmental factors including carcinogens and ultraviolet light. These factors can create chromosomal double-strand breaks which require repair to maintain genomic integrity[101]. This can be achieved through several molecular repair mechanisms including nonhomologous end joining and homologous recombination[102]. However, nonhomologous end joining can lead to gene deletion, potentially causing a malfunctioning or misfolded protein[102]. Furthermore, in the case of DNA double-strand breaks occurring in the WT allele, homologous recombination with the mutant allele will lead to loss of heterozygosity (LOH)[102]. This will consequently lead to two mutant alleles, both coding for inactivated proteins. Unsurprisingly, *RB1* LOH was observed in 72% of TNBC patients[103].

RB is a member of the retinoblastoma protein family, with the other two members being retinoblastoma-like protein 1 (p107) and retinoblastoma-like protein 2 (p130)[91]. p107 and p130 have a similar function as RB[104]; however, they are not commonly mutated in human cancers[105]. These three proteins are known as the 'pocket proteins'[91]. These proteins contain conserved protein-binding regions in the form of three distinct functional pockets: the small A/B pocket, the C pocket, and the large A/B pocket[106] (**Figure 1.6**). The small A/B pocket binds to proteins with the LXCXE motif, such as HDAC[107]. Mutations within the small A/B pocket inhibit the transcriptional repression activity of RB, confirming that RB and HDAC function as a unit to suppress gene transcription[107]. The C pocket, which is located near the C-terminus, binds to Abelson tyrosine kinase (c-Abl) in the nucleus[108]. This interaction inhibits c-Abl kinase activity. Once RB is hyperphosphorylated, c-Abl is released and its transcriptional activation function during the S phase of the cell cycle is regained[108]. Finally, the large A/B pocket binds to proteins in the E2F family[106]. As discussed briefly, RB halts cell cycle progression through its interaction with E2F. Despite having multiple pocket domains, RB's interactions with proteins in different pocket sites are independent of each other[107]. As a matter of fact, evidence shows that RB function in multiple pocket sites is required to fully regulate cell growth. For example, a mutation in the LXCXE binding site of the small A/B pocket may not have interrupted the interaction of E2F in the large A/B pocket; however, the capacity of RB to suppress cell growth is still reduced[107]. This can potentially lead to an aberrant growth of cells, which is one of the key characteristics of

cancer. Intriguingly, an *RB1* mutation detected in TNBC patient samples included the deletion of 37 base pairs from exon 12 and the addition of GT nucleotides (the conserved RNA splicing acceptor site)[28]. Sanger sequencing confirmed in-frame splicing of exon 11-13 of *RB1* which resulted in the absence of 44 amino acids within the conserved pocket domain of RB, a mutation that would likely be detrimental to RB function[28,109].

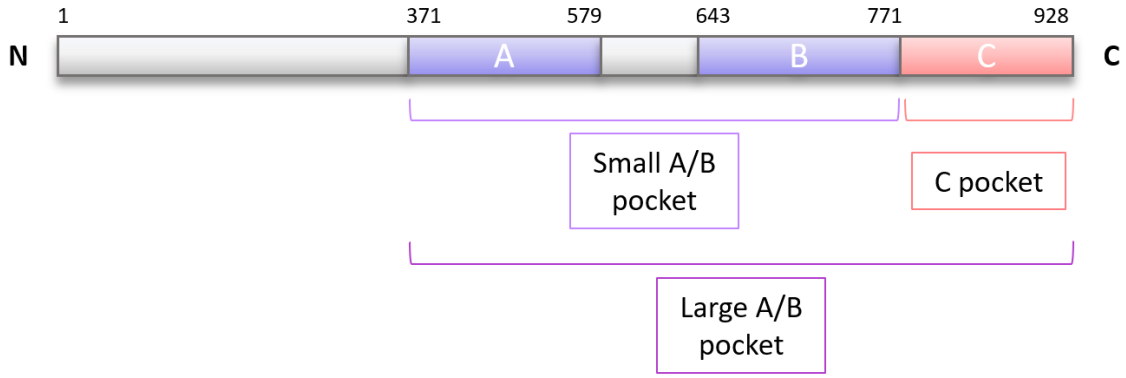

Figure 1.6. RB domain architecture.
RB contains three functional pocket domains. The small A/B pocket consists of domain A and B (aa. 371 – 579). The C pocket spans aa. 772 – 928. The large A/B pocket is a combination of the small A/B pocket and the C pocket (aa. 371 – 928). (aa. = amino acid)

On the other hand, phosphorylation at specific sites within RB can cause conformational changes in RB's structure that are detrimental to its function. For instance, the hyperphosphorylation of RB at the C pocket by Cdk4/6 and Cdk2 induces intramolecular interactions within the RB pockets, disrupting pocket structure and inactivating RB[106,110]. As well, phosphorylation at the C-terminus of RB is found to prevent its binding to c-Abl and LXCXE motif proteins[111], thus promoting cell proliferation. All in all, the three RB pocket domains exhibit a tumour suppressor function and their ability to form interactions with other proteins is tightly regulated by RB phosphorylation. Hence, mutations that modify the pocket domains or the phosphorylation sites are likely to result in a loss of tumour suppressor function.

1.3.2. Loss of function RB can promote tumour metastasis

Mutations in *RB1* often leads to a loss of tumour suppressor function and are also found to promote tumour metastasis. In TNBC samples where there is a concomitant upregulated activity of Myc proto-oncogene (Myc) and a loss of RB, an RNA

microarray showed amplification of the expression of EMT-promoting genes[112]. These genes include *integrin alpha-3* (*ITGA3*) and *fibroblast growth factor 10* (*FGF10*). Through the RB-E2F transcription factor axis, loss of RB enhances expression of genes responsible for tumour metastasis[113]. For instance, loss of RB decreases the expression of E-cadherin, an epithelial cell marker, and upregulates ZEB1 which leads to an overall promotion of EMT[114,115] (**Figure 1.7**), a process which facilitates a detachment of cancer cells from the primary tumour site. Furthermore, a non-canonical function of RB that is mediated through hypoxia signalling has recently been uncovered. Beischlag *et al*. demonstrated that RB is a negative regulator of the thyroid receptor-retinoblastoma interacting protein (TRIP230) transcriptional coactivator, a coactivator that is indispensable for hypoxia-inducible factor-1α (HIF1α) and aryl hydrocarbon receptor nuclear translocator (ARNT) (also known as HIF1β) activity[116]. In this role, RB acts as a transcriptional repressor protein of the HIF1α and HIF1β transcription factors during activated transcription[117]. Subsequently, it was demonstrated that small-interfering RNA (siRNA)-mediated knock-down of RB in MCF-7 cells (a breast cancer cell line) led to a hypoxia-dependent up-regulation of the expression of several genes associated with metastasis and tumour progression, including *C-X-C chemokine receptor 4* (*CXCR4*), *Procollagen-lysine,2-oxoglutarate 5-dioxygenase 2* (*PLOD2*), and *vascular endothelial growth factor* (*VEGF*)[118].

1.3.2.1. Hypoxia is the master regulator of cancer metastasis and survival

Hypoxia, or low oxygen conditions (pO_2 < 10 mmHg in tissues[119,120]), occurs when tumour cells over-proliferate, growing further from blood vessels and depleting their limited oxygen supply. This is common in adenocarcinomas, such as breast carcinomas. Hypoxia initiates the expression of survival genes[121] such as *solute carrier family 2 member 1* (*SLC2A1*) which encodes for glucose transporter 1 (GLUT1)[122,123], controlling glucose uptake, and *vascular endothelial growth factor A* (*VEGFA*) which enhances blood vessel formation (angiogenesis)[122], increasing oxygen supply (**Figure 1.7**). These genes are essential for the tumour cells to survive under hypoxia and are regulated by hypoxia-inducible factors (HIFs)[124,125].

Increased activity of HIFs also causes tumour cells to become metastatic[124,125]. For instance, HIFs upregulate *CXCR4* which promotes growth of primary tumour[126], as well as cell migration through enhancing angiogenesis[127,128] (**Figure 1.7**). Hypoxia-

mediated upregulation of CXCR4 and its chemoattractant ligand, CXCL12, are essential for endothelial cells (EC) proliferation[125]. Knocking-down *CXCR4* in ECs significantly decreased EC growth. Moreover, elevated CXCR4 expression in hypoxia also enhances trans-endothelial migration by responding to the increasing gradient of CXCL12. Knocking-down *CXCR4* from a human-derived TNBC cell line, MDA-MB-231, diminished the cell migration ability under hypoxia[125].

HIFs also upregulate *PLOD2* which promotes ECM remodelling[129,130] (**Figure 1.7**). Knocking down *PLOD2* from fibroblasts reduced the stiffening of ECM generated under hypoxia[129]; the stiffness caused by ECM remodeling promotes cell migration[131]. As a consequence, a co-culturing of MDA-MB-231 and ECM from fibroblasts that were cultured in hypoxia (1% O_2) resulted in MDA-MB-231 cells migrating at a much faster rate and more directional, compared to MDA-MB-231 cells that were co-cultured with ECM from fibroblasts grown under normoxic (20% O_2) conditions[129]. Moreover, PLOD2 also promotes the metastasis and invasion of breast cancer cells during *in vivo* experiments. Immunodeficient mice with MDA-MB-231 cells injected into the mammary fat pad exhibited cancer cell infiltration both in the lymph node and lungs[130]. Knocking down *PLOD2* in these cells significantly decreased their infiltration into the lymph nodes and lungs.

Furthermore, HIFs upregulate *angiopoietin like 4* (*ANGPTL4*) which facilitates lung and brain specific metastasis in breast cancer[132,133] (**Figure 1.7**). ANGPTL4 assists circulating tumour cells in extravasation, an important process for tumour cells to penetrate through blood vessels into a secondary tissue. Incubating ECs with a breast cancer cell line over-expressing ANGPTL4 led to disruptions of endothelial cell-cell junctions[132]. Additionally, immunodeficient mice injected with breast cancer cell line over-expressing ANGPTL4 exhibited a 3-fold increase in lung metastasis, compared to the control cells that do not over-express ANGPTL4[132]. Similarly, immunodeficient mice injected with MDA-MB-231 cells showed a significant decrease in brain metastasis when *ANGPTL4* was knocked-down[133].

Aside from enhancing tumour invasiveness, HIFs also allow tumours to become resistant to apoptosis[124]. Noman *et al.* found that the loss of *protein tyrosine phosphatase non-receptor type 1* (*PTPN1*), a gene which is negatively regulated by miR-210, decreases tumour cell susceptibility to cytotoxic T lymphocyte (CTL)-induced cell

lysis[134] (**Figure 1.7**). HIFs upregulate miR-210 which further suppresses the expression of *PTPN1*, which encodes for protein tyrosine phosphatase 1B (PTP1B)[134]. However, the specific mechanism of how the loss of PTP1B protects tumour cells from lysis by CTLs is currently unidentified. HIFs also upregulate programmed death-ligand 1 (PD-L1), a transmembrane protein which is recognized by programmed cell death protein 1 (PD-1) on the cell surface of CTLs[135] (**Figure 1.7**)m. The interaction between PD-L1 and PD-1 suppresses the immune activity of CTLs, thus, preventing tumour cell death[135].

Overall, current literature suggests that the loss of RB function promotes tumour progression and metastasis either by losing the ability to induce cell cycle arrest through the RB-E2F axis or by enhancing the expression of metastasis-promoting genes through the RB-HIFs axis, all of which advance tumour progression and worsen patient outcome.

Figure 1.7. The loss of RB promotes tumour progression through various mechanisms.
The loss of RB decreases E-cadherin expressing and increases ZEB1 activity which promotes epithelial-mesenchymal transition (EMT). By enhancing the HIF1α-ARNT transcriptional activity under hypoxia, the loss of RB induces overexpression of genes which are responsible for angiogenesis, extracellular matrix (ECM) modification, extravasation, lung and brain metastasis, and escaping cytotoxic T lymphocytes (CTL)-induced cell lysis.

1.4. Mutations in both *TP53* and *RB1* could concomitantly drive metastasis in TNBC

Metastasis, the spread of cancer cells to a secondary site, is the main cause of death in many types of cancer patients[136]. Metastasis is a multi-step process which requires the facilitation of different molecular pathways for cells to successfully metastasize to a secondary site. The main steps of metastasis involve local infiltration of primary tumour cells into adjacent tissue, intravasation (penetration into blood vessels), survival in the circulatory system, extravasation (exiting blood vessels into downstream tissue), and proliferation/colonization at the secondary site[137]. Indeed, mutations in both *TP53* and *RB1* possess a high potential to facilitate TNBC metastasis through various pathways.

1.4.1. Epithelial-Mesenchymal Transition (EMT)

The first step of metastasis requires cancer cells to lose epithelial cell properties and detach from a primary tumour. One important property of epithelial cells is their adherence to neighbouring cells through junction protein interactions[138]. The most well-known epithelial cell marker is a junction protein called E-cadherin[73]. Loss of E-cadherin will result in loss of cell-cell adhesion (**Figure 1.8**). As discussed previously, the loss of RB function facilitates this by decreasing the expression of E-cadherin, through the RB-E2F transcriptional axis[113] (**Figure 1.8**). Once cancer cells are detached from one another, the epithelial-like cells undergo a morphological transformation into mesenchymal cells by undergoing EMT. This process converts a polar cell into a non-polar, spindle-shaped cell which aids cell motility[73] (**Figure 1.8**). Several transcription factors and signaling pathways are known to promote the EMT process. For example, ZEB1/2, which is upregulated by both mutant p53 and the loss of RB in hypoxia (**Figure 1.8**), represses E-cadherin expression[68,125], but up-regulates the expression of N-cadherin, a mesenchymal cell marker[139]. Interestingly, mutant p53 (R175H) is found to reverse transforming growth factor β (TGF-β) function as a tumour suppressor, transforming it into a metastasis promoter[80]. The activation of TGF-β favours the formation of the mutant p53/p63 complex which in turn inhibits the EMT repression function of p63[80,81] (**Figure 1.8**). Furthermore, HIFs facilitate EMT by enhancing the formation of invadopodia, actin-rich structures that help cells to interact with ECM by protruding the cell membrane. HIFs help form these structures by upregulating the

expression of cysteine and glycine rich protein 2 (CSRP2)[140] (**Figure 1.8**). In breast cancer cell lines, CSRP2 promotes invadopodia by stabilizing actin bundles[141]. High expression levels of CSRP2 has also been found to be negatively correlated with overall survival, distant metastasis-free survival, and relapse-free survival of breast cancer patients, revealing its significant role in tumour metastasis[141].

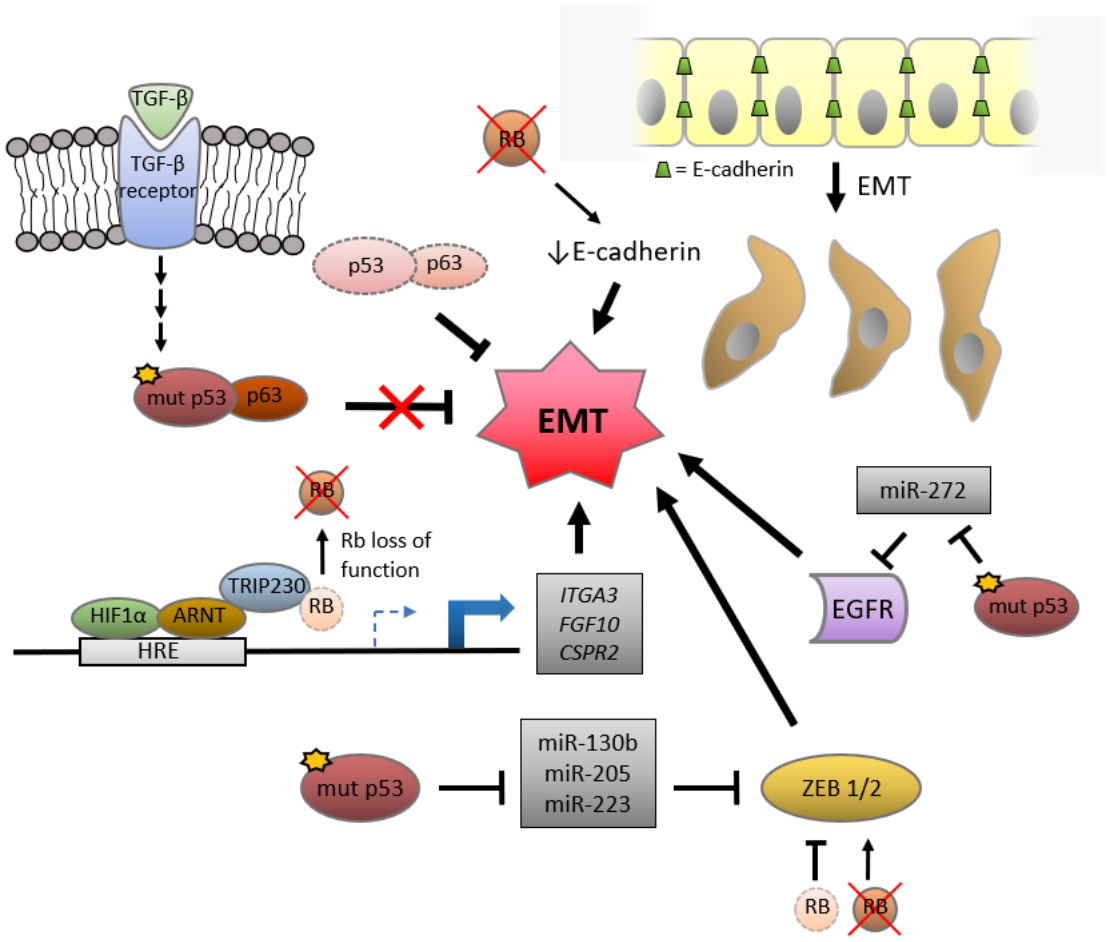

Figure 1.8. Mutant p53 and the loss of Rb promote the loss of cell-cell adhesion and epithelial to mesenchymal transition (EMT).
Activation of the TGF-β receptor induces the formation of a p53-p63 complex, which inhibits EMT. Formation of a mutant p53-p63 complex through TGF-β signaling prevents the inhibition of EMT. Mutant p53 also enhances EMT by increasing ZEB1/2 and EGFR activity via the downregulation of microRNAs. ZEB1/2 function is further upregulated by the loss of RB. Loss of RB reduces cell-cell adhesion by decreasing the expression of E-cadherin, important cell junction proteins which function to adhere neighbouring epithelial cells. The loss of RB also contributes to the exaggeration of transcription of EMT-promoting genes, regulated by the hypoxia-inducible transcription factor (HIFs) complex under hypoxia.

1.4.2. Extracellular Matrix (ECM) Remodelling

Degradation or remodelling of the extracellular matrix (ECM) is essential for tumour cells to escape through the basement membrane (BM) and intravasate into blood vessels[136]. The ECM is mainly composed of collagen and fibronectin[142]. It provides structural support for cells and helps facilitate cell-to-cell communication and cell adhesion[142]. The interaction between cells and the ECM occurs via the binding of fibronectin, which directly links the ECM to receptors (integrins) located on cell membranes[87]. As discussed previously, invadopodia formation facilitates a crosstalk between the cells and the ECM[140]. During tumour progression in various cancers, ECM proteases called matrix metalloproteinases (MMPs) are overexpressed, causing a reorganization of the ECM[143–145]. The loss of RB, together with hypoxia, increases the expression of MMP-2 and MMP-9 which are responsible for degrading the ECM[146–148] (**Figure 1.9**). Furthermore, the presence of integrins on cancer cell membranes enhances MMPs function by anchoring cells to the ECM[86]. This leads to hyperplasia (increase in cell growth) and enhancement of invasion[149]. Intriguingly, R273H p53 increases integrin recycling which facilitates cancer cells forming a meshwork with the ECM[86], enhancing ECM degradation by MMPs[148] (**Figure 1.9**). Loss of RB under hypoxic conditions also promotes the expression of PLOD2 which also induces a re-arrangement of the ECM[129] (**Figure 1.9**). PLOD2 stiffens ECM, another process which enhances ECM degradation by MMPs and facilitates the invasion of tumour cells into lymph nodes or surrounding tissues[129].

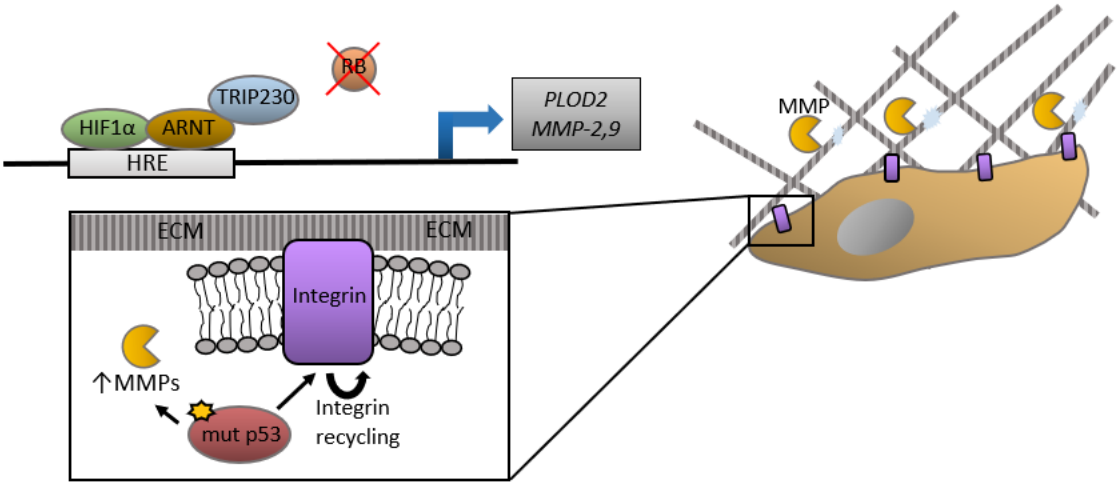

Figure 1.9. Mutant p53 and the loss of Rb enhance the degradation of the extracellular matrix (ECM).

The loss of RB promotes degradation of the ECM by upregulating genes responsible for ECM re-arrangement via HIFs complex-mediated transcription. Mutant p53 further increases ECM degradation by increasing the expression of MMPs and the recycling of integrin, promoted further cell-ECM interactions.

1.4.3. Angiogenesis

Angiogenesis, or formation of blood vessels, is another crucial step required during the initiation of metastasis. Approximately 100 years ago, it was discovered that angiogenesis is correlated with the metabolic rate of tissues or cells[150]. The density of capillaries is higher at tissues where the metabolism rate is high, as these tissues typically require an increased oxygen supply. Tumour cells, rapidly growing cells, often outgrow their oxygen supply and demand more nutrients and oxygen, which are available through blood vessels. To generate more blood capillaries, tumour cells activate HIFs complex, which is oxygen sensitive and upregulated by the loss of RB[151]. Under hypoxia, HIFs transcribe various genes which encode for proteins responsible for multi-step angiogenesis (**Figure 1.10**). For instance, VEGF increases vascular permeability, creating gaps for the formation of new blood vessels and inducing EC growth[121,152]. Also, angiopoietin-2 (ANGPT2) facilitates endothelial sprouting from existing blood vessels[153,154] (**Figure 1.10**). Meanwhile, MMP-2 and MMP-9 degrade the ECM, clearing the path for angiogenesis and inducing the release of angiogenic factors from the basement membrane[155] (**Figure 1.10**). Mutant p53 (R175H, H179L, R273H, D281G) further promotes angiogenesis by increasing the expression of CXC ligands[82],

which enhances the expression of MMP-2 and MMP-9[156] (**Figure 1.10**). As mentioned previously, mutant p53 also loses its angiogenesis inhibitory capability due to the mutations, resulting in an elevated expression of VEGF[85] (**Figure 1.10**). Similarly, while WT p53 represses the expression of CXCR4, mutant p53 (V143A and R280K) promotes the expression[157] (**Figure 1.10**). This further promotes angiogenesis through the CXCR4/CXCL12 axis, as previously discussed[128].

Aside from assisting tumour survival in hypoxia, blood vessels are also one of the main routes cancer cells utilize to migrate from the primary site to a secondary site. Angiogenesis provides new routes for cancer cells to enter the circulatory system[158]. However, the hypoxia-induced angiogenesis mechanism, also known as sprouting angiogenesis, is only utilized by tumours at the early stage of development[159]. Tumours can acquire resistance to anti-angiogenic drugs which target VEGF[159] because late stage tumours utilize another type of angiogenesis known as intussusceptive angiogenesis[160], which does not rely on VEGF function. In this type, instead of sprouting new blood vessels from existing ones, blood vessels split down in the middle into two parallel vessels[160]. Currently, little is known about this mechanism, though hypoxia is not found to be associated with intussusceptive angiogenesis[159]. A relationship between mutant p53 and this form of angiogenesis has also yet to be investigated.

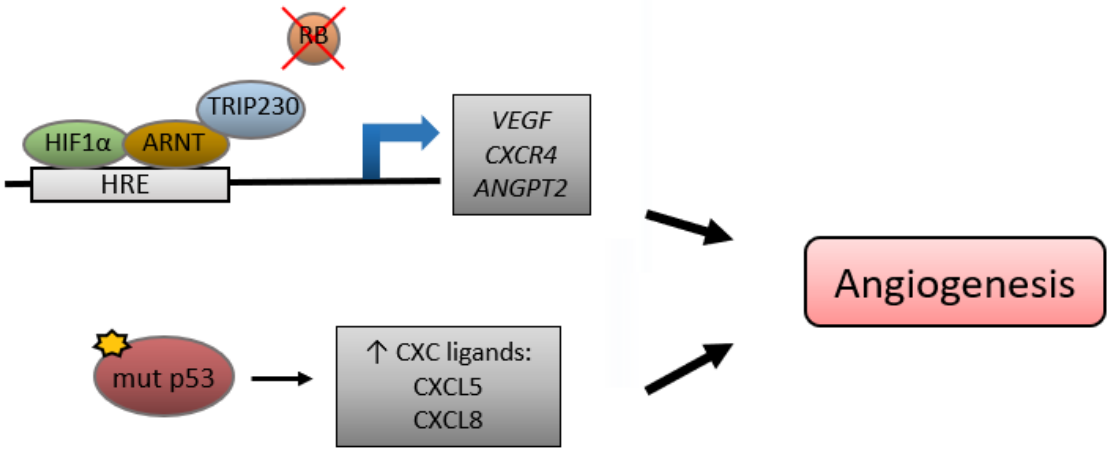

Figure 1.10. Mutant p53 and the loss of RB promotes angiogenesis.
Expression of genes, as well as chemokine ligands responsible for angiogenesis is enhanced by mutant p53 and the loss of RB via HIFs complex-mediated transcription.

1.4.4. Survival in the Circulatory System

Various mechanisms promoted by loss of RB and mutant p53 facilitate the survival of cancer cells in the circulatory system. A combination of loss of RB and hypoxic conditions recruits macrophages and mesenchymal stem cells (MSCs) to the tumour site[161] (**Figure 1.11**). The two recruitment mechanisms mainly involve CXC motif-chemokines signalling and C-C motif-chemokines signalling. Breast cancer cells initially recruit MSCs by secreting CXCL16, which binds to CXCR6 on MSCs[161] (**Figure 1.11**). In response to the recruitment by breast cancer cells, MSCs also secrete CXCL10, which is the ligand of CXCR3 on breast cancer cells[161] (**Figure 1.11**). In a similar mechanism, breast cancer cells recruit MSCs by expressing CCR5 in response to CCL5 secreted by MSCs (**Figure 1.11**). These binding events signal cancer cells to secrete macrophage colony-stimulating factor 1 (CSF1), which binds to CSF1 receptor on MSCs, subsequently recruiting macrophages[161] (**Figure 1.11**). The presence of tumour-associated macrophages (TAMs) protects cancer cells from other immune cells in the circulatory system that may target the tumour[162]. As discussed previously, enhanced HIFs activity mediated by loss of RB also protects tumour cells from CTL-induced cell lysis through increasing the expression of miR-210 and PD-L1[134,135] (**Figure 1.11**). Likewise, cancer cells expressing mutant p53 (R248W) secrete miR-1246-rich exosomes which subsequently recruits TAMs[163]. Aside from protecting tumour cells from other immune cells, TAMs also facilitate extravasation as well as prepare a pre-metastatic niche, making it easier for cancer cells to establish a new colony[162].

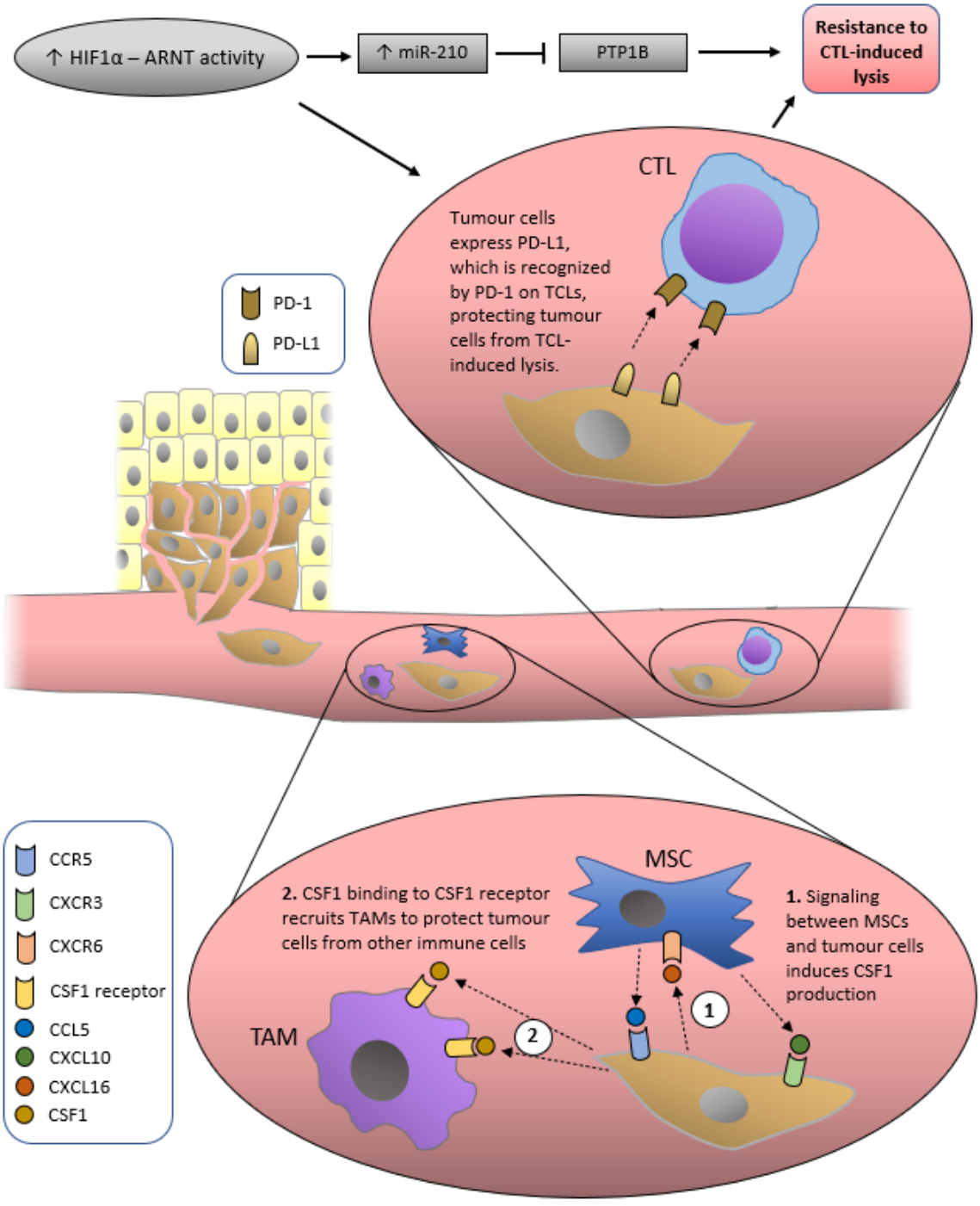

Figure 1.11. The loss of RB protects TNBC from immune cell-induced cell death via HIFs complex-mediated transcription.

Through the C-X-C chemokine receptor and ligand signaling cascades, tumour cells recruit mesenchymal stem cells (MSC) and tumour-associated macrophages (TAM) to protect against other immune cells in the circulatory system. Upregulation of PD-L1 and down regulation of PTP1B also protects tumour cells from cytotoxic T-lymphocytes (CTL)-induced cell lysis.

1.4.5. Secondary Tissue Colonization

Colonization is the final step before cancer cells successfully form a metastatic secondary tumour. For cancer cells to metastasize to a secondary site and successfully form a tumour, they must acquire the ability to penetrate through tissues of specific organs and adapt to the surrounding microenvironment. Common sites of breast cancer metastasis include bones, liver, lungs, and brain[164]. One of the factors which dictates the secondary site of a tumour is organ-specific barriers for cancer cell infiltration. For instance, capillaries in the bone marrow and liver are fenestrated, and are therefore more permissive towards circulating tumour cell infiltration[165,166]. On the other hand, lung capillaries are surrounded by ECs, basement membrane, and alveolar cells, all acting as obstacles that cancer cells must overcome to enter the lungs[167]. Similarly, the blood-brain barrier in the brain, which is composed of ECs surrounded by basement membrane, pericytes, and astrocytes, is a major obstacle for cancer cells, preventing colonization in the brain[168]. To overcome these physical barriers, cancer cells upregulate specific genes which facilitate vascular modulation and communication with the surrounding microenvironment. These genes are often overexpressed in the primary tumour.

TNBC poses a higher likelihood of metastasis to lungs or brain, compared to other types of breast cancer[19]. Upregulation of *prostaglandin-endoperoxide synthase 2* (*PTGS2*) (encodes for cyclooxygenase-2 (COX-2)) and MMP2 promote the ability of breast cancer cells to extravasate into lungs[167] (**Figure 1.12**). Mice with PTGS2- and MMP2-knockdown cell lines injected intravenously showed a reduction in lung metastasis compared to the mice injected with the parental cell line. Likewise, overexpression of ANGPTL4 dissociates endothelial cell-cell junctions around the lung capillaries, allowing cancer cells to infiltrate into the lungs[132] (**Figure 1.12**). MMP2 and ANGPTL4 are overexpressed in hypoxic cancer cells[146,169]. COX-2, which functions by responding to inflammation and promoting tumour growth and immunosuppression, is inhibited by WT p53 but not mutant p53[170].

Under hypoxic conditions, loss of RB leads to overexpression of a gene which facilitates brain metastasis. The cancer cells overexpress CXCR4 (**Figure 1.12**) which responds to chemoattractant CXCL12 secreted by astrocytes, non-neuronal cells in the brain, surrounding the blood-brain barrier[171]. Astrocytes can alter the brain

microenvironment to favour the survival and colonization of TNBC cells by secreting cytokines, such as TGF-α, TGF-β and interleukins[172]. These cytokines regulate cell growth and immune responses[173]. Astrocytes also express sphingosine-1 phosphate receptor 3 (S1P3) which, when activated by sphingosine-1 phosphate (S1P), has the downstream effect of decreasing endothelial cell-cell adhesion[174]. This aids cancer cell penetration through the blood-brain barrier, infiltrating the brain tissue. WT p53 negatively regulates sphingosine kinase (SK1), which phosphorylates sphingosine to produce S1P[175]. In the absence of p53, SK1 levels elevate resulting in an increase of S1P and activation of S1P3[175], further implicating mutation of p53 in formation of secondary tumours.

Overall, much evidence suggests that mutations in *TP53* and *RB1* display a high probability of facilitating TNBC metastasis. Their mutations promote tumour metastasis from inducing morphological transition of tumour cells which promotes a detachment from a primary site, protecting tumour cells from cell lysis by immune cells, all the way to establishing a colony at a secondary site. Through enhancing the expression of various genes, such as *CXCR4*, *PLOD2*, and *ANGPTL4*, mutations in *TP53* and/or *RB1* assist tumour metastasis by enhancing angiogenesis, assisting ECM remodelling, as well as promoting extravasation into a secondary tissue, respectively. With their high potential ability to assist each and every step of TNBC metastasis, the specific molecular mechanisms of how mutations in *TP53* and *RB1* drive TNBC aggressiveness is worth investigating.

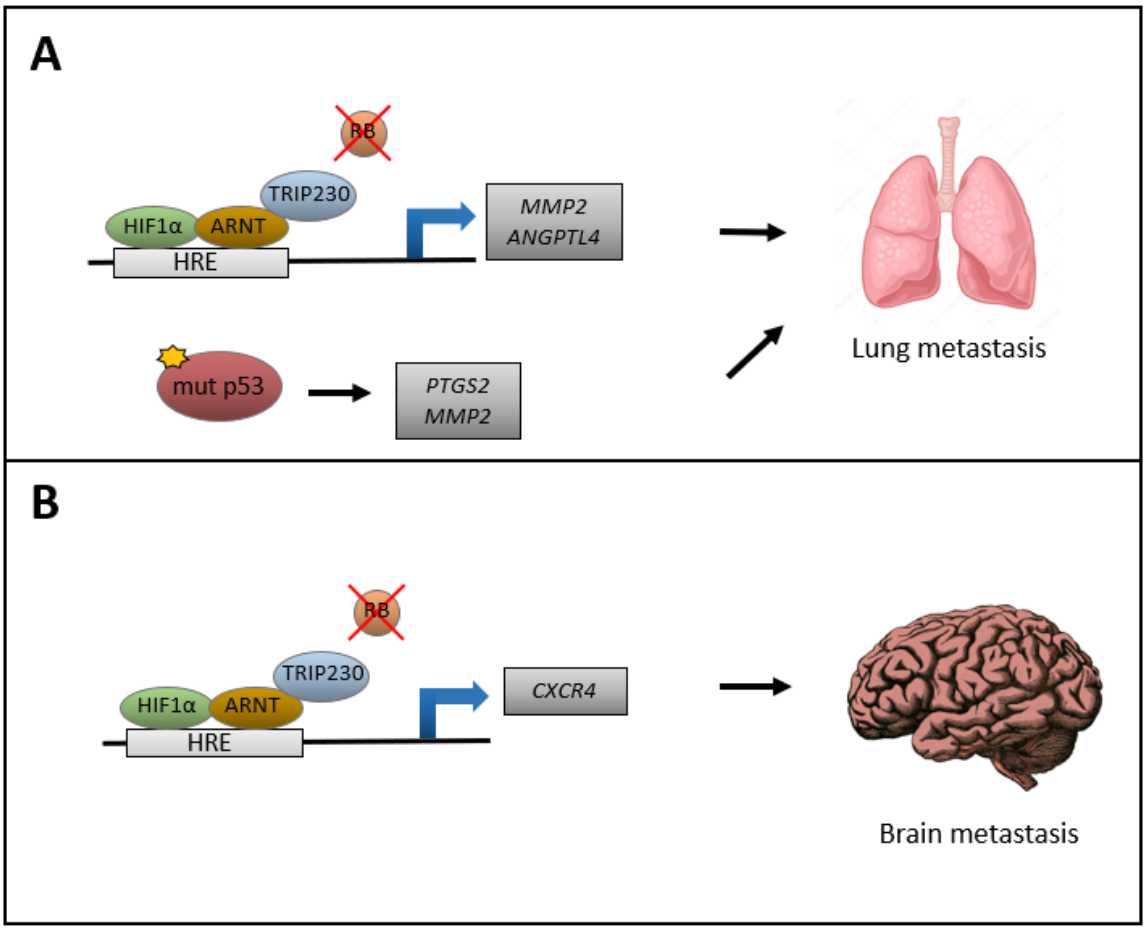

Figure 1.12. Mutant p53 and loss of RB promotes lung and brain metastasis. Through enhancing the HIFs transcriptional complex activity, the loss of RB enhances expression of genes which facilitate lung and brain metastasis. Similarly, mutant p53 increases the expression of genes which facilitate lung metastasis.

1.5. Cell line model could aid the understanding of the effect of *TP53* and *RB1* mutations in TNBC

The cell line model is an *in vitro* model in which cells extracted from a specific tissue of an individual are grown in a laboratory[176]. Adherent cells are cultured on a tissue-culture plate and suspended cells are cultured in a flask. In both cases, cells are submerged in cell culture media supplemented with essential nutrients for their growth. Cells are then incubated in conditions which favour cell proliferation, usually in a humidified incubator at 37 °C and 5% CO_2. Cells can be passaged into a new vessel to maintain their growth or to prepare them for experiments. Adherent cells are often detached from a tissue culture plate via the use of a protease (e.g., Trypsin), or a chelating agent (e.g., EDTA). To store cell lines for future usage, cells are resuspended

in an appropriate culture media supplemented with 5-10% dimethyl sulfoxide (DMSO), a cryoprotectant which reduces ice formation to prevent cell death. The resuspended cells can be stored in the gas phase of liquid nitrogen. Though cell lines can be easily grown and maintained, the growth conditions favour cell proliferation and cell survival, which do not closely mimic physiological conditions. Thus, studies using cell lines could serve as preliminary data and a model which better mimics human physiological conditions, an *in vivo* model, should be used to more accurately test a hypothesis.

Cells and cell lines used in a lab are categorized into different types, based on their life span[176]. Primary cells are cells that are extracted directly from tissues which can come from a biopsy, a surgery, or an animal model. These cells can be grown in a vessel using a similar method described previously[176]. Primary cells become cell lines once they are passaged into a new culture vessel and maintained. Generally, cell lines will continue to proliferate until they become senescent. However, genetic modifications can extend the replication ability of cells. On the other hand, aggressive cancer cell lines tend be immortalized, meaning they can continuously replicate and will not reach senescence.

Using immortal cell lines as study models can be beneficial as they are cost effective, easy to maintain and expand, and can bypass ethical concerns. Thereby, immortal cell lines are commonly used in pre-clinical research, including cancer research and therapeutic development. Notably, the establishment of several cell lines has led to the emergence of important vaccines and cancer treatment developments. For instance, HeLa cell line (cervical cancer cell line) assisted scientists in developing an anti-polio vaccine[177], and K562 and NB4 cell lines (leukemia cell lines) have driven the development of treatments for multiple types of leukemia[178,179]. These cell lines can typically be grown quickly and subsequently utilized for a broad range of *in vitro* experiments. For example, cell lines can be treated with drugs to measure how cells respond to the drugs or how certain molecular mechanisms are affected by the drugs. The genetic material or proteins can be extracted from the cells to determine the effect of the drugs on specific molecular pathways. Moreover, cell proliferation rate or apoptosis upon drug treatment can also be measured.

More importantly, cell lines can be easily manipulated genetically, which can provide meaningful information on downstream effects and functions of target genes. For

example, the underlying mechanism of how the loss of RB promotes metastasis can be investigated by suppressing the expression of *RB1* gene in a cell line and observing the genotypic as well as phenotypic changes of the cell line. Several genetic editing tools are commonly utilized to silence gene expression or even modify DNA sequences. Small interfering RNA (siRNA) and short hairpin RNA (shRNA) knockdown protein expression by inducing the RNA interference pathway[180]. An anti-sense strand of siRNA forms a complex with a complementary mRNA molecule along with an enzyme which will digest the mRNA, preventing its translation to a protein product[181]. shRNA induces protein knockdown through a similar mechanism as siRNA, except the target sequence is expressed to form an internal hairpin structure, which is processed prior to hybridizing with the targeted mRNA[182]. A more powerful gene editing tool which is widely used by researchers nowadays is clustered regularly interspaced short palindromic repeats (CRISPR)-Cas9. Rather than manipulating protein expression at the mRNA level, CRISPR-Cas9 has the ability to edit DNA genomic sequences, introducing various types of mutations to suppress the expression of the target gene[183]. This approach provides a much more stabilized silencing of protein expression as the corresponding mRNA will likely not be transcribed and, therefore, continual and active suppression of newly generated mRNA is not required.

MDA-MB-231 is a well-established TNBC cell line that is widely used in breast cancer research. The cell line was derived from a 51-year-old, Caucasian female patient with metastatic breast adenocarcinoma[184]. This cell line is particularly easy to maintain and replicates rapidly, making it a suitable model for efficient experimental data collection. More importantly, MDA-MB-231 expresses a mutant form of p53, R280K p53[185], which will allow us to directly compare cancer cell phenotypes as a consequence of either a loss of p53 function mutation or the R280K point mutation, which could be either a loss or gain of function mutation. The direct comparison will help uncover which type of *TP53* mutation could drive the aggressiveness of TNBC. As such, MDA-MB-231 was selected as the parental cell line for the generation of an *in vitro* model.

1.5.1. CRISPR *Cas-9* technology facilitates genes modification in cell line model

CRISPR-*Cas9* is a genomic editing tool derived from a natural immune defense mechanism utilized by a wide range of bacterial species[183]. These bacteria that have

been previously infected by viruses will integrate fragments of the viral genetic material into their own genome within segments called CRISPR arrays. If the bacteria are then infected with the same virus, transcription and processing of the CRISPR array generates an RNA molecule that contains a guide sequence complementary to a segment of the foreign viral genome (gRNA). This molecule associates with an RNA-guided endonuclease, such as Cas9, and binds to its complementary sequence on the viral genome, allowing the endonuclease to digest and destroy the foreign DNA, preventing infection.

Researchers have used components of this bacterial mechanism to create an immensely powerful tool for genomic editing in eukaryotic cells. Cells can be transfected with expression vectors encoding both customized gRNA sequences and the Cas9 endonuclease[183]. The gRNA can then guide Cas9 to whichever segment of the genome the gRNA has been designed to complement, providing the segment contains a protospacer adjacent motif (PAM) sequence. At this specific site, Cas9 will generate a DNA-double stranded break (DSB) within the targeted segment or gene. DNA repair machinery will attempt to mend the DSB in order to maintain genomic stability by two main mechanisms, non-homologous end joining and homologous recombination. These repair mechanisms often result in insertion/deletion mutations (indels) which introduce frameshifts and stop codons, potentially resulting in a functional knockout of the gene. Successful gene knockouts can then be screened by single cell colony propagation followed by immunoblotting for the gene knockout product of interest. In this way, researchers have the ability to create a wide range of different cell lines with stable gene knockouts of interest for further study.

1.6. Rationale

TNBC patients suffer from a lack of specialized treatments and thus exhibit a poor prognosis. The underlying mechanisms which drive TNBC progression and metastasis are not well studied; however, *TP53* and *RB1* are commonly mutated together in TNBC. Mutations in *TP53* and/or *RB1* have evidently been shown to promote aggressive tumour progression and metastasis. Hence, creating a TNBC cell line model utilizing CRISPR-Cas9 to knockout *TP53* and *RB1* could provide a useful tool to unveil the tumour progression driving mechanisms controlled by p53 and RB. The valuable

information gained from experimentation on this model could prove beneficial to the eventual development of therapeutics for TNBC.

1.7. Hypothesis

We hypothesize that our established *TP53* and *RB1* knockout cell lines will exhibit an enhancement in tumour aggressive traits, specifically in increased cell cycle progression, elevated metastasis-promoting genes expression, and better response to chemoattractant for migration. We further hypothesize that *TP53* – *RB1* double knockout (DKO) MDA-MB-231 will be the most aggressive, compared to *TP53* or *RB1* single knockout.

1.8. Objectives

The aim of this thesis is to generate cell line models to elucidate the role of concomitant mutations in *TP53* and *RB1* in promoting TNBC aggressiveness. Our specific objectives are:

1. To genetically modify the MDA-MB-231 cell line by knocking out both *TP53* and *RB1* utilizing CRISPR-Cas9 technology
2. To validate that the established cell lines present changes in the molecular mechanisms regulated by p53 and/or RB under normoxic and hypoxic conditions. The specific mechanisms include:
    - Cell distribution in different phases of cell cycle
    - Expression of metastatic-promoting genes
    - Migration of cells via responding to chemoattractant

Chapter 2.

Experimental Procedures

2.1. Cell culture

MDA-MB-231 (ATCC) cells were cultured in Dulbecco's Modified Eagle Medium, high glucose, glutaMAX (DMEM; Gibco) supplemented with 10% Fetal Bovine Serum (FBS; Gibco) and 1% of 10,000 units (U)/mL penicillin and 10,000 µg/mL streptomycin (Pen/Strep; Gibco). Cells were incubated in a humidified incubator at 37°C and 5% CO_2. Once cells reach approximately 80% confluency, cells were passaged at a 1:20 split ratio to allow cells to continue to grow. To passage cells, cell media was aspirated, and cells were washed with warm 1x phosphate-buffered saline (PBS - 137 mM NaCl, 2.7 mM KCl, 10 mM Na_2HPO_4, and 1.8 mM KH_2PO_4, pH 7.4). Subsequently, PBS was removed, and cells were detached by incubating with a small volume of Trypsin EDTA (0.25% Trypsin, 0.1% EDTA; Corning) for 1 min at room temperature. For a 10-cm tissue culture plate, 1 mL of Trypsin EDTA was used. Once cells were detached, 4 mL of culture media was added to neutralize Trypsin EDTA. Cells were then passaged on to a new tissue culture plate.

2.2. CRISPR-Cas9 gene knockout

TP53-knockout (KO), *RB1*-KO, and *TP53*-*RB1*-double knockout (DKO) MDA-MB-231 cell lines were generated in collaboration with Robert Payer from the Beischlag lab, Faculty of Health Sciences (FHS), Simon Fraser University (SFU). *TP53*-KO and *RB1*-KO MDA-MB-231 cell lines were generated by Robert Payer (**Table 2.1**), and I generated *TP53-RB1* DKO cell lines by knocking out *TP53* from one of the *RB1*-KO MDA-MB-231 cell lines generated by Robert Payer. The list of sgRNA sequences used by Robert Payer can be found in **Appendix A**.

Table 2.1. Knockout cell lines generated by Robert Payer

Knockout cell lines	Referred to as
TP53-KO1 MDA-MB-231 (sgRNA 3-3)	p53-KO1
TP53-KO2 MDA-MB-231 (sgRNA 4-7)	p53-KO2
RB1-KO1 MDA-MB-231 (sgRNA 3-1)	RB-KO1
RB1-KO2 MDA-MB-231 (sgRNA 4-1)	RB-KO2

Note: The first number to follow sgRNA indicates the specific sgRNA sequence found in **Appendix A**. The next number indicates the specific clone.

2.2.1. CRISPR-Cas9 plasmid preparation

pSpCas9(BB)-2A-Neo, which will be referred to as PX495-Neo from here onward, was a gift from Ken-Ichi Takemaru (Addgene plasmid # 127762; http://n2t.net/addgene:127762 ; RRID:Addgene_127762) and it was used as a backbone plasmid (**Figure 2.1**). To prepare the plasmid for single guide RNA (sgRNA) insertion, 1 µg PX459-Neo was digested with 10 U *Bbs*I enzyme from New England Biolabs (NEB) in 10x NEBuffer 2.1 (NEB). The reaction was incubated in a 37 °C water bath for 3.5 h followed by heat inactivation in a 65 °C water bath for 20 min. The digested PX459-Neo plasmid was loaded and ran on a 0.8% agarose gel and was purified from the gel utilizing the Monarch DNA Gel Extraction Kit (NEB) as per manufacturer's protocol.

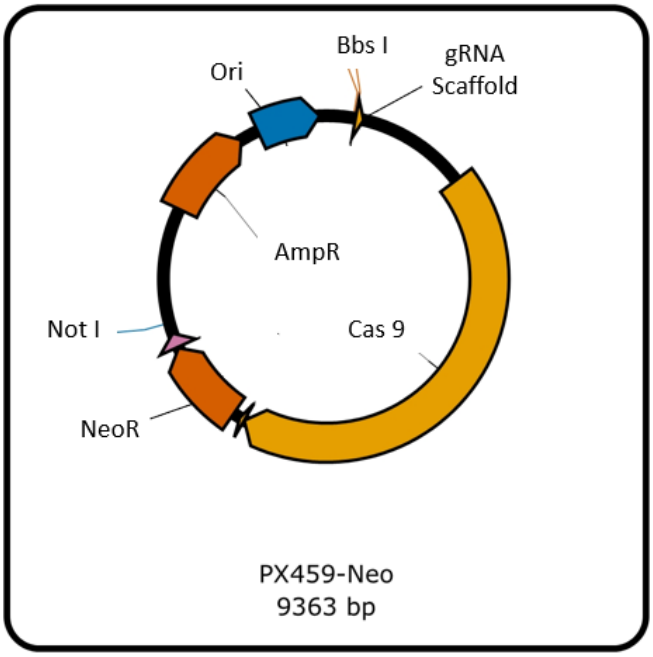

Figure 2.1. pSpCas9(BB)-2A-Neo (PX459-Neo) Plasmid Map
A simplified PX459-Neo plasmid map, showing the important components including origin of replication (Ori), gRNA scaffold, Cas9, neomycin resistance gene (NeoR), ampicillin resistance gene (AmpR), and digestion sites for *Not* I and *Bbs* I. The figure was generated by PlasmaDNA Software.

sgRNA oligos targeting *TP53* (**Table 2.2**) were designed using a web-based tool, CHOPCHOP[186], with the following parameters - Target: *TP53*, In: *Homo sapiens* (hg38/GRCh38), Using: CRISPR/Cas9, For: Knock-out. Four sgRNA sequences were selected using the following guidelines: 40 – 80% GC content, no direct off-targets, and targets the conserved exons in all of the p53 isoforms.

Table 2.2. sgRNA sequences targeting TP53

sgRNA	Sequence (5' → 3')	Targeted *TP53* Exon	Amino acid preceding the cut site	Targeted p53 domain
sgRNA 1	F: caccgCCGGTTCATGCCGCCCATGC R: aaacGCATGGGCGGCATGAACCGGc	Exon 6	N247	DBD
sgRNA 2	F: caccgCAGACCTCAGGCGGCTCATA R: aaacTATGAGCCGCCTGAGGTCTGc	Exon 5	Y220	DBD
sgRNA 3	F: caccgGCGCCGGTCTCTCCCAGGAC R: aaacGTCCTGGGAGAGACCGGCGCc	Exon 7	C277	DBD
sgRNA 4	F: caccgGGTGCCCTATGAGCCGCCTG R: aaacCAGGCGGCTCATAGGGCACCc	Exon 5	P222	DBD

Note: F = forward, R = reverse. Lowercase sequences indicate specific sequence required for plasmid cloning. Uppercase sequences indicate specific targets on *TP53*. DBD = DNA binding domain.

The designed sgRNA oligos were purchased from Integrated DNA Technology (IDT) and were re-constituted in TE buffer (10 mM Tris-HCl, pH 8, 1 mM EDTA). To prepare the sgRNA oligos for ligation into the PX459-Neo plasmid, 100 µM of forward and reverse sgRNA oligos were simultaneously phosphorylated by 10 U T4 polynucleotide kinase (NEB) in 10x T4 polynucleotide buffer (NEB) and annealed using a thermocycling program.

Thermocycling parameters:

37 °C	30 min
95 °C	5 min
95 °C → 25 °C	5 °C/min

Fifty ng of the digested PX459-Neo plasmid and 1 µL of each phosphorylated sgRNA duplex were subsequently ligated by 5 U T4 DNA ligase (NEB) in 10x T4 ligase buffer (NEB). The reactions were incubated at room temperature for 2 h. The ligated product was later transformed into competent TOP10 *Escherichia coli* (*E. coli*) by adding 5 µL of the product into 50 µL of the bacterial cells and mixing gently. The cells were incubated on ice for 20 min, followed by a heat shock incubation in a 42 °C water bath for 45 seconds (sec). Afterwards, the transformed bacteria were incubated on ice for 2 min before plating onto Luria-Bertani agar containing 100 µg/mL ampicillin (Amp), selecting for bacterial colonies containing PX459-Neo plasmid expressing an ampicillin resistant gene (**Figure 2.1**). The plated bacteria were grown overnight (12 – 16h) at 37 °C. Approximately 20-30 colonies were observed per plate compared to 0 colonies for the negative control, which was plated with TOP10 *E. coli* transformed with 5 µL Milli-Q water. To purify the ligated plasmid, well-isolated single colonies were inoculated into 5 mL of lysogeny broth (LB), containing 100 µg/mL Amp, and the bacterial culture was agitated (225 revolution per min) at 37 °C overnight (12 – 16h). The plasmids were purified using QIAprep Spin Miniprep Kit (QIAGEN) according to manufacturer's protocol and eluted with nuclease-free water.

To validate the successful insertion of sgRNA into the PX459-Neo plasmid, a restriction digestion of 1 µg of the purified plasmids by 10 U *Bbs*I and 20 U *Not*I-HF enzymes was setup in NEBuffer 2.1 (NEB).The reactions were incubated in a 37 °C water bath for 3.5 h and subsequently ran on a 0.8% agarose gel to monitor the ability of enzymes to digest at their restriction sites. If the sgRNA was successfully inserted into

the PX459-Neo plasmid, the *Bbs*I digestion site would be destroyed. This would result in a singular linearized plasmid, as only *Not*I-HF will have an intact restriction site to digest. On the other hand, if the plasmid spontaneously re-ligated prior to sgRNA insertion or sgRNA simply failed to insert, both restriction sites would remain intact. Therefore, the plasmid would be digested by both *Bbs*I and *Not*I-HF, resulting in two distinct DNA plasmid fragments. In my case, all four reactions (one for each sgRNA) exhibited a single band on the agarose gel, indicating the successful insertion of all sgRNA candidates.

2.2.2. Transfection of CRISPR-Cas9 plasmids into MDA-MB-231 cells

The plasmid delivery cell transfection method chosen for this research was lipofection, a liposome-based method for DNA product delivery into cells[187]. At 24 h prior to transfection, *RB1*-KO2 MDA-MB-231 cells, which will be referred to as RB-KO2 from here onward, were seeded onto a 6-well tissue culture dish, targeted at approximately 40% - 50% confluency. Plasmid constructs with the four candidate sgRNA insertions were transfected independently, along with a negative control plasmid containing no sgRNA insertions. Lipofectamine 3000 Transfection Reagent (Invitrogen) was used to transfect the cells as per manufacturer's protocol, with the exception of replacing the Opti-MEM I Reduced Serum Medium (Gibco) with Dulbecco's Modified Eagle Medium with 4.5 g/L glucose, 0.11 g/L sodium pyruvate, without L-glutamine and phenol red (Corning). 2.5 µg of each prepared CRISPR-Cas9 plasmid construct was transfected into RB-KO2 cells. At 24 h after transfection, the culture media was replaced with DMEM supplemented with 10% FBS and 1% Pen/Strep to allow recovery of cells from the transfection process. At 48 h after transfection, media was replaced with DMEM supplemented with 10% FBS and 1% Pen/Strep with an addition of geneticin selective antibiotic (G418 sulfate) (Gibco) at 1 mg/mL, to select for cells expressing the neomycin-resistance gene from the transfected plasmid (**Figure 2.1**). Culture media was replaced every 2-3 days until all the parental cells (untransfected) were dead. Surviving resistant cells were diluted to 0.5 cells/ 200 µL, and 200 µL of resuspended cells were plated onto each well of 96-well plates for single-colony selection. After incubation at 37 °C for several days, wells with small single colonies (likely originating from a single cell) were identified and expanded to screen for successful knockout.

2.2.3. Immunoblotting for *TP53* knockout screening

Immunoblotting was used to screen for cells in which *TP53* was successfully knocked out, by confirming the absence of p53 protein expression. The identified single colonies from 96-well plates were expanded until they reached approximately 90% confluency on a 10-cm tissue culture plate. At this point, cells were harvested for immunoblotting. The culture media was aspirated, and cells were washed with ice-cold 1x PBS. Cells were dislodged from the plate using a cell scraper and transferred into a microfuge tube. Subsequently, cells were pelleted by centrifugation at 1000 x g for 5 min at 4 °C. The supernatant was removed, and the cell pellet was resuspended and lysed on ice for 1 h in 200 µL of RIPA buffer (150 mM NaCl, 10 mM NaF, 50 mM Tris-HCl pH 7.4, 1 mM EDTA, 1% Triton X-100, 0.1% SDS, 0.5% Sodium deoxycholate, 1/2800 β-mercaptoethanol (β-ME)) supplemented with 1x protease inhibitor cocktail (BioShop). During incubation, the cells were periodically vortexed every 15 min. After lysis, cells were centrifuged at 17,000 x g for 15 min at 4 °C. The supernatant (cell lysate) was collected and protein quantification was performed by the reducing agent and detergent compatible (*RC DC*) protein assay using the reagents and protocol provided by the *RC DC* protein assay kit (BioRad). Using the SmartSpec Plus Spectrophotometer (BioRad), the absorbance of each lysate was measured at 750 nm. The protein concentration was quantified according to Beer-Lambert law[188] against a generated standard curve. All samples were then diluted in RIPA buffer to the same protein concentration and equal volume of each sample was loaded on a 10% SDS-PAGE gel. The gel was run at 60 V until the dye front entered the resolving gel (30 min) and then at 110 V until the dye front ran off the gel edge. The protein content of the gel was transferred at 4 °C, overnight (15 h) at 4 mÅ to polyvinylidene fluoride membranes (PVDF, Thermo Fisher) submerged in Towbin Transfer Buffer (25 mM Tris, 192 mM glycine, 20% v/v methanol, pH 8.3) using a Western Blot transfer sandwich setup. The membranes were air dried and re-activated by submerging briefly in methanol. To minimize non-specific binding of antibodies, membranes were blocked with 5% skim milk in 1x Tris-buffered saline - Tween (TBS-T, 2.5 mM Tris, 140 mM NaCl, 2.5 mM KCl, 0.5% Tween-20) and incubated at room temperature for 1 h. The membranes were thoroughly washed with 1x TBS-T before incubation with primary antibody (probing against either β-tubulin (β-tub), p53, or RB) overnight at 4 °C. The membranes were then thoroughly washed with 1x TBS-T 3 times for 10 min each. After the washes, the membranes were incubated with horseradish

peroxidase (HRP)-conjugated secondary antibody for 1 h at room temperature, followed by 3 more washes with 1x TBS-T. The immunoblots were visualized using the chemiluminescence property of HRP by incubating the membranes with Immobilon Crescendo Western HRP substrate (Millipore) for 5 min. GeneSnap software (Syngene) was used to image the immunoblots and GeneTools (Syngene) was used for band quantification. Band intensity of the protein of interest was normalized against β-tub (band intensity on the blot from the same sample.

2.2.3.1 Antibodies for immunoblotting

Primary Antibodies:

- p53 – 1/1000 of Recombinant Anti-p53 antibody [E26] (ab32389) (Abcam)
- RB – 1/2000 of Recombinant Anti-Rb antibody [EPR17512] (ab181616) (Abcam)
- β-tub – 1/10000 of Anti-beta Tubulin antibody – Loading Control (ab6046) (Abcam)

Anti-p53 and Anti-RB antibodies are rabbit monoclonal. Anti-β-tubulin antibody is rabbit polyclonal. The antibodies were diluted in 1x TBS-T 0.05% sodium azide.

Secondary Antibody:

Goat Anti-Rabbit IgG H&L Horseradish Peroxidase (HRP) - conjugated (HRP) (ab6721) (Abcam). The antibody was diluted in 5% skim milk 1x TBS-T with 1/10000 dilution factor.

2.3. Flow cytometry-based cell cycle assay

Guava cell cycle reagent (Luminex) was used to determine the proportions of cells in different phases of the cell cycle, based on DNA content. The reagent contains propidium iodine which binds to DNA. The measured intensity of the propidium iodine dye is proportional to the DNA quantity in the cells. The experiment was setup as per the manufacturer's protocol for the high-throughput Guava system. *TP53*-KO, *RB1*-KO, *TP53*-*RB1*-DKO MDA-MB-231 cells, as well as MDA-MB-231 cells transfected with PX459-Neo plasmid without sgRNA insertion (vector control), and untransfected MDA-MB-231 cells (parental) were seeded onto a 12-well tissue culture plate to a targeted

60% confluency. Cells were incubated for 48 h in a humidified incubator at 37 °C, 5% CO_2, and either under normoxia (20% O_2) or hypoxia (1% O_2). Subsequently, cells were trypsinized and transferred onto a 96-well plate (each sample in triplicate). The cells were fixed with ice-cold 70% ethanol, followed by staining with Guava cell cycle reagent (Luminex). Cell cycle analysis was performed by Guava easyCyte Flow Cytometer (Luminex) using InCyte 3.1 program from GuavaSoft Software with the setting parameters described in the manufacturer's protocol. A minimum of 2000 gated events for each sample were collected. The percentage of cells in each phase of cell cycle was determined by FlowJo analysis software, using the Watson Pragmatic algorithm from the Cell Cycle analysis tool of the software.

2.4. Quantitative Polymerase Chain Reaction (qPCR)

TP53-KO, *RB1*-KO, *TP53-RB1*-DKO, vector control, and parental MDA-MB-231 cells were cultured to approximately 85% confluency on a 10-cm tissue culture plate. Cells were further incubated in a humidified incubator for 24 h at 37 °C and 5% CO_2, either under normoxia (20% O_2) or hypoxia (1% O_2). After incubation, cells were washed with ice-cold 1x PBS and RNA samples were extracted from the cells using TRI Reagent Solution (Invitrogen) following the manufacturer's protocol. The RNA quantity and quality was assessed using the NanoDrop 2000 Spectrophotometer (Thermo Fisher). To test for RNA degradation, the RNA extracts were run on a 1% agarose gel with 0.5% v/v bleach via electrophoresis. Next, cDNA was generated from 2 µg of RNA from each cell line by performing a reverse transcription reaction using High-Capacity cDNA Reverse Transcription Kit (Applied Biosystems). The reaction was setup as per the manufacturer's protocol

Thermocycling parameters:

25 °C	10 min
37 °C	120 min
85 °C	5 min
4 °C	hold

To amplify and detect specific cDNA, qPCR was setup using the PowerUp SYBR Green Master Mix (Applied Biosystems). The synthesized cDNA was diluted 1/15 in nuclease-

free water and 3 μM of forward and reverse primer mix was used. Each sample was run in triplicate for each of three different targeted genes of interest (*CXCR4*, *PLOD2*, and *ANGPTL4*) and a *β-actin* housekeeping gene, with the following thermocycling program:

Thermocycling parameters:

45 Cycles:	
95 °C	15 s
60 °C	60 s
Melt Curve:	
95 °C	15 s
60 °C	60 s
60 °C → 95 °C	0.3 °C/min
95 °C	15 s

qPCR output was analyzed by StepOnePlus System (Applied Biosystems). Primers were ordered from IDT and their sequences can be found in **Table 2.3**.

Table 2.3. Primer sequences for qPCR

Gene	Forward primer (5' → 3')	Reverse primer (5' → 3')
CXCR4	TCTGTGACCGCTTCTACC	AGGATGAGGATGACTGTGG
PLOD2	GCGTTCTCTTCGTCCTCATC	GTGTGAGTCTCCCAGGATGC
ANGPTL4	TCCACCGACCTCCCGTTAG	CTGTTCTGAGCCTTGAGTTGTG
β-actin	GAGAAAATCTGGCACCACACC	ATACCCCTCGTAGATGGGCAC

Gene expression quantification was computed by extrapolating the obtained cycle threshold (Ct) value against the standard curve, generated by a dilution series of cDNA from the untransfected MDA-MB-231. The quantified gene expression values for the genes of interest were normalized against the gene expression value of the house keeping gene, β-actin.

2.5. Boyden chamber migration assay

The Boyden chamber assay, or transwell migration, was utilized to observe the migration ability of *TP53*-KO, *RB1*-KO, and *TP53*-*RB1*-DKO MDA-MB-231 cells, compared to the vector control and parental MDA-MB-231 cells. 24 h prior to seeding for the assay, the cells were serum starved by replacing the culture media with DMEM, supplemented with 1% Pen/Step (starved media). After 24 h, cells were trypsinized, diluted to 200 cells/µL in starved media, and 40,000 cells were seeded onto 6.5 mm Tissue Culture Plate Inserts, Polyester (PET) Membrane, 8.0 µm pore size (VWR). These inserts sit atop a 24-well tissue culture plate. The wells below the inserts contained either starved media as a negative control, or DMEM, supplemented with 10% FBS and 1% Pen/Strep, as a chemoattractant to promote migration. Cells were incubated for 24 h in a humidified incubator at 37 °C and 5% CO_2, either under normoxia (20% O_2) or hypoxia (1% O_2). Each KO cell line was seeded in triplicate under each condition. After incubation, the inserts were washed with ice-cold 1x PBS and the cells on the inserts were fixed with ice-cold methanol for 15 min, incubated at -20 °C. The inserts were washed again with ice-cold 1x PBS and the cells were subsequently stained with 0.4% toluidine blue in 1x PBS, incubated at room temperature for 5 min. The inserts were gently rinsed with distilled water after staining. Cotton swabs were used to remove cells inside the inserts that did not migrate to the other side of the membrane. The migrated cells were counted under a light microscope at the 20x objective magnification. Three random fields were selected, and the counted cell numbers were averaged.

2.6. Statistical Analysis

Each data point represents mean value + standard deviation (SD). All the assays were performed in biological triplicate, except for *CXCR4* expression and migration assays which were done in biological duplicate. The statistically significant values were determined by Student's T-test with two-tailed distribution, using two-sample equal variance. P-value < 0.05 is indicated as * and P-value < 0.01 is indicated as **.

Chapter 3.

Results

3.1. *TP53* and *RB1* were both knocked out from MDA-MB-231 by CRISPR-Cas9

To explore the metastasis promoting ability of *TP53* and *RB1*, we generated, using CRISPR-Cas9 technology, an *in vitro* model of TNBC MDA-MB-231 lacking both genes. MDA-MB-231 expresses mutant (R280K) p53 and WT RB. To create the double KO, we used single *TP53* and *RB1* KO MDA-MB-231 cell lines previously generated by Robert Payer (**Table 2.1**). In an attempt to knock out the potential p53 isoform presence in *TP53* KO MDA-MB-231 cell lines (p53-KO1 and p53-KO2, **Figure 3.3**), I designed a new set of sgRNA targeting the conserved domains among p53 isoforms (**Table 2.2**). Subsequently, RB-KO2 was used as the parental cell line to generate *TP53* and *RB1* DKO MDA-MB-231 cell lines, with the aim of completely knocking out the potential p53 isoform as well as the full length p53. Four different sgRNA sequences (**Table 2.2**) were incorporated into a CRISPR-Cas9 plasmid, PX459-Neo. The cells that remained from geneticin drug selection after the transfection were expanded and the *TP53* knockout was validated by an immunoblotting assay. Initially, the cell pools were harvested and validated before proceeding to the single colony selection. Cells transfected with sgRNA 4 showed the greatest decrease in p53 expression levels, whereas sgRNA 3 showed the smallest (**Figure 3.1**). Out of the 41 tested single colonies, 11 showed a loss of expression of the main p53 isoform at ~53 kDa (**Figure 3.2**). However, as the sgRNAs were designed to target exons 5-7 of p53, truncated forms of the full length p53 could be expressed. For the simplification of the report, the status of p53 protein of the cell lines that do not express full length p53 will be referred to as knockout, despite the potential expression of the truncated forms. Interestingly, all of the 11 clones that exhibited p53 KO were transfected with PX459-Neo plasmid incorporated with sgRNA 2 or sgRNA 4, suggesting a difference in knockout efficiency among the four sgRNAs. Despite the loss of main p53 isoform expression, the prominent band at ~42 kDa remained in all the samples. Moreover, clone 4-3 also showed a band at ~35 kDa (**Figure 3.2**). Knocking out *TP53* from the RB-KO2 cell line did not alter or recover the expression of RB (**Figure 3.2B**). Clones 2-2 and 4-6, which established a successful knockout of both *TP53* and

RB1 (**Figure 3.2**) were chosen for subsequent experiments and were referred to as DKO1 and DKO2, respectively (**Figure 3.3**). These two clones were chosen to reduce the cell damage from repeated freeze-thaw cycles, as the other clones which exhibited p53 KO were already stored at -80 °C. However, these additional clones could be used in future validation experiments to further support the data presented in this thesis. **Table 3.1** contains a full list of knockout cell lines used in the following experiments, along with shortened names as to which they will be referred.

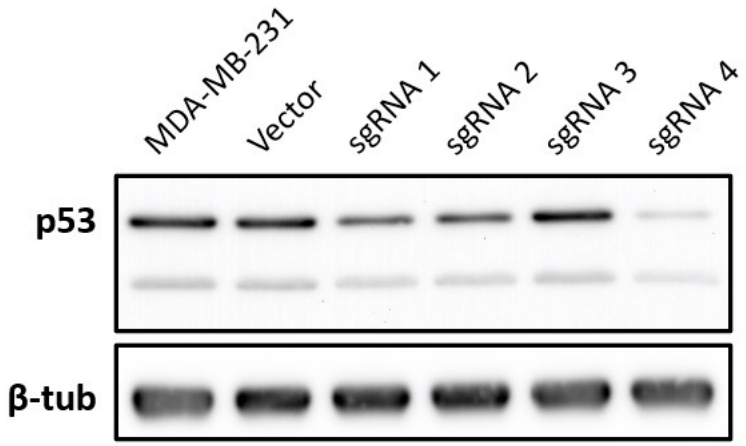

Figure 3.1. p53 protein expression status of the transfected cell pools.
Parental (MDA-MD-231), PX459-Neo without sgRNA-transfected cells (Vector), and cell pool of PX459-Neo sgRNA1, sgRNA2, sgRNA3, and sgRNA4 transfected (sgRNA sequences listed in **Table 2.2**) were harvested and lysed. Cell lysate of each sample was run on a 10% SDS-PAGE gel followed by transfer of the protein content onto PVDF membranes. p53 was probed by 1/1000 of Recombinant Anti-p53 rabbit monoclonal antibody [E26] (ab32389, Abcam). β-tub was used as a loading control and was probed by 1/10000 of Anti-beta Tubulin polyclonal rabbit antibody – Loading Control (ab6046, Abcam). 1/10000 Goat Anti-Rabbit IgG H&L (HRP) (ab6721, Abcam) was used as the secondary antibody.

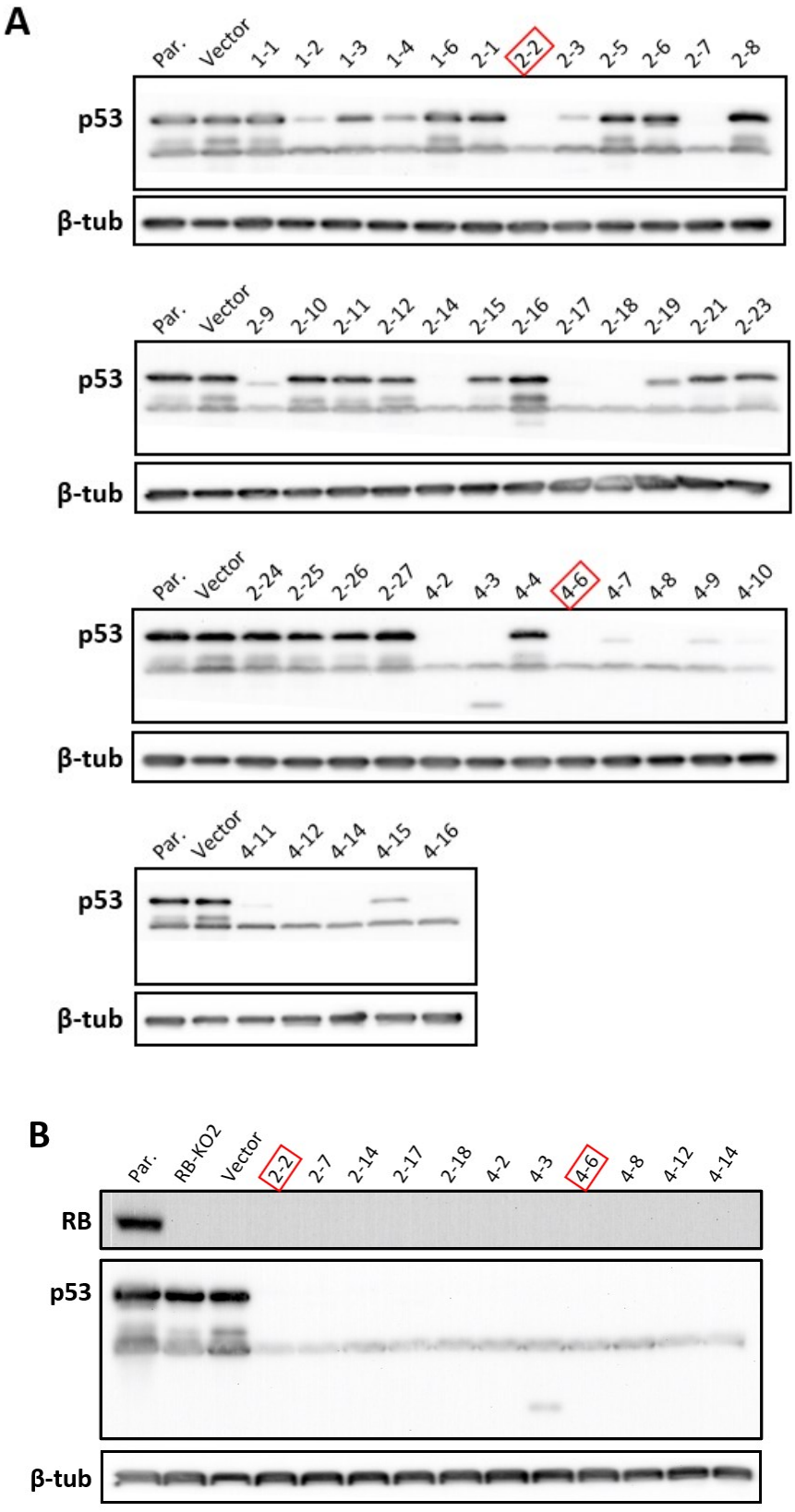
A
Par.
Vector
1-1
1-2
1-3
1-4
1-6
2-1
2-2
2-3
2-5
2-6
2-7
2-8
p53
β-tub
Par.
Vector
2-9
2-10
2-11
2-12
2-14
2-15
2-16
2-17
2-18
2-19
2-21
2-23
p53
β-tub
Par.
Vector
2-24
2-25
2-26
2-27
4-2
4-3
4-4
4-6
4-7
4-8
4-9
4-10
p53
β-tub
Par.
Vector
4-11
4-12
4-14
4-15
4-16
p53
β-tub
B
Par.
RB-KO2
Vector
2-2
2-7
2-14
2-17
2-18
4-2
4-3
4-6
4-8
4-12
4-14
RB
p53
β-tub

Figure 3.2. Single colony selection of TP53 and RB1 DKO MDA-MB-231.
RB-KO2 cells were lipo-transfected with PX459-Neo plasmid incorporated with either sgRNA 1, 2, 3, or 4, targeting *TP53* (**Table 2.2**). Successfully transfected cells were selected by Geneticin treatment. Subsequently, the cells were diluted in DMEM to 0.5 cells/μL, seeded onto each well of 96-well plates, and expanded until there were enough cells to be harvested for an immunoblot. Harvested cells were lysed and cell lysate of each sample was run on a 10% SDS-PAGE gel followed by transfer of the protein content onto PVDF membranes (**A**). Cell lysate of all the clones that exhibited p53 KO was run on another 10% SDS-PAGE gel and the protein content was subsequently transferred onto PVDF membranes (**B**). p53 and RB were probed by 1/1000 of Recombinant Anti-p53 rabbit monoclonal antibody [E26] (ab32389, Abcam) and 1/2000 of Recombinant Anti-Rb rabbit monoclonal antibody [EPR17512] (ab181616, Abcam), respectively. β-tub was used as a loading control and was probed by 1/10000 of Anti-beta Tubulin polyclonal rabbit antibody – Loading Control (ab6046, Abcam). 1/10000 Goat Anti-Rabbit IgG H&L (HRP) (ab6721, Abcam) was used as the secondary antibody. Par. refers to the parental, untransfected MDA-MB-231. Vector refers to MDA-MB-231 cells transfected with PX459-Neo without sgRNA. For each clone, the first number indicates a specific sgRNA and the second number indicates a clone number. Clones 2-2 and 4-6, shown in red boxes, were selected for further analyses.

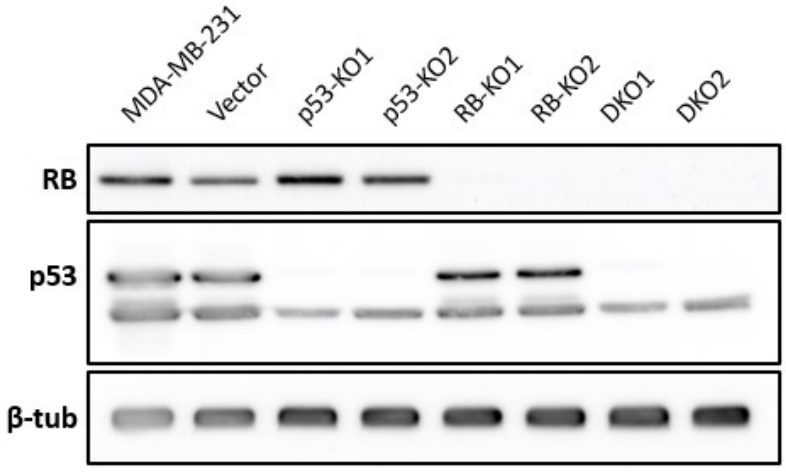

Figure 3.3. p53 and RB protein expression status of cell lines used in the validation experiments.
Parental (MDA-MD-231), PX459-Neo without sgRNA-transfected (Vector), *TP53* single knockout (p53-KOs), *RB1* single knockout (RB-KOs), and double *TP53* and *RB* knockout (DKOs) cells were harvested and lysed. Cell lysate of each sample was run on a 10% SDS-PAGE gel followed by transfer of the protein content onto PVDF membranes. p53 and RB were probed by 1/1000 of Recombinant Anti-p53 rabbit monoclonal antibody [E26] (ab32389, Abcam) and 1/2000 of Recombinant Anti-Rb rabbit monoclonal antibody [EPR17512] (ab181616, Abcam), respectively. β-tub was used as a loading control and was probed by 1/10000 of Anti-beta Tubulin polyclonal rabbit antibody – Loading Control (ab6046, Abcam). 1/10000 Goat Anti-Rabbit IgG H&L (HRP) (ab6721, Abcam) was used as the secondary antibody. The full name of each clone is listed on **Table 3.1**. Vector control, p53-KOs, and RB-KOs are approximately 6-7 passages higher than the parental control; whereas DKOs are approximately 16-17 passages higher than the parental control.

Table 3.1. Knockout cell lines used in experiments

Cell line	Short Name
MDA-MB-231	Parental
PX459-Neo MDA-MB-231	Vector Control
TP53-KO1 MDA-MB-231 (sgRNA 3-3)	p53-KO1
TP53-KO2 MDA-MB-231 (sgRNA 4-7)	p53-KO2
RB1-KO1 MDA-MB-231 (sgRNA 3-1)	RB-KO1
RB1-KO2 MDA-MB-231 (sgRNA 4-1)	RB-KO2
TP53-RB1-DKO1 MDA-MB-231 (sgRNA 2-2)	DKO1
TP53-RB1-DKO2 MDA-MB-231 (sgRNA 4-6)	DKO2

Note: The first number to follow sgRNA indicates the specific sgRNA sequence. sgRNA sequences for *TP53* and *RB1* single KO can be found in **Appendix A**. sgRNA sequences for *TP53* and *RB1* DKO can be found in **Table 2.2**. The next number indicates the specific clone.

3.2. Flow cytometry reveals complex changes in cell cycle regulation networks in *TP53* and *RB1* knockouts

Both p53 and RB play direct and indirect roles in cell cycle regulation. In order to monitor the effect of their knockouts on MDA-MB-231 TNBC cell lines, I employed the Guava cell cycle assay, which stoichiometrically measures the amount of DNA in the cells of each knockout. A proportional distribution of the number of cells in each phase is generated to determine if the cell cycle has been disrupted (**Figure 3.4**). Accumulation of cells in the G1 phase indicates G1/S arrest, whereas accumulation of cells in the G2 phase indicates G2/M arrest. I compared the relative distributions of cells in these cell cycle phases between the vector control and p53-KOs, RB-KOs, and DKOs, under both normoxia and hypoxia.

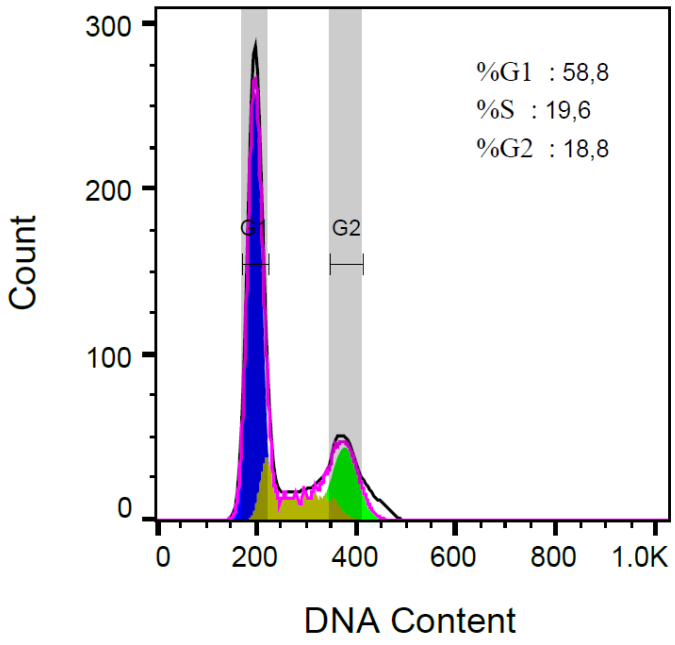

Figure 3.4. A representative cell cycle distribution of MDA-MB-231.
Untransfected MDA-MB-231 cells were distributed into three cell cycle phases according to the measured propidium iodine intensity, which is proportional to DNA quantity. Cells were seeded to a targeted confluency of 60% and incubated in a humidified incubator at 37 °C, 5% CO_2, and 20% O_2 for 48 h. Subsequently, cells were fixed with ice-cold 70% ethanol and stained with Guava cell cycle reagent (Luminex). Percentages of cell distribution in phases G1, S, and G2/M were analyzed by Guava easyCyte Flow Cytometer (Luminex) using the InCyte 3.1 program from the GuavaSoft software. A minimum of 2000 gated samples were collected. The data collected was analyzed by FlowJo analysis software. Cell cycle analysis was applied to the gated cells. G1 (blue) and G2 (green) peaks were determined using Watson Pragmatic model. S phase population (yellow) falls between G1 and G2 population.

Under normoxia, the vector control exhibited a cell cycle phase distribution of 44.9% G1, 22.5% S, and 13.2% G2 (**Figure 3.5A**), with the remaining cells being broadly distributed in the DNA quantity range higher than G2. G1 distribution was not significantly different when comparing the vector control to any knockout lines (**Figure 4.3A).** However, p53-KO1, DKO1, and DKO2 showed a significant increase in the distribution of cells in the G2 phase compared to the vector control, with G2 distributions of 22.6%, 17.2%, and 23.1%, respectively (**Figure 3.5A**). p53-KO1 also had an accompanying drop in S phase distribution to 15.6% (**Figure 3.5A**).

Under normoxia, direct comparisons between p53-KOs and DKOs cell cycle distributions were made to determine if the loss of RB further disrupts cell cycle regulation in the absence of p53. G1 phase distributions remained relatively similar between the p53-KO1 and DKOs (42.20% vs. 44.86% and 39.59%) (**Figure 3.5A**). However, DKO1 exhibited a substantial increase in S phase distribution compared to

p53-KO1 (22.53% vs. 15.64%) (**Figure 3.5B**). Moreover, both DKO1 and DKO2 had an increase in G2 phase distribution compared to p53-KO2 (17.2%/23.1% vs. 14.0%, respectively) (**Figure 3.5B**). Conversely, DKO1 showed a significant reduction in G2 distribution compared to p53-KO1 (**Figure 3.5B**). This revealed that different KO clones, despite having the same gene knocked out, can behave differently in the context of cell cycle activity.

Differences in cell cycle distributions of RB-KOs vs DKOs may reveal how p53 regulates the cell cycle in the absence of RB and if regulatory functions are completely disrupted when both p53 and RB are knocked-out. Although the RB-KOs did not have significant changes in cell cycle distribution under normoxia compared to the vector control, both RB-KO1 and RB-KO2 had a significantly higher accumulation of cells in G1 (53.0% and 55.5%, respectively) compared to both DKO1 and DKO2 (44.9% and 39.6%, respectively) (**Figure 3.5C**). Accompanying this, both DKO1 and DKO2 exhibited an increase in G2 accumulation compared to RB-KO2 (17.2%/23.1% vs. 14.5%, respectively) (**Figure 3.5C**). Comparing results between RB-KO2 and the DKOs is especially valuable as both DKO lines stem from RB-KO2 originally.

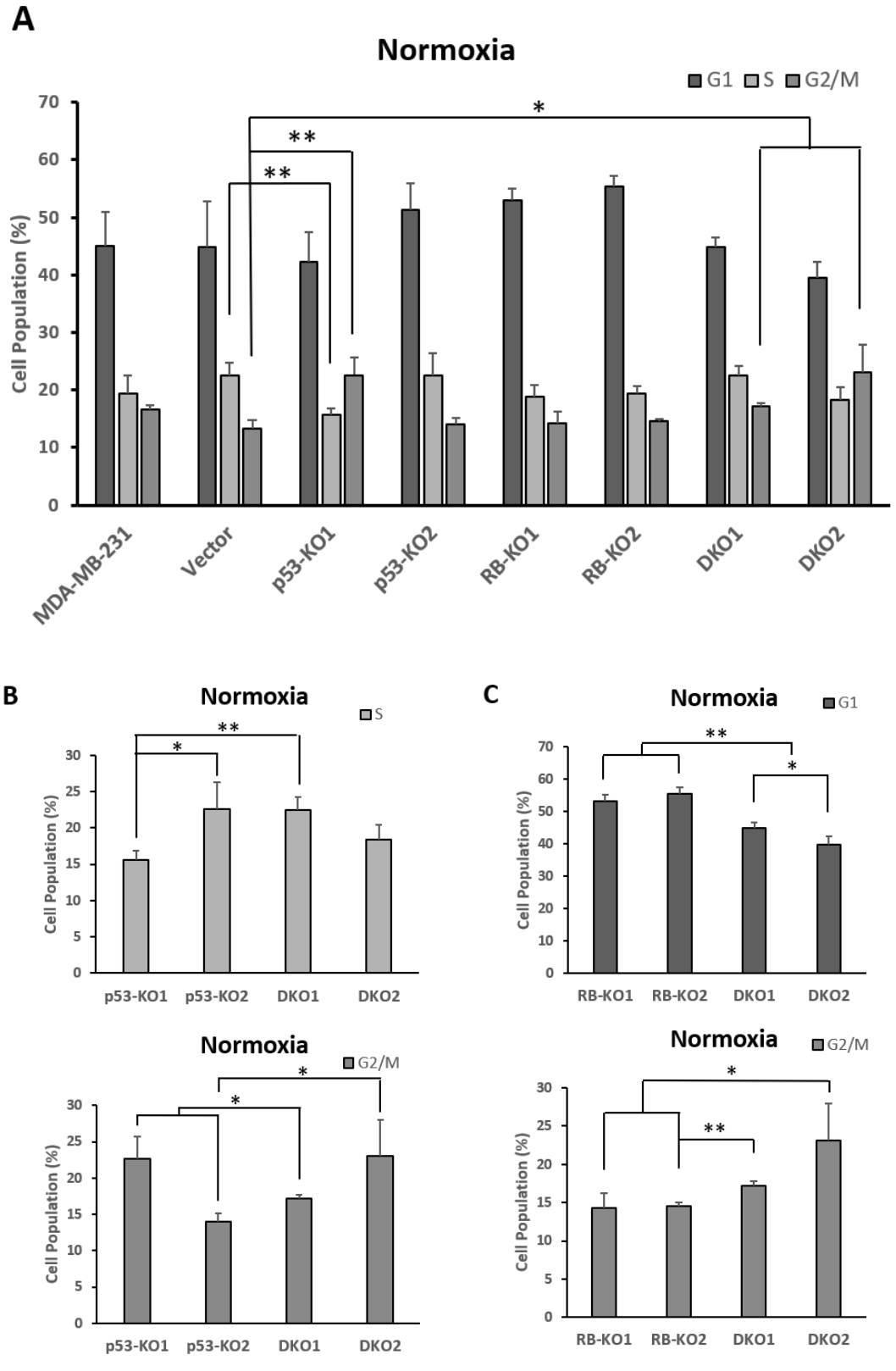
A
Normoxia
G1
S
G2/M
Cell Population (%)
MDA-MB-231
Vector
p53-KO1
p53-KO2
RB-KO1
RB-KO2
DKO1
DKO2
B
Normoxia
S
Cell Population (%)
p53-KO1
p53-KO2
DKO1
DKO2
Normoxia
G2/M
Cell Population (%)
p53-KO1
p53-KO2
DKO1
DKO2
C
Normoxia
G1
Cell Population (%)
RB-KO1
RB-KO2
DKO1
DKO2
Normoxia
G2/M
Cell Population (%)
RB-KO1
RB-KO2
DKO1
DKO2

Figure 3.5. Cell cycle phase distribution by p53 and RB expression status under normoxia.

Cell cycle phase distribution of each cell line is plotted as a bar graph, with percentage of total cells within each specific cell cycle phase plotted on the y-axis. Statistical comparisons of each cell line to the vector (**A**), direct comparisons between p53-KOs vs. DKOs (**B**), and RB-KOs vs. DKOs (**C**) were analyzed. Cells were seeded to a targeted confluency of 60% and incubated in a humidified incubator at 37 °C, 5% CO_2, and 20% O_2 for 48 h. Subsequently, cells were fixed with ice-cold 70% ethanol and stained with Guava cell cycle reagent (Luminex). Percentages of cell distribution in phases G1, S, and G2/M were analyzed by Guava easyCyte Flow Cytometer (Luminex) using the InCyte 3.1 program from the GuavaSoft software. A minimum of 2000 gated samples were collected. The data collected was analyzed by FlowJo analysis software. Error bars represent standard deviation. The statistical analysis was done using Student's T-test. *, ** indicate p-value < 0.05 and < 0.01, respectively.

The cell cycle phase distributions were also monitored with the same set of knockout cell lines and controls under hypoxic conditions (1% O_2). This was done to determine if changes in molecular machinery and pathways that are regulated by hypoxia affect the progression of the cell cycle, in the context of p53-KO, RB-KO, and DKO. When compared to the vector control, the only significant changes in phase distribution observed under hypoxia was an increase in G2 for both p53-KO1 and DKO2 (12.7% for control, 22.6% for p53-KO1, and 26.9% for DKO2) (**Figure 3.6**). Interestingly, this increase in G2 cell distribution in DKO2 was significant when compared against every other cell line in the experiment, except p53-KO1 (**Figure 3.6B-C**). This showed that this particular DKO may be prone to G2/M arrest in the context of tumour cells under both normoxia and hypoxia.

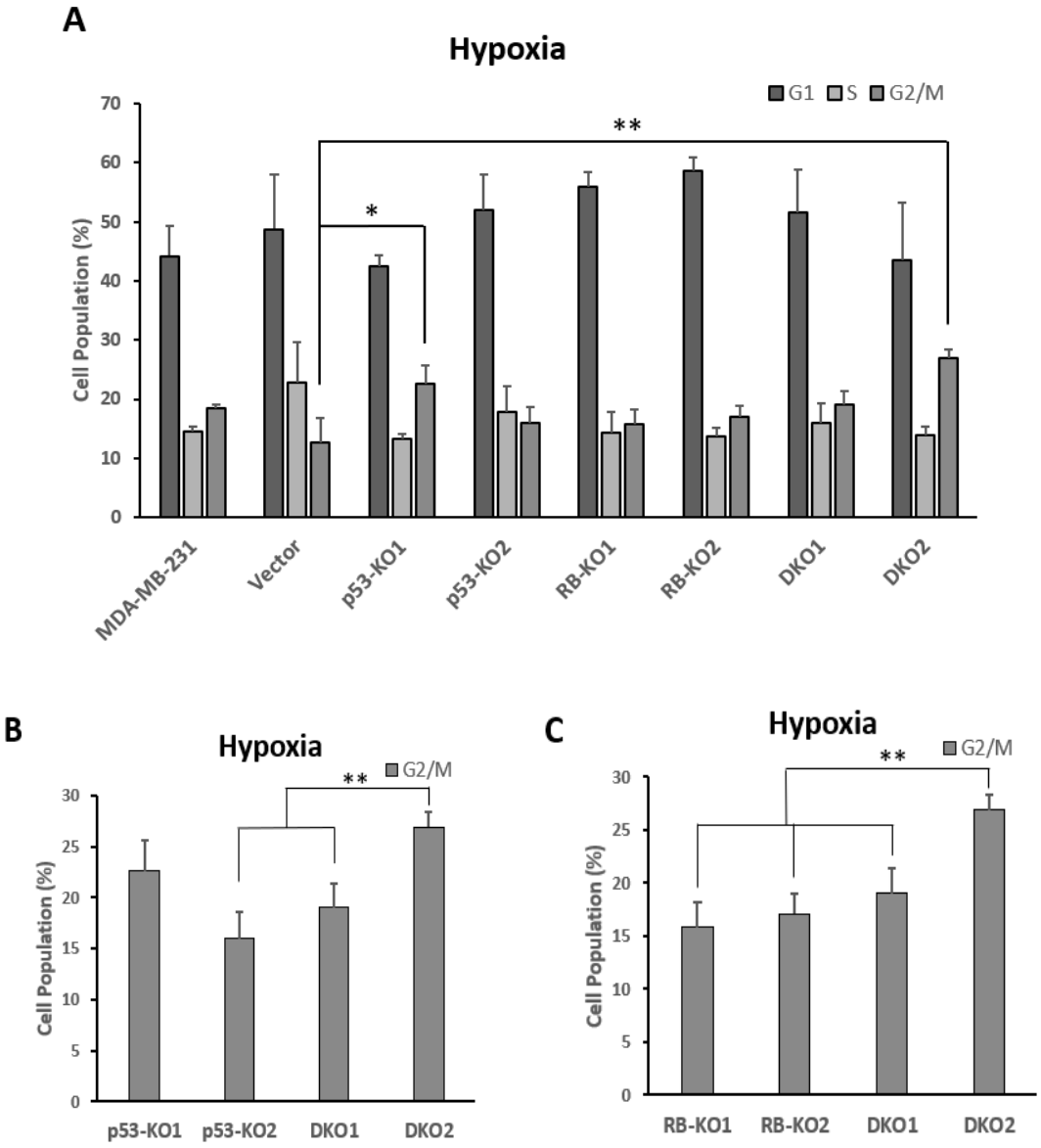

Figure 3.6. Cell cycle phase distribution by p53 and RB expression status under hypoxia.

Cell cycle phase distribution of each cell line is plotted as a bar graph, with percentage of total cells within each specific cell cycle phase plotted on the y-axis. Statistical comparisons of each cell line to the vector (**A**), direct comparisons between p53-KOs vs. DKOs (**B**), and RB-KOs vs. DKOs (**C**) were analyzed. Cells were seeded to a targeted confluency of 60% and incubated in a humidified incubator at 37 °C, 5% CO_2, and 1% O_2 for 48 h. Subsequently, cells were fixed with ice-cold 70% ethanol and stained with Guava cell cycle reagent (Luminex). Percentages of cell distribution in phases G1, S, and G2/M were analyzed by Guava easyCyte Flow Cytometer (Luminex) using the InCyte 3.1 program from the GuavaSoft software. A minimum of 2000 gated samples were collected. The data collected was analyzed by FlowJo analysis software. Error bars represent standard deviation. The statistical analysis was done using Student's T-test. *, ** indicate p-value < 0.05 and < 0.01, respectively.

When directly comparing results between the same cell lines grown under either normoxic or hypoxic conditions, there are no significant differences in either G1 or G2 phase distributions. However, the amount of cells in the S phase decreases for some cell lines when hypoxic conditions are introduced (**Figure 3.7**). This includes RB-KO2 (decrease from 19.3% to 13.7%), DKO1 (22.5% to 16.0%), and DKO2 (18.3% to 13.9%). Loss of cells distributed in the S phase could be another sign of G1/S arrest, as it could reveal a lack of cells entering the replication phase. Overall, the many differences in cell cycle phase distributions observed in these flow cytometry experiments reveal that p53 and RB play a complex role in the cell cycle regulation of these TNBC cell lines, both under normoxic and hypoxic conditions.

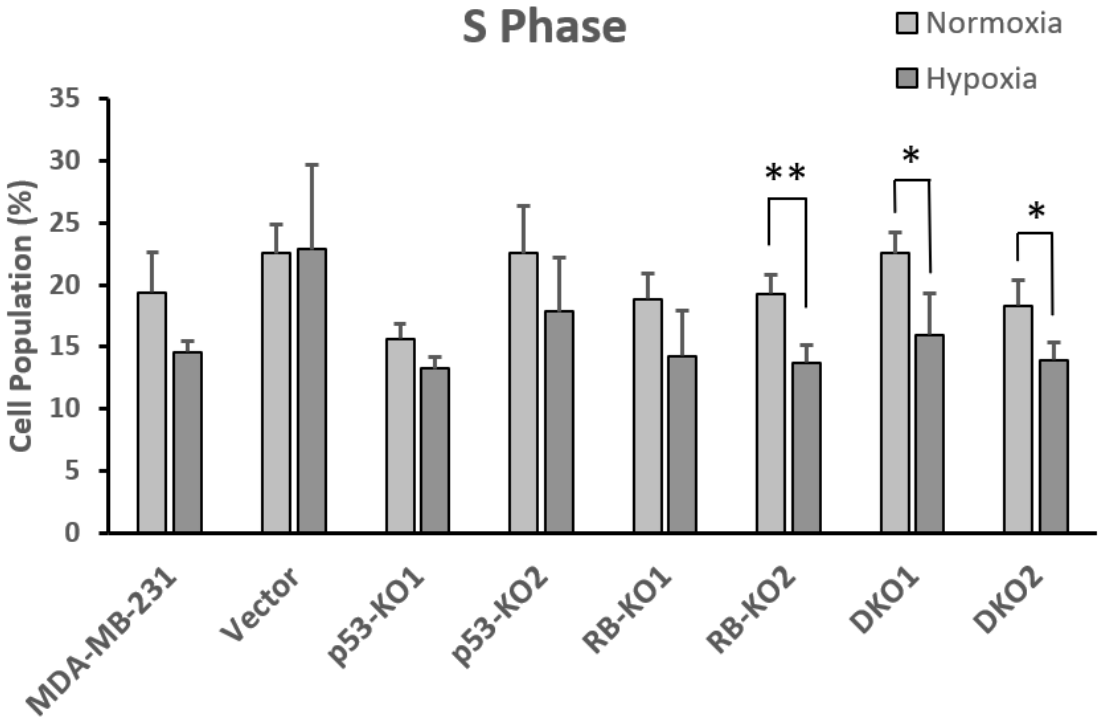

Figure 3.7. Cell population in the S phase of RB-KO2 and DKO were affected by hypoxia.

Cells were seeded to a targeted confluency of 60% and incubated in a humidified incubator at 37 °C, 5% CO_2, and either at 20% O_2 (normoxia) or 1% O_2 (hypoxia) for 48 h. Subsequently, cells were fixed with ice-cold 70% ethanol and stained with Guava cell cycle reagent (Luminex). Percentages of cell distribution were analyzed by Guava easyCyte Flow Cytometer (Luminex) using the InCyte 3.1 program from the GuavaSoft software. A minimum of 2000 gated samples were collected. The data collected was analyzed by FlowJo analysis software. Error bars represent standard deviation. The statistical analysis was done using Student's T-test. *, ** indicate p-value < 0.05 and < 0.01, respectively.

3.3. Knockout of *TP53* and *RB1* affect the expression patterns of hypoxia-inducible genes

Mutations in both p53 and RB can directly or indirectly enhance the activity of molecular pathways that promote tumour progression and metastasis. To investigate how p53 and RB knockout may exacerbate those pathways in MDA-MB-231 TNBC cells, I measured the change in expression patterns of three genes that are involved in various processes of cancer metastasis: *CXCR4, PLOD2,* and *ANGPTL4*, under both normoxic and hypoxic conditions. *CXCR4* regulates primary tumour cell proliferation and trans-endothelial migration, *PLOD2* assists primary tumour escape and intravasation through ECM remodeling, and *ANGPTL4* facilitates secondary tissue invasion through dissociating endothelial cell-cell junctions. The expression of these three genes under normoxia vs. hypoxia was monitored by harvesting RNA and performing qPCR on controls, p53-KOs, RB-KOs, and DKOs, and normalizing the results to the mRNA expression of the housekeeping gene *β-actin*.

Monitoring *CXCR4* expression produced some surprising results. As expected, the parental MDA-MB-231 TNBC cells exhibited a measurable increase in expression of *CXCR4* under hypoxia (*CXCR4*/*β-actin* normalized expression value shifted from 0.25 under normoxia to 0.73 under hypoxia) (**Figure 3.8A**). This general trend continued for the other cell lines, though the expression increase was only statistically significant for p53-KO1, with the normalized expression value shifting 3-fold from 0.11 to 0.35 (**Figure 3.8**). However, the *CXCR4* expression level in the vector control increased considerably compared to the parental control, suggesting that the transfection process may influence *CXCR4* expression level. Interestingly, general expression of *CXCR4* under both normoxia and hypoxia was reduced drastically for many KOs, compared to the vector control, including p53-KO1, RB-KO2, DKO1, and DKO2 (**Figure 3.8**). For example, under hypoxia the normalized expression level for the vector control was 10.17, while the level for these four knockouts were 0.35, 0.08, 0.01, and 0.15, respectively. Surprisingly, *CXCR4* expression levels significantly decreased in the DKOs compared to some single KOs (**Figure 3.8C-D**). Under hypoxia, p53-KO2 and RB-KO1 had normalized expression of 6.81 and 4.05, respectively, while DKO1 and DKO2 *CXCR4* expression was 0.01 and 0.15, respectively. DKO1 also had significantly reduced expression compared to p53-KO1, under both normoxia and hypoxia (**Figure 3.8C**).

Despite low variation between data points of technical replicates, *β-actin*-normalized expression levels fluctuated greatly between biological replicates. To both mask the effect of this fluctuation and compare the differences between the controls and KOs in *CXCR4* expression when cells are shifted from normoxia to hypoxia, the fold change was plotted for each cell line (**Figure 3.8E**). This revealed that DKO2 had the highest overall fold increase in expression from normoxia to hypoxia, at 6.64. This was higher than any other cell line, especially RB-KO1 at a 1.44 increase, a significantly smaller increase compared to DKO2. Overall, monitoring *CXCR4* expression reveals that the gene's role in cell migration likely changes in different tumour contexts depending on the presence or absence of p53 and RB and under normoxia vs. hypoxia. However, as the vector control behaved differently from the parental control, these observed changes are potentially caused by the off-target effect from the transfection.

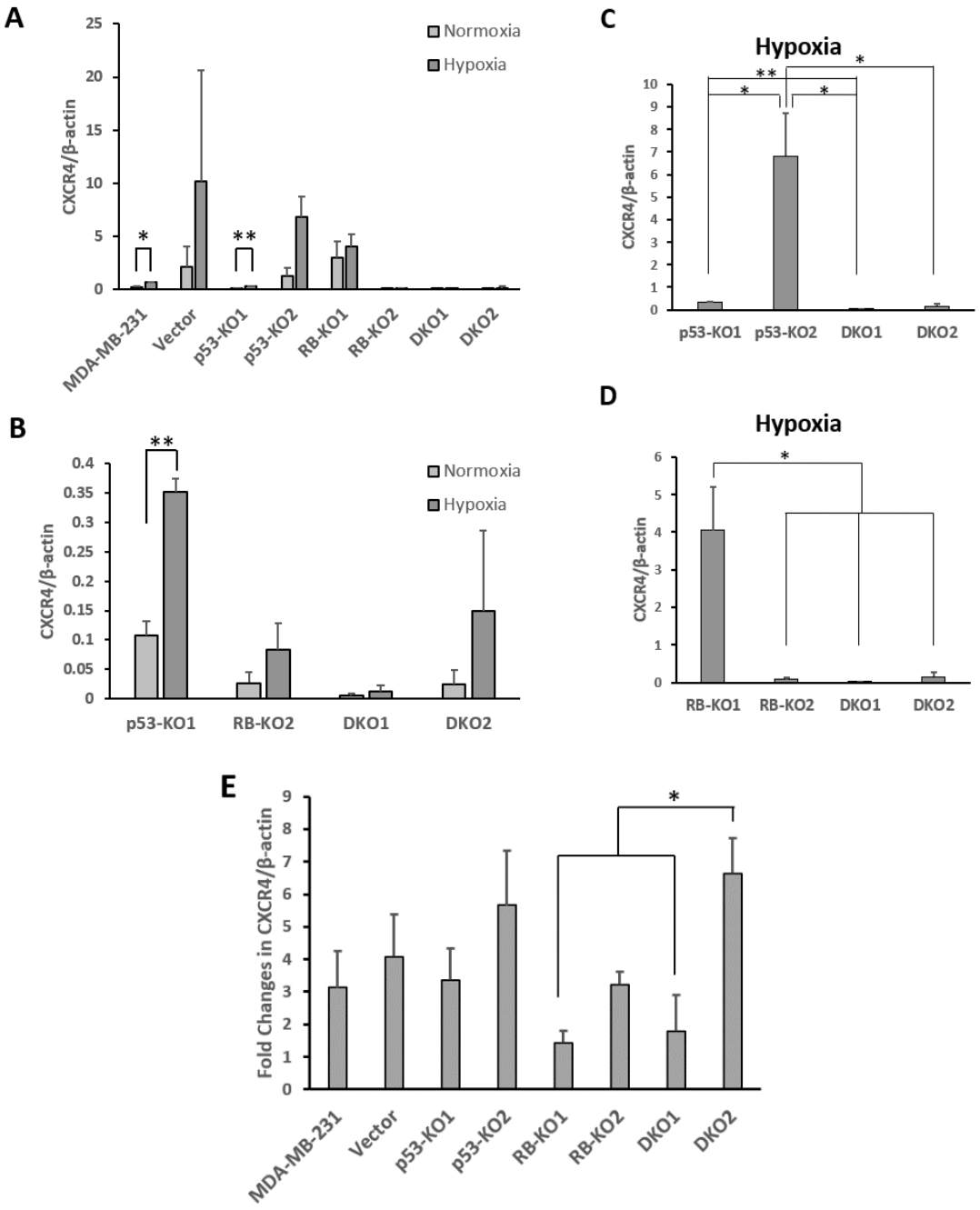

Figure 3.8. The expression of CXCR4 was influenced by TP53 and/or RB1 mutations both under normoxia and hypoxia.

Bar graphs plot relative *CXCR4* expression levels, normalized to *β-actin* expression, in each cell line under normoxia and hypoxia (**A**), with extremely low normalized expression values displayed in a separate, re-scaled bar graph, for readability (**B**). Statistical comparisons of each cell line to the vector as well as *CXCR4* expression level under normoxia vs. hypoxia of each cell line were analyzed. Direct comparisons between p53-KOs vs. DKOs (**C**), and RB-KOs vs. DKOs (**D**) under hypoxia were analyzed. Fold increase in gene expression from normoxia to hypoxia for each cell line, with statistical comparisons of each cell line to the vector, p53-KOs vs. DKOs, and RB-KOs vs. DKOs were also analyzed (**E**). Cells were cultured to ~ 85% confluency and incubated in a

humidified incubator at 37 °C, 5% CO_2, and either at 20% O_2 (normoxia) or 1% O_2 (hypoxia) for 24 h. Subsequently, RNA samples were extracted using TRI Reagent solution (Luminex). mRNA was reverse transcribed into cDNA and qPCR was set up using the PowerUp SYBR Green Master Mix (Applied Biosystems). *CXCR4* expression levels were normalized against the expression level of *β-actin*. Error bars represent standard deviation. Statistical analysis was performed using Student's T-test. *, ** indicate p-value < 0.05 and < 0.01, respectively.

PLOD2 expression profiles had some similarities with *CXCR4*, and some obvious distinctions, due to its different role in tumour growth and metastasis. The normalized *PLOD2* expression increased with a normoxia to hypoxia shift for all controls and KO lines; however, this increase was only statistically significant for DKO2 (from 0.17 to 0.60) (**Figure 3.9A**). Comparative data also produced no significant differences in expression levels under normoxia or hypoxia between any tested cell lines (**Figure 3.9A**). When fold increase in expression of *PLOD2* from normoxia to hypoxia was plotted, the only significant difference observed was p53-KO2 having a significant greater fold increase (5.62) compared to RB-KO1 (1.60) (**Figure 3.9B**). This data illustrates that hypoxia-inducible mechanisms enhanced by *TP53* and *RB1* double knockout in TNBC may not necessarily involve *PLOD2*. However, similar to the observation made for *CXCR4* expression, the vector control behaved differently from the parental control; thus, any observed changes are likely caused by the off-target effects from the transfection.

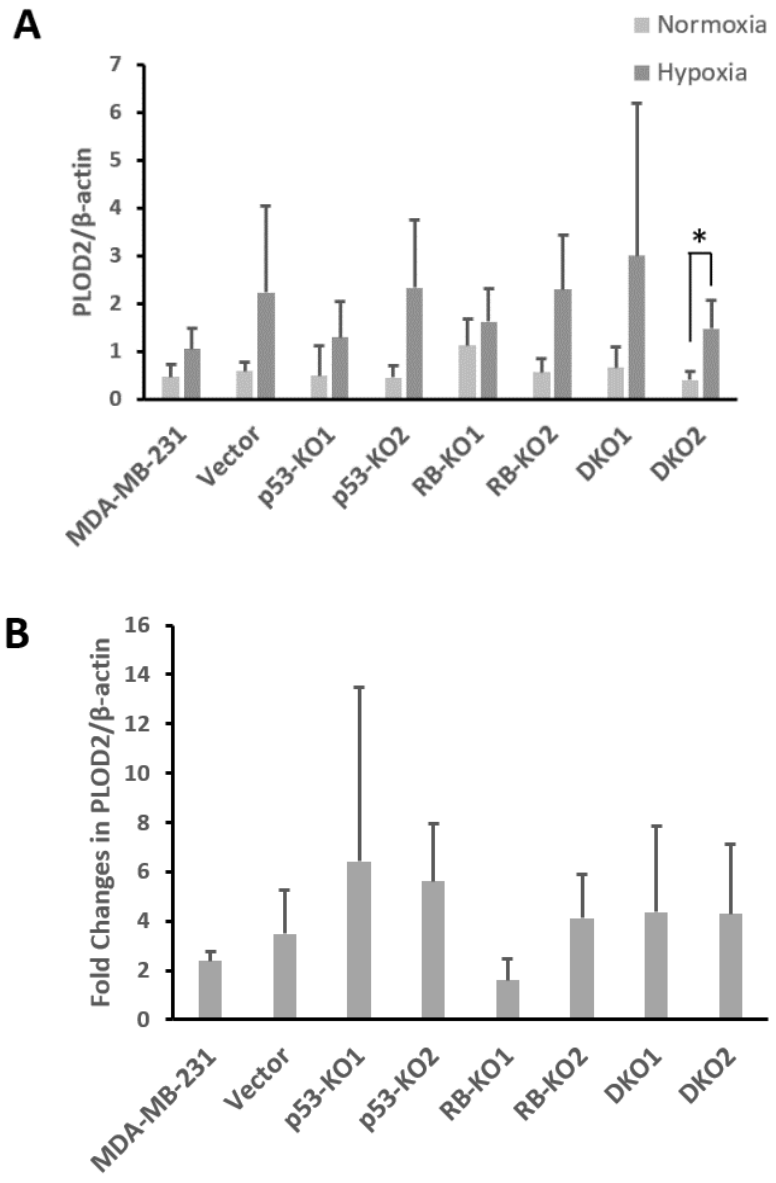

Figure 3.9. TP53 and/or RB1 mutations did not affect PLOD2 expression neither under normoxia nor hypoxia.

Bar graphs plot relative *PLOD2* expression levels, normalized to *β-actin* expression, in each cell line under normoxia and hypoxia (**A**). Statistical comparisons of each cell line to the vector as well as *PLOD2* expression level under normoxia vs. hypoxia of each cell line were analyzed. Fold increase in gene expression from normoxia to hypoxia for each cell line, with statistical comparisons of each cell line to the vector were also analyzed (**B**). Cells were cultured to ~ 85% confluency and incubated in a humidified incubator at 37 °C, 5% CO_2, and either at 20% O_2 (normoxia) or 1% O_2 (hypoxia) for 24 h. Subsequently, RNA samples were extracted using TRI Reagent solution (Luminex). mRNA was reverse transcribed into cDNA and qPCR was set up using the PowerUp SYBR Green Master Mix (Applied Biosystems). *PLOD2* expression levels were normalized against the expression level of *β-actin*. Error bars represent standard deviation. Statistical analysis was performed using Student's T-test. * indicates p-value < 0.05.

ANGPTL4-targeted qPCR expression data, again, suggested that the gene is hypoxia-inducible in MDA-MB-231 TNBC cells (**Figure 3.10A**). Under the circumstances of untransfected cells, the normalized expression increase was drastic, rising from 0.05 under normoxia to 0.99 under hypoxia. This pattern of drastic increases continued for all transfected cells, with statistical significance identified for DKO2 (from 0.03 to 0.50). Overall, the hypoxia-inducible expression of *ANGPTL4* was the most significant among the three genes evaluated by qPCR in this study. When comparing the normalized *ANGPTL4* expression between cell lines, no significant differences or patterns were observed, not under normoxia nor hypoxia.

Fold increase in *ANGPTL4* expression for cells under hypoxia vs. normoxia was also monitored and revealed some significant patterns (**Figure 3.10B-C**). Though the vector control exhibited an overall higher expression of *ANGPTL4*, both under normoxia and hypoxia, compared to the parental control, the fold increase did not differ. p53-KO2, RB-KO2, and DKO1 had a strong hypoxia-inducible effect on expression, with fold increases of 50.34, 73.79, and 52.70, respectively. These were all significantly greater than the fold increase of the vector control, at 20.99 (**Figure 3.10B**). Interestingly, the fold increase was measurably higher for DKO1 (52.70) compared to RB-KO1 (25.39) (**Figure 3.10C**), suggesting the possibility that double knockout of p53 and RB could enhance hypoxic inducible effects in some contexts.

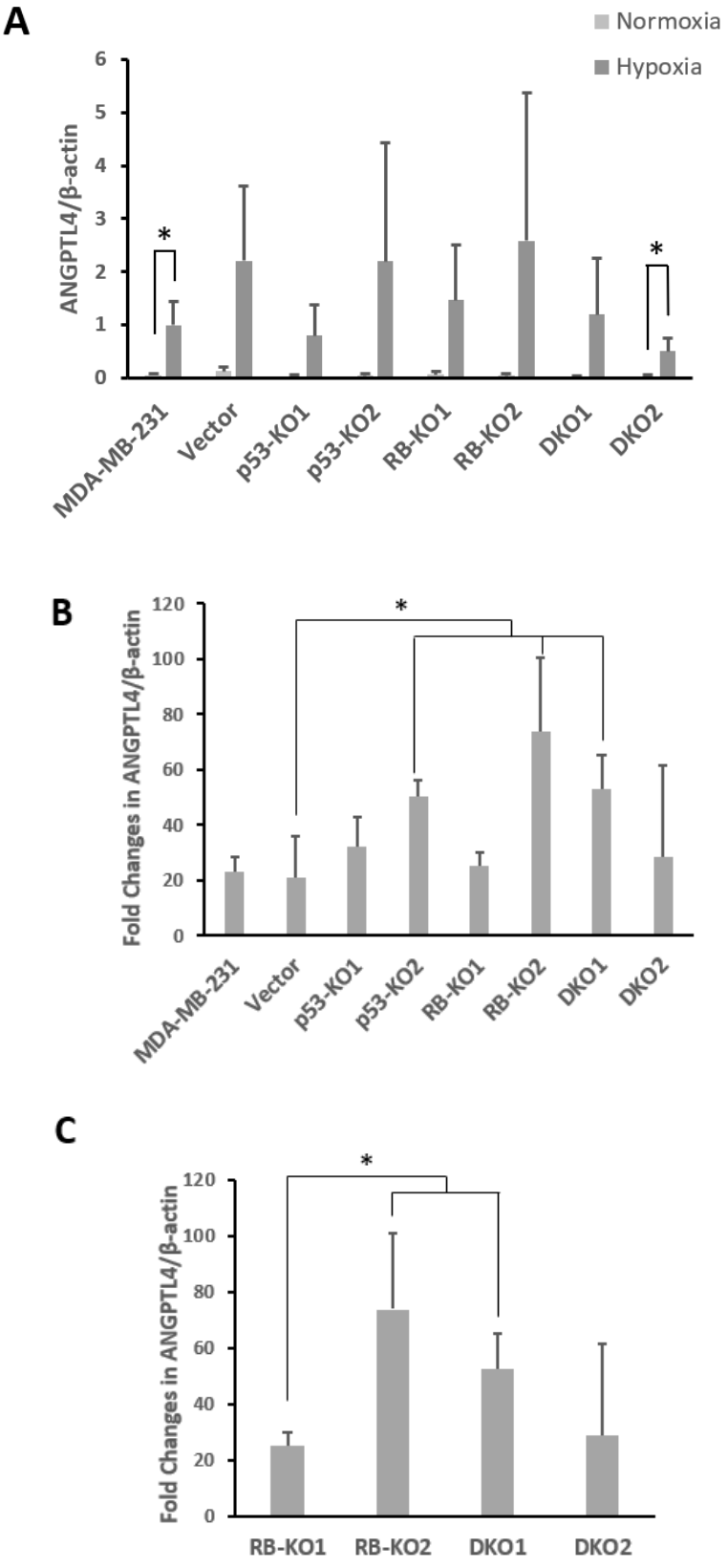
A
Normoxia
Hypoxia
ANGPTL4/β-actin
0
1
2
3
4
5
6
*
*
MDA-MB-231
Vector
p53-KO1
p53-KO2
RB-KO1
RB-KO2
DKO1
DKO2
B
Fold Changes in ANGPTL4/β-actin
0
20
40
60
80
100
120
*
MDA-MB-231
Vector
p53-KO1
p53-KO2
RB-KO1
RB-KO2
DKO1
DKO2
C
Fold Changes in ANGPTL4/β-actin
0
20
40
60
80
100
120
*
RB-KO1
RB-KO2
DKO1
DKO2

Figure 3.10. The expression of ANGPTL4 was influenced by TP53 and/or RB1 mutations both under normoxia and hypoxia.

Bar graphs plot relative *ANGPTL4* expression levels, normalized to *β-actin* expression, in each cell line under normoxia and hypoxia (**A**). Statistical comparisons of each cell line to the vector as well as *ANGPTL4* expression level under normoxia vs. hypoxia of each cell line were analyzed. Fold increase in gene expression from normoxia to hypoxia for each cell line, with statistical comparisons of each cell line to the vector were also analyzed (**B**), with a direct comparison between RB-KOs vs. DKOs presented in a separate graph (**C**). Cells were cultured to ~ 85% confluency and incubated in a humidified incubator at 37 °C, 5% CO_2, and either at 20% O_2 (normoxia) or 1% O_2 (hypoxia) for 24 h. Subsequently, RNA samples were extracted using TRI Reagent solution (Luminex). mRNA was reverse transcribed into cDNA and qPCR was set up using the PowerUp SYBR Green Master Mix (Applied Biosystems). *ANGPTL4* expression levels were normalized against the expression level of *β-actin*. Error bars represent standard deviation. Statistical analysis was performed using Student's T-test. *, ** indicate p-value < 0.05 and < 0.01, respectively.

Overall, the expression data presented here represented just a small snapshot of the complex hypoxia-inducible gene expression profile of TNBC tumour cells. The three representative genes chosen appear to act as hypoxia-inducible in the MDA-MB-231 cancer model. Their relationship to regulation by p53 and RB appears to be complex in this model, but no definite conclusions can be drawn as the vector control reveals that there is likely an off-target effect caused by the transfection process.

3.4. Neither hypoxic conditions nor knocking out *TP53* and *RB1* enhanced MDA-MB-231 cell migration ability

As previously discussed, mutations in both p53 and RB play a complex and multifaceted role in cancer cell metastasis. Enhanced migration ability of cells is an important hallmark of metastatic tumours. To measure the migratory properties of the p53-KOs, RB-KOs, and DKOs, I employed the Boyden Chamber assay, in which cells are seeded on top of a porous, semi-permeable membrane and the number of cells that traverse this membrane is quantified. A negative control for migration was set up for all cell lines tested, in which the media that cells can migrate into across the membrane does not contain the chemoattractant FBS. As expected, minimal to no cells were able to migrate in these control experiments, both under normoxia and hypoxia. The experimental assay, in which an increasing FBS gradient was presented to cells that could traverse the membrane, resulted in a drastic increase in the number of migrated cells across all control and knockout cell lines, for both normoxic and hypoxic conditions (**Figure 3.11**).

Despite relatively high counts, the number of migrated cells varied drastically between experiments. Each biological replicate was composed of 3 technical replicates and within each technical replicate, cells within 3 separate fields of view were counted and averaged. Migrated cell numbers remained very consistent between technical replicates, however, differences in counts between biological replicates were large. These discrepancies were as drastic as 3-fold for some cell lines. For example, the most radical difference between biological replicates occurred with DKO1 (**Figure 3.11A**). Under normoxia, biological replicate raw counts differed from 120 to 425 and under hypoxia they shifted from 58 to 385 (data not shown). As a result, there was no statistical significance observed when comparing the cell migration abilities between any KO clones used in the experiments. This was true under both normoxic and hypoxic conditions. When comparing the difference in migrated cell numbers between normoxia and hypoxia, for the same clone, I also observed no significant change for any control or knockout lines (**Figure 3.11A**). These results reveal a few possibilities: either the p53 and RB knockouts have little to no effect on the MDA-MB-231 tumour cell migration ability, the knockout effect is extremely sporadic and not fully captured in this limited data set, or uncontrollable error is not being accounted for between biological replicates.

To potentially eliminate any systematic error that may spontaneously occur between biological replicates, the fold change of migrated cell counts for cells under normoxia vs. hypoxia was calculated for individual biological replicates before averaging the replicates (**Figure 3.11B**). This change in cell migration ability under normoxia vs. hypoxia was observed for each control and knockout. There was still no significant difference in this change between cell lines. In a final attempt to eliminate potentially uncontrollable count fluctuation between biological replicates, the raw counts for all knockout lines were normalized to the vector control before averaging. This also did not reveal any significant patterns or changes in cell migration abilities between clones or between normoxia vs. hypoxia (**Figure 3.11C**). Ultimately, this data reveals that with these specific cell lines and under the specific conditions of this cell migration assay, there is no discernable change in cell migration with the knockout of p53, RB, or both, and hypoxic conditions do not introduce any changes to this cell migration ability.

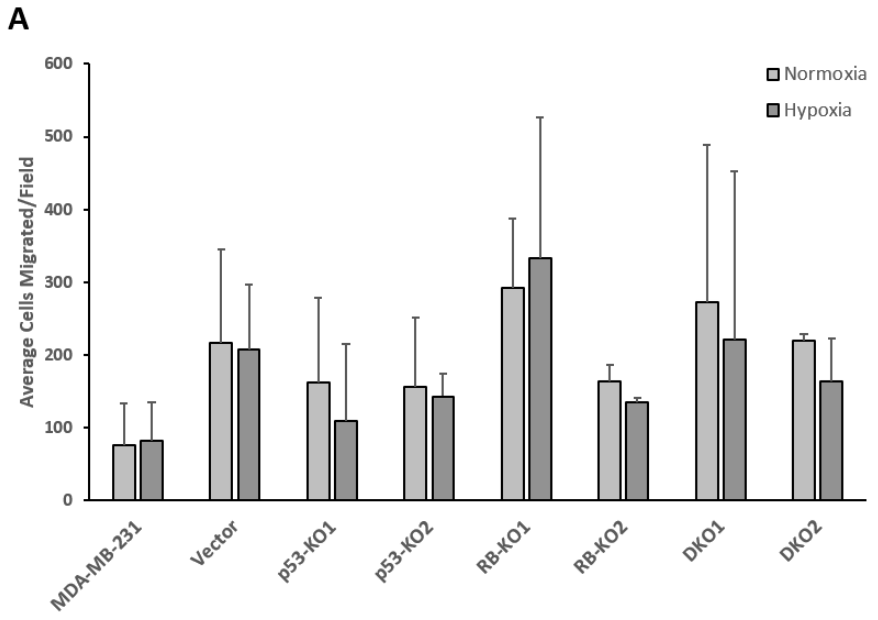
A
Normoxia
Hypoxia
Average Cells Migrated/Field
600
500
400
300
200
100
0
MDA-MB-231
Vector
p53-KO1
p53-KO2
RB-KO1
RB-KO2
DKO1
DKO2

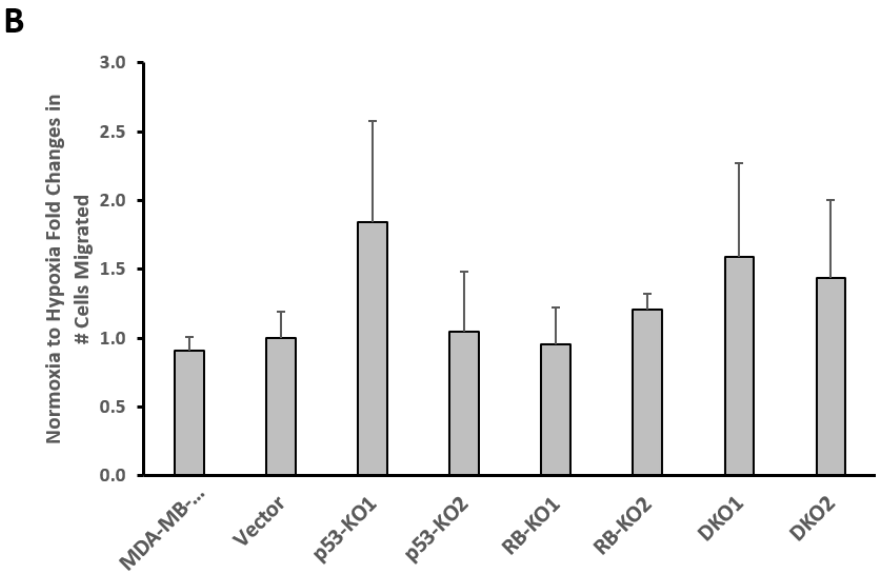
B
Normoxia to Hypoxia Fold Changes in # Cells Migrated
3.0
2.5
2.0
1.5
1.0
0.5
0.0
MDA-MB-...
Vector
p53-KO1
p53-KO2
RB-KO1
RB-KO2
DKO1
DKO2

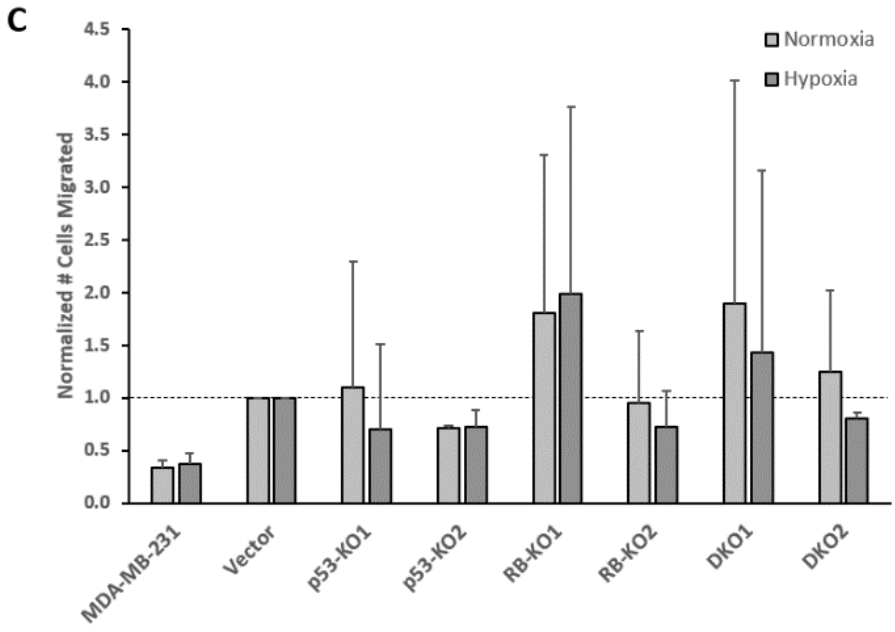

Figure 3.11. Mutations in TP53 and/or RB1 showed a minimal effect on MDA-MB-231 cell migration.

Bar graphs plot the average raw # of cells migrated per field viewed under 20x objective lens under normoxia and hypoxia for each cell line (**A**)**.** Fold change in the average # of cells migrated from normoxia to hypoxia of each cell line was analyzed (**B**). The average # of cells migrated for each cell line under normoxia and hypoxia were also normalized to the vector control (**C**). Cells were cultured in a serum starved media for 24 h. 4 x 10^4 cells were seeded onto 6.5 mm Tissue Culture Plate Inserts, Polyester (PET) Membrane, 8.0 µm pore size (VWR). The inserts were placed on top of the wells of 24-well tissue culture plates filled with either serum starved media (no FBS) or DMEM with 10% FBS. Cells were incubated in a humidified incubator at 37 °C, 5% CO_2, and either at 20% O_2 (normoxia) or 1% O_2 (hypoxia) for 24 h. Subsequently, cells were fixed with -20 °C methanol and stained with 0.4% toluidine blue. The stained/migrated cells were counted under a light microscope at a 20x objective magnification. Error bars represent standard deviation. Statistical analysis was performed using Student's T-test. There was no significant difference in cell migration when comparing each cell line to the vector.

Chapter 4.

Discussion

Specific treatments for TNBC remain underdeveloped as the underlying mechanisms that drive TNBC to progress more aggressively than other breast cancer subtypes are not fully understood. Here we generated an *in vitro* cell line model, double-knocking out *TP53* and *RB1*, to serve as a tool to study the metastasis-promoting mechanisms of two genes that are commonly mutated together in TNBC. The model was investigated for phenotypic consequences of single and double gene knockouts by a cell cycle assay, gene expression analysis, and a cell migration assay. The interpretation of these data is discussed below.

4.1. Generation of an *in vitro* model of double *TP53* and *RB1* mutated TNBC

In this investigation, we established p53 and RB DKO TNBC cell lines that express a non-detectable amount of full length p53 and RB proteins by immunoblot. However, the truncated forms of p53 and RB potentially remained expressed. One of the possible reasons why these truncated proteins are not detectable by immunoblot is the epitope of the antibodies used is likely located at the C-terminal region of the proteins, which would have not been expressed in the truncated forms, due to a frameshift mutation and potentially an introduction of a premature stop codon as a result of CRISPR-Cas9 gene editing. The truncated p53 and RB could also be thermodynamically unstable and become degraded immediately after expression. Furthermore, as multiple sgRNAs were designed to target multiple exons of p53 and RB, different truncated proteins in each KO cell line are likely expressed as in each cell, double-stranded break-induced DNA repair could introduce different frameshift mutations. Thus, the existence of distinct truncated p53 and RB should be considered when analyzing the data from the validation experiments, as these may contribute to the changes observed in KO cell lines.

Interestingly, despite designing all of the sgRNAs to target the conserved exons among all p53 isoforms, we observed striking differences in the knockout efficiency of

cells transfected with PX459-Neo incorporated with different sgRNAs (**Figure 3.1**). The cell pool transfected with sgRNA 3 showed very little decrease in p53 expression level compared to the untransfected cells; meanwhile, the cell pool transfected with sgRNA 4 showed a drastic decrease (**Figure 3.1**). One possible explanation for these variations in knockout efficiency could be that, although each sgRNA targets the same gene, accessibility to certain regions of the gene may be reduced through packaging of DNA as chromatin. For instance, sgRNA 3 may target a genomic region that is tightly wrapped around histones, reducing the accessibility for Cas9 to generate a DSB. Whereas, sgRNA 4 may target an area that is readily exposed to Cas9. Moreover, MDA-MB-231 cell line is an aggressive TNBC cell line which likely exhibits great genome instability, frequently introducing new mutations to various regions of the genome as the cell lines are passaged generation to generation. These mutations could alter the DNA sequences of the sgRNA-targeted regions, reducing the affinity for the sgRNA to the genome and thus, producing less efficient knockouts. Another possibility could be that errors were introduced during plasmid preparation, resulting in a disruption of the sgRNA sequence and preventing its interaction with the *TP53* target site. Sequencing the plasmids after sgRNA ligation could have been performed to avoid this possibility.

Intriguingly, a recent study by Clarke *et al*. showed that the gene knockout efficiency is highly dependent on the DNA strand that sgRNA targets[189]. If the sgRNA is designed to target the template strand of the genome DNA, which is the same strand uses by RNA polymerase machinery to perform DNA transcription, the knockout efficiency is drastically improved compared to sgRNA that targets the coding strand. This is because once the Cas9 enzyme introduces a DSB, it remains bound to the DNA, preventing access of DNA repair proteins to the repair site. However, RNA polymerase machinery that is translocating along the genome can dislodge Cas9 from the DSB DNA if the sgRNA targeted the template strand, thereby, allowing for DSB repair and enhancing efficiency of the genomic edit. In alignment with the observations by Clarke *et al*., sgRNA 4, which targeted the template strand of *TP53*, showed the highest knockout efficiency, compared to the other sgRNAs which targeted the coding strand (**Figure 3.1**). Hence, to maximize gene knockout efficiency, the targeted DNA strand should be taken into consideration when designing sgRNAs.

The targeted exon of the gene of interest may also influence knockout efficiency. Generally, sgRNAs should be designed to target the most upstream exons of a gene

structure, especially if they code for a functional domain of the protein. The purpose of this is to introduce an indel mutation early in the gene, which could potentially create a frameshift, and subsequently lead to the introduction of a premature stop codon. Consequently, the translated protein would be misfolded and/or non-functional. On the other hand, targeting exons that are situated further downstream in the gene structure will decrease the possibility of introducing a premature stop codon, as there will be fewer nucleotides remaining downstream of the targeted site. In agreement with this, the cell pool transfected with sgRNA 3, which targeted exon 7, exhibited the lowest *TP53* knockout efficiency, compared to the cell pools transfect with sgRNA 1, 2, and 4, which targeted exon 6, 5, and 5, respectively (**Figure 3.1**). Due to the low knockout efficiency, cells transfected with sgRNA 3 did not proceed to the single clone selection process.

Another factor to take into consideration when designing a gene knockout experiment is the method of genetic material delivery to target cells. While lipofection may be an efficient, cost-effective method to knockout a gene of interest, it can also cause cell cytotoxicity. An investigation by Nguyen *et al*. revealed an increase in apoptotic induction after cells were lipotransfected[190]. Within this study, microarray experiments also showed an upregulation of apoptosis-related genes in the lipo-transfected cells. During single clone selection, it was observed that cells transfected with sgRNA 1 proliferated much slower than the cells transfected with sgRNA 2 or sgRNA 4. Differences in proliferation rates could be due to the potential genomic instability of the MDA-MB-231 cell line. This instability may cause certain cell pools to be more prone to cytotoxicity than others. Therefore, it is plausible that the clone transfected with sgRNA 1 had acquired genomic variations that enhanced its susceptibility to lipofection-induced cytotoxicity. As a result, the single clones selected to proceed to validation were either from cells transfected with sgRNA 2 or sgRNA 4 (**Figure 3.2**).

Not only can lipofection-induced cytotoxicity reduce knockout efficiency, changes in gene expression levels as a result of lipofection can interfere with the observation of potential changes in cell genotypes and/or phenotypes cause by a gene knockout. Therefore, multiple knockout clones should be validated to identify which changes are a direct effect of the gene knockout. Alternatively, another non-cytotoxicity-inducing method to deliver genetic materials into cells for gene knockout, such as lentiviral transduction, could be employed. For this method, cells are ‘infected’ by lentivirus

packaged with genetic material encoding Cas9 and sgRNA targeting a gene of interest[191]. However, as the genetic material transduced by lentivirus can be integrated into the host cell genome, there is potential for disruption of gene sequences in the integrated site, causing further genomic instability. Maintenance and preparation of effective lentivirus systems may also require specialized expertise and may not be as cost-effective. All in all, each transfection method has its own advantages and disadvantages, and an appropriate method to perform gene knockout should be selected according to the needs and expertise of the researchers.

During knockout experiments in typical diploid eukaryotic cells, partial gene knockout may occur, as the cells contain two copies of each gene. However, the MDA-MB-231 cell line was derived from a tumour of a breast cancer patient with a chromosomal count of nearly triploid. Specifically, MDA-MB-231 contains four copies *TP53* and two copies of *RB1*[192], making it increasingly difficult to completely knockout the expression of p53. This is a potential reason as to why some clones, such as clone 1-2, 2-3, and 4-7, showed a partial reduction of p53 protein expression (**Figure 3.2A**) and why generating a knockdown with undetectable p53 levels was relatively difficult in these experiments.

Although the expression of the main isoform of p53 was not detectable by an immunoblot in successful knockout clones, a band at ~42 kDa was rather prominent in all the clones (**Figure 3.2**). This band could represent two distinct possibilities: the presence of another p53 isoform resistant to the sgRNA knockout or non-specific binding of the antibody to an unknown target. A possible approach to determine if such a band represents an isoform of the target protein vs. a non-specific interaction could involve immunoblotting with an antibody that targets a different epitope of the same protein. If a different p53 antibody still generated the same band as the initial antibody, the interaction is very likely a true, specific antibody-antigen interaction. However, if no band is generated, then the initial antibody likely forms a strong, non-specific interaction with another protein, and the knockout of p53 is complete. However, it is also possible that the p53 isoform may not contain a specific epitope recognized by the new p53 antibody. To circumvent this, polyclonal p53 antibodies, targeting multiple p53 epitopes, could be used for validation.

A number of studies have found expression of p53 isoforms, particularly the Δ40p53 isoform, in breast cancer patients and cell lines[193,194]. This isoform lacks the first 39 amino acids, which encode the transactivation domain (TAD) 1, caused by various alternative splicing events[195]. The molecular weight of this isoform is 42 kDa, making it a strong suspect candidate as the protein that represents the prominent band in the knockout clone blots. Strengthening this prediction is evidence that, besides the full length p53, the Δ40p53 isoform is the most commonly expressed isoform in breast cancer[194]. Furthermore, the high expression of Δ40p53 is most prominent in TNBC cells[194]. However, while other antibody-reacting p53 isoforms potentially present in the parental MDA-MB-231 cells were knocked out, the 42 kDa remained prominent in all of the clones (**Figure 3.2**). Additionally, the exons targeted by all sgRNAs in these experiments were within the protein coding region of all isoforms, including Δ40p53, eliminating the possibility that the isoform could evade knockout by the exclusion of the genomic changes induced by the sgRNA-targeted mutation. This suggests that the unidentified 42 kDa band is likely a non-specific interaction by the antibody. Nonetheless, until a definite answer is achieved, the potential of persistent Δ40p53 expression in the clones used in the subsequent experiments should be considered during data interpretation.

The specific role of Δ40p53 in promoting breast cancer progression and metastasis is currently unclear. However, Δ40p53 expression level is elevated in breast cancer cell lines, compared to normal breast epithelial cell lines[194]. Moreover, a high expression of Δ40p53 relative to the full length p53 is associated with a decrease in metastatic-free survival rate[196]. These observations suggest a possibility of Δ40p53 involvement in breast cancer metastasis; thereby, the results obtained from the subsequent experiments could potentially be influenced by the presence of Δ40p53.

Interestingly, clone 4-3 also shows a band at ~35 kDa (**Figure 3.2**). Unlike the 42 kDa band, this band only appeared in one clone; thus, it is likely not due to a non-specific binding event. Although this is still a possibility, as the high genomic instability of the cell lines could result in genomic re-arrangements or mutations that create a novel, non-specific binding partner for the antibody that is not present in any other single colony clone. But more likely, it represents a p53 isoform, Δ133p53. This isoform lacks the first 133 amino acids, which encode TAD 1 and 2[195]. In contrast to the generation of Δ40p53, Δ133p53 is produced by the initiation of transcription at an internal promoter of the *TP53*

gene[195]. Despite sgRNA 4 targeting exon 5, located downstream of this promoter, Δ133p53 remained expressed. A possible explanation for this could be that only partial knockout of this isoform was achieved, due to the presence of multiple copies of the gene. Interestingly, expression of full length p53 by clone 4-3 was not detectable (**Figure 3.2**). It is possible that an off-target effect introduced by the transfection process may have enhanced the internal promoter activity to express Δ133p53, specifically. Currently, little is known about this p53 isoform; though, Δ133p53 has been found to be an antagonist to full length p53, preventing full length p53-mediated apoptosis as well as G1/S cell cycle arrest[194]. Resistance to apoptosis is one of the main features of cancer. Hence, the relationship between Δ133p53 and cancer may be worth investigating. However, for the following cell line validation experiments, clone 4-3 was not pursued, as the potentially unknown effects of the isoform on cell line characteristics would over-complicate data interpretation and could mask the effects of gene knockouts.

Though the 42 kDa protein band in all of the clones and the 35 kDa protein band shown in clone 4-3 could represent Δ40p53 and Δ133p53 isoforms, respectively, it is likely not the case. As discussed previously, these KO clones could potentially express the truncated forms of p53; however, those were not detectable by immunoblot, indicating the epitope recognized by the p53 antibody used is likely located at the C-terminal end of p53. Both Δ40p53 and Δ133p53 isoforms are missing domains from the N-terminal but also express 10 missense mutations within the C-terminal domains[195]. Hence, the p53 antibody used likely does not have the affinity specifically for these mutations, suggesting that the 42 kDa and 35 kDa bands represent non-specific binding of the p53 antibody.

Overall, the *TP53* and *RB1* DKO clones 2-2 (DKO1) and 4-6 (DKO2), along with p53-KOs and RB-KOs, were selected (**Figure 3.3**) for further clone validation as well as investigation of the potential TNBC metastatic promoting ability *in vitro* of double mutated *TP53* and *RB1* cells. Clones 2-2 and 4-6 were two among several clones that appear to show non-detectable levels of full length p53 expression (**Figure 3.2B**). The RB expression status of these clones also remained non-detectable, assuring *RB1* was stably knocked out (**Figure 3.2B**). An advantage of selecting two clones that were targeted by different sgRNAs is that if the results from the two clones are identical, the changes observed from the validation experiments, compared to the vector control, are likely due to the gene KO. However, as discussed previously, the potential of different

truncated forms of p53 being expressed in these two clones could also lead to variation the outcome. Thus, selecting two clones targeted by the same sgRNA could possibly eliminate this variation.

As lipofection may alter gene expression and potentially causes other off-target effects, the data obtained from these KO clones were compared to the vector control cells to eliminate the effects that may have resulted from the lipofection. It is also worth noting that MDA-MB-231 cells express a mutated form of p53, specifically R280K p53, and not the WT[185]. This mutation occurs in the DNA binding domain of p53[47], altering residue 280 arginine to lysine, both positively charged amino acids. Thus, the comparisons between cell lines were made based on the p53 and RB status shown in **Table 4.1**.

Table 4.1. p53 and RB status of cell lines used in the experiment

Cell line	p53 status	RB status
Parental	R280K	WT
Vector Control	R280K	WT
p53-KOs	KO	WT
RB-KOs	R280K	KO
DKOs	KO	KO

Note: KO = knocked out, WT = wildtype

4.2. Mutations in *TP53* and *RB1* promote TNBC cell growth and survival

p53 and RB are key cell cycle regulators, specifically known to induce G1/S cell cycle arrest. Cell cycle assays aimed to validate the KO cell lines by monitoring the cell cycle phase distribution of each KO clone. WT p53 induces G1/S arrest by activating p21 expression, which promotes RB expression[39]. Phosphorylated RB then binds to E2F, preventing E2F gene transcription activity and subsequently the progression of the cell cycle to the S phase[91,92]. Interestingly, a number of studies have indicated that R280K p53 decreases G1/S arrest[47,197]. Specifically, the R280K point mutation introduces a conformational change in p53, altering its p21 promoter binding site[47]. As a result, the downstream G1/S arrest cascade is disrupted. Supporting this, Bae *et. al* showed that knocking down R280K p53 increased G1 phase cell population but decreased S phase population, indicating G1/S arrest[197]. In alignment with this, p53-KO1

showed a significant reduction of S phase cell population, compared to the vector control, supporting the hypothesis that R280K p53 suppresses G1/S arrest (**Figure 3.5A**). Conversely, when RB function was already lost, knocking out R280K p53 decreased G1 cell population (RB-KOs vs. DKOs, **Figure 3.5C**), further reducing G1/S arrest. While evidence suggested that R280K p53 suppresses G1/S arrest, which can be rescued by knocking out R280K p53, the absence of RB, instead, prevented the rescue and further reduced G1/S arrest. This suggested that there could be another WT p53 induced-molecular pathway responsible for cell cycle arrest; this WT p53 function however may not be compromised by the R280K mutation. Therefore, knocking out R280K p53 could decrease G1/S arrest through the suppression of this alternate pathway.

Though it has not been studied recently, p53 has been found to regulate G2/M arrest by inhibiting Cdk2, a kinase required for cells to enter mitosis[198]. However, the relationship between R280K p53 and G2/M arrest is currently unknown. Interestingly, p53-KO1, DKO1, and DKO2 showed a significant increase in G2/M cell population, relative to the vector control (**Figure 3.5A**). The accumulation of cells in the G2 phase indicates G2/M arrest potentially caused by knocking out R280K p53. Similarly, in the absence of RB, knocking out R280K p53 increased G2/M phase cell distribution (RB-KOs vs DKOs, **Figure 3.5C**) Thus, besides suppressing G1/S arrest, R280K p53 could potentially relegate tumour suppressor function of WT p53 by suppressing G2/M arrest, independently of RB. Consequently, TNBC tumours with a R280K mutant p53 could potentially exhibit over proliferation through uncontrolled regulation of the G2/M checkpoint, and therapeutic intervention to regain control of this checkpoint could be considered for these patients.

In contrast, RB-KOs did not show any significant changes to any of the cell phase populations, compared to the vector control (**Figure 3.5A**). This could be because RB regulates cell cycle arrest downstream of p53. Inhibition of p21 expression by R280K p53 may have already diminished RB function in inducing cell cycle arrest. However, in the absence of both the WT and R280K p53, knocking out *RB1* showed an increase in cell population in the S phase as well as a decrease in cell population in the G2/M phase (p53-KO1 vs. DKO1, **Figure 3.5B**), which are indications of a decrease in G1/S arrest and G2/M arrest, respectively. The observation suggests a possibility that other molecular pathway(s) independent of p53 could activate RB, allowing it to retain the

tumour suppressor function of inducing cell cycle arrest. Contradictory to this finding, DKOs showed an increase in G2/M cell population compared to p53-KO2 (**Figure 3.5B**), indicating an induction of G2/M arrest when *RB1* is knocked out. Notably, the cell distribution in both S and G2/M phases are significantly different among p53-KO1 and p53-KO2, implying these two clones do not behave identically. The genomic instability of the cancer cells or off-target effects from lipofection may have interfered with the phenotypes. For that reason, examining more clones can strengthen the data by identifying the shared characteristics among different clones and eliminating any outliers.

Hypoxia is a low oxygen microenvironment that is common in solid tumours such as breast adenocarcinomas[121]. Under hypoxic conditions, HIFs form a complex and induce cell cycle arrest via the upregulation of p21 expression[199]. Thus, we explored how the mutation status of p53 and RB may influence cell cycle arrest under hypoxia. As RB is involved in G1/S cell cycle arrest by being the downstream target of p21, I predicted that the loss of RB function would decrease G1/S arrest under hypoxia. Surprisingly, compared to normoxic conditions, RB-KO2, DKO1, and DKO2 showed a significant decrease in the S phase cell population under hypoxia (**Figure 3.7**), indicating an increase in G1/S arrest. RB has a non-canonical role of negatively regulating HIFs-mediated gene transcription; therefore, loss of RB function will lead to an exaggeration of HIFs-mediated gene transcription[118]. Thus, it is possible that the loss of RB could have promoted the expression of HIFs-mediated genes which are involved in pathway(s) responsible for inducing G1/S arrest.

In contrast to RB, there are currently no known relationship between p53 and cell cycle arrest that is regulated by hypoxia. I observed that under hypoxia, p53-KO1 showed an increase in G2 cell population compared to the vector control, indicating G2/M arrest (**Figure 3.6A**). This was similar to the observation made under normoxia, in which knocking out R280K p53 restored G2/M arrest, suggesting hypoxia did not alter R280K p53 function in inhibiting G2/M arrest. However, the loss of RB together with the loss of R280K p53 significantly increased G2/M cell population under hypoxia (DKO2 vs. every other clones except for p53-KO1, **Figure 3.6A-C**). The elevated G2/M arrest of DKO2 could be the result of the combined effect of the loss of R280K p53, releasing G2/M arrest inhibition, as well as the loss of RB, promoting overexpression of HIFs-mediate genes involved in cell cycle arrest. Typically, one major characteristic of cancer is aberrant proliferation. Conversely, under hypoxia where oxygen and glucose supplies

are limited, it would be strategic for cancer cells to reprogram to conserve the limited resources and focus on increasing access to these resources through mechanisms such as angiogenesis. Thus, it is deemed to be more beneficial for cancer cells to undergo cell cycle arrest under hypoxia, which could explain the observations made from the cell cycle experiments. Patients with p53-negative and RB-negative TNBC tumours, for instance, may have HIFs playing an enhanced role in tumour survival through cell cycle regulation, thus hinting at yet another set of strong candidates for therapeutic intervention.

Through the cell cycle assay, I displayed the importance of p53 and RB in regulating the cell cycle in TNBC and how the mutations of these proteins may disrupt this regulation. Under normoxia, R280K p53 suppresses cell cycle arrest, while RB induces the arrest in the absence of R280K p53. However, when both R280K p53 and RB are knocked out, the suppression of cell cycle arrest becomes more prominent, promoting tumour cell proliferation. On the other hand, loss of RB, especially when accompanied by the loss of R280K p53, increases cell cycle arrest under hypoxia. This could allow tumour cells to conserve the limited resources required for cell growth, promoting tumour cell survival under hypoxia. Overall, mutations in *TP53* and *RB1* enhance tumour cell growth and survival under various circumstances. Nonetheless, the data strongly suggests that multiple pathways, both dependent and independent of p53 or RB, regulate cell cycle checkpoints. These alternate pathways are worth investigating as they could ultimately rescue cell cycle arrest functions when p53/RB pathways are disrupted. More importantly, members of these pathways could serve as potential therapeutic targets in p53 and RB negative tumours. To strengthen the predictions derived from these results, other assays including cell proliferation and apoptosis assays should also be incorporated. This would give a more complete outlook of the cell survival and proliferation profile of TNBC cells in the context of p53 and RB mutation in TNBC.

4.3. p53 and RB mutations exert little to no effect on *CXCR4*, *PLOD2*, and *ANGPTL4* expression

Existing data suggest that mutations in *TP53* and/or *RB1* enhance expression of metastasis-promoting genes. Thus, monitoring the expression of genes known to be regulated by p53 or RB under normoxia and/or hypoxia was performed as another approach to validate the generated *TP53* and *RB1* DKO *in vitro* model. In this

investigation, gene expression level of *CXCR4*, *PLOD2*, and *ANGPTL4* were explored, as evidence suggests they also acquire the ability to promote tumour metastasis in some breast cancers.

Up-regulation of *CXCR4* assists cell migration, specifically by enhancing the chemoattractant-responding ability of tumour cells. As an aspect of its tumour suppressor function, WT p53 was previously found to repress CXCR4 expression, while the mutant R280K p53 promoted the expression[200]. In alignment with this, I showed that the absence of R280K p53 in p53-KOs and DKOs decreased CXCR4 expression level under both normoxia and hypoxia (**Figure 3.8A**). On the other hand, the loss of RB function in hypoxia was previously found to up-regulate CXCR4 expression[118]; thus I would expect RB-KOs to show an increase in CXCR4 expression level, especially under hypoxia. Contradictory to the existing data in literature, I observed a reduction of CXCR4 levels in RB-KOs under hypoxia (**Figure 3.8A**). Interestingly, a study by Nobutani *et al*. revealed a down-regulation of CXCR4 in metastasized breast cancer cells[201]. Flow cytometry analysis showed a significant decrease in cell surface expression of CXCR4 in lung metastasized tumour cells, compared to the primary tumour cells. They also observed that the metastasized tumour cells entered a dormant state, which is a mechanism utilized by tumour cells to protect against immune attack[202]. There is a possibility that knocking out *TP53* and *RB1* promote tumour aggressive traits which mimic the characteristics of metastasized tumour cells. Hence, all of the KO clones, especially the DKOs, consistently showed a substantial decrease in CXCR4 expression (**Figure 3.8A-D**).

Similarly, high expression of PLOD2 has been previously proven to facilitate tumour metastasis by promoting ECM re-modelling[129,130]. The loss of RB in hypoxia was shown to exaggerate PLOD2 expression under hypoxia[118]. However, in this investigation, neither knocking out p53 nor RB altered the PLOD2 expression level in normoxia or hypoxia (**Figure 3.9**); though, there is currently no known relationship between p53 and PLOD2 expression. Nonetheless, it is important to highlight that an increase in PLOD2 expression under hypoxia, accompanied by the loss of RB, was demonstrated in MCF-7 cell line[118]. MCF-7 is a breast cancer cell line, categorized as subtype luminal A[203], which is much less aggressive than TNBC. This indicates that the expression level of PLOD2 could be at its maximum potential in an aggressive TNBC

cell line like MDA-MB-231, thereby, masking the effects mutated *TP53* and *RB1* may have on increasing the expression level of PLOD2.

Metastasis of TNBC, specifically to the lungs and brain, is enhanced by an overexpression of ANGPTL4, which assists tumour cells in extravasation[132,133]. Similarly to PLOD2, ANGPTL4 expression levels have previously been shown to dramatically increase under hypoxia when accompanied by the loss of RB[151], but a relationship between ANGPTL4 and p53 expression remains undetermined. Knocking out *TP53* and/or *RB1* from MDA-MB-231, however, did not alter the expression levels of ANGPTL4, neither under normoxia nor hypoxia (**Figure 3.10**). The unexpected lack of change in expression levels of ANGPTL4 may be explained through reasoning similar to the PLOD2 expression data. The previously demonstrated increase in ANGPTL4 expression due to the loss of RB under hypoxia occurred in the LNCaP cell line, which represents early-stage prostate cancer cells[204]; whereas, MDA-MB-231 represents an aggressive breast cancer subtype which may already express high levels of ANGPTL4, regardless of RB status.

Overall, the expression data suggested mutations in *TP53* and *RB1* exert little to no effect on the expression of PLOD2 and ANGPTL4. Knocking out p53 and RB may have shown a decrease in CXCR4 expression, but a clear pattern was not established. One possible explanation for this lack of clarity could involve the high discrepancies of the results between each replicate, which may have stochastically influenced the overall gene expression patterns. Nonetheless, the fold increase analysis, in which the gene expression values in hypoxia are normalized to their corresponding normoxia value, revealed that *CXCR4*, *PLOD2*, and *ANGPTL4* genes remain hypoxia-inducible, despite p53 and/or RB knockout. In most cases, p53-KOs, RB-KOs, and DKOs showed a substantial fold increase in gene expression, compared to the vector control, indicating that mutation in *TP53* and *RB1* could better promote tumour cell survival under hypoxia. As p53 and RB can promote metastasis through various molecular pathways, it is possible that *PLOD2* and *ANGTPL4* are not their target genes in TNBC. Thus, an analysis that fully encapsulates the gene expression of the entire genome, such as RNA-sequencing analysis, could unveil the specific pathways that are influenced by p53 and RB mutations in TNBC.

4.4. TNBC cell migration was not affected by mutations in *TP53* or *RB1*

Collective evidence from existing literature suggests a high potential for concomitant *TP53* and *RB1* mutations to drive TNBC metastasis, supporting each step of the process from leaving the primary tumour to colonizing at a secondary site. Particularly, mutations in these genes have been shown to enhance EMT[68,113], ECM re-arrangement[86,146,147], as well as the expression of chemoreceptors and chemokines[118,200]. All of these are crucial processes for effective cell migration through tissue. Furthermore, by negatively mediating a master regulator of metastasis, HIF1α, RB attenuates the expression of hypoxia-inducible metastasis-promoting genes[118]. Thereby, the loss of RB enhances cancer metastasis under hypoxia[118]. As such, it is important to validate the generated *TP53* and *RB1* DKO *in vitro* model by observing metastatic phenotypes of the cell model both under normoxia and hypoxia.

A major factor that influences cell migratory properties is the ability of cells to respond to chemical stimuli, called chemoattractants. This mechanism is especially commonly utilized by immune cells to communicate and elicit immune responses[205]. In this investigation, cell migration in response to an increasing gradient of chemoattractant was monitored, with FBS acting as the chemoattractant. I predicted that cells would not migrate when the chemoattractant gradient was absent. Indeed, none of the clones migrated to the other side of the membrane of the insert when FBS was absent from the bottom chamber, but they all responded to the chemotactic signal and migrated towards to the bottom chamber when FBS was present (**Figure 3.11A**). This suggests that *TP53* and *RB* mutations in TNBC cells do not hinder the ability of the cells to utilize chemotactic signaling as a method of tumour cell migration and metastasis.

One mechanism by which mutations in both *TP53* and *RB1* promote cell migration is through enhancing the expression of CXCR4, a chemokine receptor that responds to specific chemoattractants. WT p53 represses CXCR4 expression, while R280K p53 rescues the expression[200]. Likewise, through mediating hypoxia-inducible gene transcription, RB downregulates CXCR4 expression, but the expression is exaggerated when RB function is lost[118]. Overexpression of CXCR4 has been previously shown to induce migration under hypoxia in MCF-7 cells[118]. However, in the MDA-MB-231 cell lines utilized in these experiments, knocking out p53 and RB did not enhance

migration under hypoxia (nor normoxia) (**Figure 3.11A**). Considering that CXCR4 expression was also not promoted in the knockouts, this result is less surprising. It is of note that the previously mentioned experiments with MCF-7 cells utilized a different migration assay than the assay presented here. Those experiments utilized a Matrigel-based migration assay, which includes membranes containing components that mimic the ECM for the cells to migrate through[118]. This assay provides a better measure of a tumour cells ability to migrate in tissues, compared to the migration assay used here, which is simply a measure of cell ability to respond to chemoattractants. Perhaps mutation of p53 and/or RB allow breast cancer cells to navigate the ECM more effectively through molecular re-arrangement of ECM components, and these effects were not captured in the migration assay. Moreover, a trans-endothelial migration assay, in which a monolayer of ECs is coated on the membrane to better mimic the tumour microenvironment, performed by Jin *et. al* showed that MDA-MB-231 cells were able to migrate in a hypoxia-inducible manner[128]. It is important to note that the chemoattractant used in the experiment was CXCL12, which is the CXCR4 ligand. Hence, the ability of mutation in *TP53* and *RB1* to enhance TNBC cell migration may be hindered by the absence of the specific chemokine ligand to CXCR4. Overall, testing the cell lines developed here against a migration assay that takes into account the components of the ECM, ECs, and the specific molecular interactions involved in chemotactic signalling of tumour cells could provide useful insight into the roles of p53 and RB in TNBC migration and metastasis.

4.5. Future Directions

Despite CRISPR-Cas9 being chosen as the method to knockout *TP53* and *RB1*, alternative methods, such as siRNA and shRNA, could also be utilized, each of which provide their own advantages and disadvantages. CRISPR-Cas9 knocks out genes of interest at the genomic level and can stabilize the knockout[183]. This will likely prevent the re-expression of the genes of interest during experimentation. On the other hand, siRNA and shRNA suppress protein expression at the RNA level[180]. These two methods only transiently knock down target proteins and the protein of interest may be re-expressed. However, to observe an immediate effect of a loss of protein expression, siRNA and shRNA would be more suitable approaches as they are not time consuming to generate a knockdown. Whereas CRISPR-Cas9 requires several passages of cell line to establish

a knockout. During experimentation, any changes observed from the KO cell lines compared to the control could potentially be the result of the genomic changes caused by cell passaging or the adaptation of the cells to the knockout, rather than an immediate effect by the knockout.

Though the *TP53* and *RB1* DKO *in vitro* model generated here revealed some insights into how mutations of these genes influence TNBC cell growth and survival, invasion-promoting gene expression levels, as well as tumour cell migration, there remained indisputable limitations that may have hindered clear interpretation of some data. First, cancer cell lines such as MDA-MB-231 harbour significant levels of genomic instability. As an unintended and unavoidable consequence of this, when cell cultures are split and propagated in isolation, any new genomic changes that occur in the following generations can manifest as genotypic and phenotypic variations. Specifically, vector control, p53 KOs, and RB KOs are approximately 6-7 passages higher than the parental control and the DKOs are approximately 16-17 passages higher than the parental control. This can interfere with the ability to make direct comparisons between cell lines as the changes observed in the KO cell lines could potentially be caused by genomic changes from cell passaging. Additionally, the potential off-target effects from lipofection, as well as the expression of various truncated p53 and RB may also contribute to the discrepancies in the genotypes and phenotypes of the cell lines. As shown in the statistical analysis of gene expression and migration assay data, lack of reproducibility was unfortunately a common theme. A possible approach to mitigate this could involve re-pooling knockout clones after single clone selection before proceeding to validation. This would provide a cell line that is genetically representative of several different clonal lines, which would eliminate the genotypic variations between single colony clones of the same knockout.

Undeniably, the choice of the parental cell line for this investigation represents non-negotiable caveats, though the options were limited. MDA-MB-231 is categorized as a mesenchymal TNBC subtype, which represents a late-stage cancer[25]. This could be beneficial, as it provides the opportunity to study how late-stage cancer cells behave differently from early-stage cancer cells and which molecular pathways are involved in promoting aggressive phenotypes. However, using a highly aggressive TNBC model could mask the effects that *TP53* and *RB1* mutations may typically have on the ability of tumour cells to promote metastasis, as there are potentially many more genetic

variations at play that may already be driving cancer phenotypes. Moreover, MDA-MB-231 has an existing p53 mutation which eliminates comparison of the results to a WT p53 model. Validation experiments with a cell line model expressing WT p53 could help determine whether R280K p53 behaves more similarly to p53 KO, which represents a loss of function mutation, or whether it acts as a gain of function mutation. Hence, choosing a parental line that represents an early-stage cancer and expresses WT p53 could be beneficial to gain a better understanding of how p53 and RB knockout specifically and directly influences tumour progression and metastasis.

Unfortunately, most existing TNBC cell lines likely represent late-stage cancers already, as TNBC typically exhibits an early aggressive trait. Moreover, TNBC also often expresses a mutant form of p53. One approach to circumvent the lack of WT p53 is to exogenously express WT p53 in the p53-KO cell lines. Using this approach, p53 constructs with specific mutations generated by site-directed mutagenesis could also be introduced into breast cancer cell line models. Therefore, mutational hotspots that are found in the TNBC patient population, but not in commonly used cell line models, can be studied. This approach would allow for a more personalized characterization of breast cancers, possibly assisting the development of specific treatments depending on p53 mutation.

To obtain a better grasp on specifically which molecular pathways are up- or down-regulated by the mutated *TP53* and *RB1*, RNA-sequencing analysis could be performed on the models generated. Similar to qPCR, RNA from the cell lines would be extracted to perform the analysis. But instead of monitoring the expression of a few genes of interest, mRNA transcription levels of the entire genome could be determined. Comparative large-scale analysis of the full transcriptome between different knockout cell lines could pinpoint if members of any specific metastasis-promoting pathways or mechanisms are consistently upregulated in p53- and/or RB-negative TNBC. This could highlight potential molecular candidates for therapeutic intervention. Besides mRNA analysis, total RNA-sequencing analysis could also give an insight into the regulation of non-coding RNA in TNBC. Though they do not code for proteins, non-coding RNA, such as micro RNAs, play important roles in regulating protein expression and can contribute to cancer progression. It is crucial to consider that the parental MDA-MB-231 cell lines also have mutations in other genes which could influence the expression status of genes of interest. Hence, generating the DKO models in different parental TNBC cell lines and

perform RNA-sequencing analysis to compare analysis between cell lines with differing genetic backgrounds could provide more complete insight into which pathways are affected by mutated p53 and RB.

Once the generated *in vitro* model developed in this investigation is fully validated, that is, the vector control behaves similarly to the parental control and the data generated is reproducible in multiple validation experiments, the cell line will become a powerful tool that can be used to study TNBC metastasis in various ways. To start, the cells could be co-cultured with other molecules or cell types to gain information on how the model interacts with components of a typical tumour microenvironment, and not just in the isolated system of a petri dish with media. For instance, to better represent the physical barriers for cell migration, ECM proteins can be coated on top of the membrane in the transwell migration assay, monitoring the ability of cells to remodel ECM. Culturing the cell line with ECs could be helpful for exploring the extravasation ability of the cell line, observing for endothelial cell-cell contact disruption. Finally, co-culturing the cell line with immune cells could provide insights into whether mutations in *TP53* and *RB1* protect cells from CTL-induced cell lysis, a mechanism utilized by tumour cells to survive in the circulatory system during metastasis. The co-culturing experiments suggested above could act as a first step towards understanding the mechanisms involved in the different phases of metastasis in TNBC, before costly and time-consuming *in vivo* experiments are utilized.

In vitro experiments do not accurately represent the molecular microenvironment that tumour cells typically experience. Besides hypoxia, which is also considered an aspect of the tumour microenvironment, many proteins, such as ECM, or other cells, such as stromal cells and immune cells are also components of the tumour microenvironment[206]. Thus, any data obtained from *in vitro* experiments may not be directly applicable to cancer cells in the context of the human body. An *in vivo* study, on the other hand, can utilize animal models, which provide a much more accurate mimic of the complex network of interactions involving cells and other factors occurring inside the tissues of a cancer patient. To transform our *in vitro* cell line model into an *in vivo* model, the cell lines could be orthotopically transplanted into mice to establish a mouse xenograft. Phenotypic effects, such as metastasis of the tumour cells to a secondary site, could then be observed and compared between cell knockout lines. Moreover, the metastasized cells could be harvested to perform RNA-sequencing analysis as well, as

the more accurate tumour microenvironment may influence the transcriptome through new mechanisms induced by factors in the microenvironment that were not captured by *in vitro* experiments. This could again reveal crucial information, pinpointing which molecular pathways may have a heavy impact on cancer metastasis in the context of p53 and RB mutations.

Besides exploring the underlying mechanisms on how mutations in *TP53* and *RB1* could promote the most aggressive form of TNBC, it is critical to search for potential therapeutic targets for TNBC expressing these mutations, as there is still a lack of specific, non-toxic induced treatments for TNBC patients. As mammalian cell networks are incredibly complex, we need a screening method which will cover the entire genome rather than focusing on specific pathways. An emerging new technique which researchers are using to identify therapeutic targets for cancer is known as synthetic lethality screening. Synthetic lethality occurs when a perturbation of two or more genes leads to cell death but deficiencies in any one of those genes alone result in viable cells[207]. Since cancer cells have known underlying mutations, synthetically lethal gene partners to these pre-existing mutated genes could be considered candidate therapeutic targets. Healthy cells would not be killed by targeting these candidates, as they do not possess the underlying, cancer-associated mutations.

A synthetic lethality screen can be performed using a combination of CRISPR-Cas9 techniques by transfecting cancer cell lines with lentivirus containing genomic library plasmids to target a wide array of different genes independently[208,209]. At least two cell pools, with and without the underlying mutation of interest, would need to be transfected. Lethal targets could then be identified by deep sequencing of the plasmids in the live cells, using next-generation sequencing technology. A comparison of the gene profile would be performed between the wild-type cell pool and the mutated cell pool. The genes which are present in the wild-type pool (indicating cell viable) but are missing from the mutated cell pool (indicating cell death) would be considered as potential synthetic lethal candidates.

Computational methods can also be used to identify synthetic lethal targets. DAISY (Data mining synthetic lethality identification pipeline) identifies synthetic lethal pairs by screening for gene pairs which fall into three specific categories[210]. DAISY combines data from both clinical samples and cancer cell lines. The first category is

known as ‘genomic survival of the fittest’ which identifies genes that are co-inactivated and eliminated early within the cell population. This is because if the genes are a synthetic lethal pair, inactivation of both will result in cell death. The identification of gene pairs can be done by analyzing somatic copy number alteration and somatic mutation data. Genes which appear to be less co-inactivated will be selected. The second category entails gene pairs which when one of the genes from a pair is under-expressed, the other gene’s activity increases. This can be identified by a shRNA screen in combination with transcriptome analysis. The third category is genes which are co-expressed, as genes in a synthetic lethal gene pair often have similar biological functions. A gene pair which falls into all three categories would be identified by the program as a synthetic lethal pair. These candidate pairs could then be transitioned to *in vitro* experiments to determine if they act as synthetically lethal in the context of tumour cells.

Overall, a synthetic lethal screen could bring us closer to identifying potential therapeutic targets for TNBC. For instance, possible candidates could be p107 or p130 which function similarly to RB in regulating cell cycle arrest but are not commonly mutated in cancers[104,105]. Targeting these identified genes would not be toxic to the healthy cells as the synthetic lethality screen would only screen for targets which, when inhibited in *TP53* and *RB1* mutated cells specifically, result in cell death. These synthetic lethality screens provide a powerful tool that could complement well the cell line models developed in this investigation. This would move us towards the end goal of this research, the development of more specific therapeutics to improve TNBC patient outcomes.

4.6. Conclusion

TNBC presents patients with several clinical challenges and poor prognoses, derived from a complete lack of effective targeted therapies. Generalized treatments such as radiotherapy and chemotherapy have inherent drawbacks, especially for patients with secondary metastases, as the introduced toxicities do not selectively target cancer cells, resulting in damage to healthy cells and tissues. The molecular characteristics of TNBC specifically, compared to other types of breast cancer, make treatment development more difficult as common approaches, like hormonal therapy, are not effective. Therefore, the search for TNBC targeted therapies that do not induce

toxicities in healthy cells remains at the forefront of TNBC research. To facilitate the search for therapeutic targets, we have developed an *in vitro* model that expresses mutations in *TP53* and *RB1*, genes than are commonly mutated together in TNBC. Mutations in the two well-known tumour suppressors, *TP53* and *RB1*, have proven to play major roles in numerous mechanisms that drive the steps of TNBC metastasis. Mutant p53 abolishes many of its WT tumor-suppressor functions that keeps cell proliferation in check. As demonstrated in this study, loss of p53 function in TNBC promotes tumour proliferation and survival. Similarly, loss of function RB causes cells to lose the ability to control cell cycle progression but promotes cell survival under hypoxia when p53 function is also lost. With such a complex network of cancer-related molecular mechanisms that involve both *TP53* and *RB1*, there is substantial evidence that mutations in these genes may work together to enhance breast cancer metastasis. Studies have linked the mechanisms altered by either *TP53* or *RB1* mutation to all steps of metastatic cancer development, including EMT, blood vessel intravasation, angiogenesis, and colonization at secondary sites. However, the effect of mutated *TP53* and *RB1*, together, on promoting TNBC metastasis has yet to be investigated. Due to limitations in our experiments, *TP53* and *RB1* did not alter metastasis-promoting gene expression or cell migration, contradictory to previous findings. Though once modifications to our current model have been implemented, as suggested above, the model could serve as a useful tool to explore the metastasis promoting ability of concomitantly mutated *TP53* and *RB1* in TNBC. More importantly, as there are no current specific treatments for TNBC, our model could be utilized for therapeutic development. An approach such as genome-wide synthetic lethality screen using *TP53*- and *RB1*-mutated TNBC cancer cells could identify potential targets, perhaps some of which have been discussed in this thesis.

References

1. Metastatic Cancer: When Cancer Spreads. *NIH: National Cancer Institute* https://www.cancer.gov/types/metastatic-cancer (2020).

2. Canadian Cancer Society. Cancer-Specific Stats 2022. (2022).

3. Sung, H. *et al.* Global Cancer Statistics 2020: GLOBOCAN Estimates of Incidence and Mortality Worldwide for 36 Cancers in 185 Countries. *CA. Cancer J. Clin.* **71**, 209–249 (2021).

4. Weigelt, B., Geyer, F. C. & Reis-Filho, J. S. Histological types of breast cancer: How special are they? *Mol. Oncol.* **4**, 192–208 (2010).

5. Krecke, K. N. & Gisvold, J. J. Invasive lobular carcinoma of the breast: mammographic findings and extent of disease at diagnosis in 184 patients. *Am. J. Roentgenol.* **161**, 957–960 (1993).

6. Wasif, N., Maggard, M. A., Ko, C. Y. & Giuliano, A. E. Invasive Lobular vs. Ductal Breast Cancer: A Stage-Matched Comparison of Outcomes. *Ann. Surg. Oncol.* **17**, 1862–1869 (2010).

7. Pike, M. C., Spicer, D. V., Dahmoush, L. & Press, M. F. Estrogens, Progestogens, Normal Breast Cell Proliferation, and Breast Cancer Risk. *Epidemiol. Rev.* **15**, 17–30 (1993).

8. Xu, R. *et al.* Amplification of Her-2/neu Gene in Her-2/neu-Overexpressing and -Nonexpressing Breast Carcinomas and Their Synchronous Benign, Premalignant, and Metastatic Lesions Detected by FISH in Archival Material. *Mod. Pathol.* **15**, 116–124 (2002).

9. Allred, D. C. & Mohsin, S. K. Biological Features of Premalignant Disease in the Human Breast. *J. Mammary Gland Biol. Neoplasia* 14 (2001).

10. Rubin, I. & Yarden, Y. The basic biology of HER2. *Ann. Oncol.* **12**, S3–S8 (2001).

11. Voduc, K. D. *et al.* Breast Cancer Subtypes and the Risk of Local and Regional Relapse. *J. Clin. Oncol.* **28**, 1684–1691 (2010).

12. Cheang, M. C. U. *et al.* Ki67 Index, HER2 Status, and Prognosis of Patients With Luminal B Breast Cancer. *JNCI J. Natl. Cancer Inst.* **101**, 736–750 (2009).

13. Inic, Z. *et al.* Difference between Luminal A and Luminal B Subtypes According to Ki-67, Tumor Size, and Progesterone Receptor Negativity Providing Prognostic Information. *Clin. Med. Insights Oncol.* **8**, CMO.S18006 (2014).

14. Desmedt, C. *et al.* Genomic Characterization of Primary Invasive Lobular Breast Cancer. *J. Clin. Oncol.* **34**, 1872–1881 (2016).

15. Loibl, S. & Gianni, L. HER2-positive breast cancer. *The Lancet* **389**, 2415–2429 (2017).

16. Incorvati, J. A., Shah, S., Mu, Y. & Lu, J. Targeted therapy for HER2 positive breast cancer. *J. Hematol. Oncol.J Hematol Oncol* **6**, 38 (2013).

17. Kennecke, H. *et al.* Metastatic Behavior of Breast Cancer Subtypes. *J. Clin. Oncol.* **28**, 3271–3277 (2010).

18. Anders, C. K. & Carey, L. A. Biology, Metastatic Patterns, and Treatment of Patients with Triple-Negative Breast Cancer. *Clin. Breast Cancer* **9**, S73–S81 (2009).

19. Foulkes, W. D. & Reis-Filho, J. S. Triple-Negative Breast Cancer. *N Engl J Med* 11 (2010).

20. Pommier, R. M. *et al.* Comprehensive characterization of claudin-low breast tumors reflects the impact of the cell-of-origin on cancer evolution. *Nat. Commun.* **11**, 3431 (2020).

21. De Laurentiis, M. *et al.* Treatment of triple negative breast cancer (TNBC): current options and future perspectives. *Cancer Treat. Rev.* **36**, S80–S86 (2010).

22. Dent, R. *et al.* Triple-Negative Breast Cancer: Clinical Features and Patterns of Recurrence. *Clin. Cancer Res.* **13**, 4429–4434 (2007).

23. Brian D Lehmann & Jennifer A Pietenpol. Identification and use of biomarkers in treatment strategies for triple-negative breast cancer subtypes. *J. Pathol.* **232**, 142–150 (2014).

24. Badve, S. *et al.* Basal-like and triple-negative breast cancers: a critical review with an emphasis on the implications for pathologists and oncologists. *Mod. Pathol.* **24**, 157–167 (2011).

25. Lehmann, B. D. *et al.* Identification of human triple-negative breast cancer subtypes and preclinical models for selection of targeted therapies. *J. Clin. Invest.* **121**, 2750–2767 (2011).

26. Gerratana, L. *et al.* Androgen receptor in triple negative breast cancer: A potential target for the targetless subtype. *Cancer Treat. Rev.* **68**, 102–110 (2018).

27. Engebraaten, O., Vollan, H. K. M. & Børresen-Dale, A.-L. Triple-Negative Breast Cancer and the Need for New Therapeutic Targets. *Am. J. Pathol.* **183**, 1064–1074 (2013).

28. Craig, D. W. *et al.* Genome and Transcriptome Sequencing in Prospective Metastatic Triple-Negative Breast Cancer Uncovers Therapeutic Vulnerabilities. *Mol. Cancer Ther.* **12**, 104–116 (2013).

29. Jones, R. A. *et al.* RB1 deficiency in triple-negative breast cancer induces mitochondrial protein translation. *J. Clin. Invest.* **126**, 19 (2016).

30. Harris, C. C. Structure and Function of the p53 Tumor Suppressor Gene: Clues for Rational Cancer Therapeutic Strategies. *JNCI J. Natl. Cancer Inst.* **88**, 1442–1455 (1996).

31. Harbour, J. W. & Dean, D. C. Rb function in cell-cycle regulation and apoptosis. *Nat. Cell Biol.* **2**, E65–E67 (2000).

32. Shah, S. P. *et al.* The clonal and mutational evolution spectrum of primary triple-negative breast cancers. *Nature* **486**, 395–399 (2012).

33. Perou, C. M. Molecular Stratification of Triple-Negative Breast Cancers. *The Oncologist* **15**, 39–48 (2010).

34. Fernandez, S. V. *et al.* TP53 mutations detected in circulating tumor cells present in the blood of metastatic triple negative breast cancer patients. *Breast Cancer Res.* **16**, 445 (2014).

35. Madic, J. *et al.* Circulating tumor DNA and circulating tumor cells in metastatic triple negative breast cancer patients: ctDNA and CTC in Metastatic Triple Negative Breast Cancer. *Int. J. Cancer* **136**, 2158–2165 (2015).

36. Lo Nigro, C. *et al.* High frequency of complex TP53 mutations in CNS metastases from breast cancer. *Br. J. Cancer* **106**, 397–404 (2012).

37. Bingham, C. *et al.* Mutational studies on single circulating tumor cells isolated from the blood of inflammatory breast cancer patients. *Breast Cancer Res. Treat.* **163**, 219–230 (2017).

38. Shieh, S.-Y., Ikeda, M., Taya, Y. & Prives, C. DNA Damage-Induced Phosphorylation of p53 Alleviates Inhibition by MDM2. *Cell* **91**, 325–334 (1997).

39. Xiong, Y. *et al.* p21 is a universal inhibitor of cyclin kinases. *Nature* **366**, 701–704 (1993).

40. Smith, M. *et al.* Interaction of the p53-regulated protein Gadd45 with proliferating cell nuclear antigen. *Science* **266**, 1376–1380 (1994).

41. Sengupta, S. & Harris, C. C. p53: traffic cop at the crossroads of DNA repair and recombination. *Nat. Rev. Mol. Cell Biol.* **6**, 44–55 (2005).

42. Toshiyuki, M. & Reed, J. C. Tumor suppressor p53 is a direct transcriptional activator of the human bax gene. *Cell* **80**, 293–299 (1995).

43. Honda, R., Tanaka, H. & Yasuda, H. Oncoprotein MDM2 is a ubiquitin ligase E3 for tumor suppressor p53. *FEBS Lett.* **420**, 25–27 (1997).

44. McCann, A. *et al.* Amplification of the MDM2 gene in human breast cancer and its association with MDM2 and p53 protein status. *Br. J. Cancer* **71**, 981–985 (1995).

45. David Malkin *et al.* Germline Mutations of the p53 Tumor-Suppressor Gene in Children and Young Adults with Second Malignant Neoplasms. *N. Engl. J. Med.* **326**, 1309–1315 (1992).

46. Hollstein, M., Sidransky, D., Vogelstein, B. & Harris, C. p53 mutations in human cancers. *Science* **253**, 49–53 (1991).

47. Emamzadah, S., Tropia, L. & Halazonetis, T. D. Crystal Structure of a Multidomain Human p53 Tetramer Bound to the Natural CDKN1A (p21) p53-Response Element. *Mol. Cancer Res.* **9**, 1493–1499 (2011).

48. Olivier, M. The Clinical Value of Somatic TP53 Gene Mutations in 1,794 Patients with Breast Cancer. *Clin. Cancer Res.* **12**, 1157–1167 (2006).

49. Olivier, M. *et al.* The IARC TP53 database: New online mutation analysis and recommendations to users. *Hum. Mutat.* **19**, 607–614 (2002).

50. Joerger, A. C., Ang, H. C. & Fersht, A. R. Structural basis for understanding oncogenic p53 mutations and designing rescue drugs. *Proc. Natl. Acad. Sci.* **103**, 15056–15061 (2006).

51. D. P. Lane & L. V. Crawford. T antigen is bound to a host protein in SY40-transformed cells. *Nature* **278**, 261–263 (1979).

52. Linzer, D. I. H. & Levine, A. J. Characterization of a 54K Dalton cellular SV40 tumor antigen present in SV40-transformed cells and uninfected embryonal carcinoma cells. *Cell* **17**, 43–52 (1979).

53. Zakut-Houri, R., Bienz-Tadmor, B., Givol, D. & Oren, M. Human p53 cellular tumor antigen: cDNA sequence and expression in COS cells. *EMBO J.* **4**, 1251–1255 (1985).

54. Wolf, D., Harris, N. & Rotter, V. Reconstitution of p53 Expression in a Nonproducer Ab-MuLV-Transformed Cell Line by Transfection of a Functional p53 Gene. *Cell* **38**, 119–126 (1984).

55. Eliyahu, D., Michalovitz, D. & Oren, M. Overproduction of p53 antigen makes established cells highly tumorigenic. *Nature* **316**, 158–160 (1985).

56. Jenkins, J. R., Rudge, K. & Currie, G. A. Cellular immortalization by a eDNA clone encoding the transformation- associated phosphoprotein p53. 651–654 (1984).

57. Cook, A. & Milner, J. Evidence for allosteric variants of wild-type p53, a tumour suppressor protein. *Br. J. Cancer* **61**, 548–552 (1990).

58. Mowat, M., Cheng, A., Kimura, N., Bernstein, A. & Benchimol, S. Rearrangements of the cellular p53 gene in erythroleukaemic cells transformed by Friend virus. *Nature* **314**, 633–636 (1985).

59. Chow, V., Ben-David, Y., Bernstein, A., Benchimol, S. & Mowat, M. Multistage Friend erythroleukemia: independent origin of tumor clones with normal or rearranged p53 cellular oncogenes. *J. Virol.* **61**, 2777–2781 (1987).

60. Eliyahu, D., Michalovitz, D., Eliyahu, S., Pinhasi-Kimhi, O. & Oren, M. Wild-type p53 can inhibit oncogene-mediated focus formation. *Proc. Natl. Acad. Sci.* **86**, 8763–8767 (1989).

61. Finlay, C. A. & Levine, J. The p53 Proto-Oncogene Can Act as a Suppressor of Transformation. *Cell* **57**, 1083–1093 (1989).

62. Chicas, A., Molina, P. & Bargonetti, J. Mutant p53 Forms a Complex with Sp1 on HIV-LTR DNA. *Biochem. Biophys. Res. Commun.* **279**, 383–390 (2000).

63. Sampath, J. *et al.* Mutant p53 Cooperates with ETS and Selectively Up-regulates Human MDR1 Not MRP1. *J. Biol. Chem.* **276**, 39359–39367 (2001).

64. Do, P. M. *et al.* Mutant p53 cooperates with ETS2 to promote etoposide resistance. *Genes Dev.* **26**, 830–845 (2012).

65. Stambolsky, P. *et al.* Modulation of the Vitamin D3 Response by Cancer-Associated Mutant p53. *Cancer Cell* **17**, 273–285 (2010).

66. Masciarelli, S. *et al.* Gain-of-function mutant p53 downregulates miR-223 contributing to chemoresistance of cultured tumor cells. *Oncogene* **33**, 1601–1608 (2014).

67. Piovan, C. *et al.* Oncosuppressive role of p53-induced miR-205 in triple negative breast cancer. *Mol. Oncol.* **6**, 458–472 (2012).

68. Dong, P. *et al.* Mutant p53 gain-of-function induces epithelial–mesenchymal transition through modulation of the miR-130b–ZEB1 axis. *Oncogene* **32**, 3286–3295 (2013).

69. Wang, W., Cheng, B., Miao, L., Mei, Y. & Wu, M. Mutant p53-R273H gains new function in sustained activation of EGFR signaling via suppressing miR-27a expression. *Cell Death Dis.* **4**, e574–e574 (2013).

70. Li, G. *et al.* miRNA-223 upregulated by MYOD inhibits myoblast proliferation by repressing IGF2 and facilitates myoblast differentiation by inhibiting ZEB1. *Cell Death Dis.* **8**, e3094–e3094 (2017).

71. Greene, S. B., Herschkowitz, J. I. & Rosen, J. M. The ups and downs of miR-205: Identifying the roles of miR-205 in mammary gland development and breast cancer. *RNA Biol.* **7**, 300–304 (2010).

72. Gregory, P. A. *et al.* The miR-200 family and miR-205 regulate epithelial to mesenchymal transition by targeting ZEB1 and SIP1. *Nat. Cell Biol.* **10**, 593–601 (2008).

73. Lamouille, S., Xu, J. & Derynck, R. Molecular mechanisms of epithelial–mesenchymal transition. *Nat. Rev. Mol. Cell Biol.* **15**, 178–196 (2014).

74. Milner, J. & Medcalf, E. A. Cotranslation of Activated Mutant p53 with Wild Type Drives the Wild-Type p53 Protein into the Mutant Conformation. *Cell* **65**, 765–774 (1991).

75. Rong-Zong Liu *et al.* NFIB promotes cell survival by directly suppressing p21 transcription in TP53-mutated triple-negative breast cancer. *J. Pathol.* **247**, 186–198 (2019).

76. Semenova, E. A. *et al.* Transcription Factor NFIB Is a Driver of Small Cell Lung Cancer Progression in Mice and Marks Metastatic Disease in Patients. *Cell Rep.* **16**, 631–643 (2016).

77. Karnoub, A. E. *et al.* Mesenchymal stem cells within tumour stroma promote breast cancer metastasis. *Nature* **449**, 557–563 (2007).

78. Annie Yang *et al.* Relationships between p63 Binding, DNA Sequence, Transcription Activity, and Biological Function in Human Cells. *Mol. Cell* **24**, 593–602 (2006).

79. Ihrie, R. A. *et al.* Perp Is a p63-Regulated Gene Essential for Epithelial Integrity. *Cell* **120**, 843–856 (2005).

80. Adorno, M. *et al.* A Mutant-p53/Smad Complex Opposes p63 to Empower TGFβ-Induced Metastasis. *Cell* **137**, 87–98 (2009).

81. Girardini, J. E. *et al.* A Pin1/Mutant p53 Axis Promotes Aggressiveness in Breast Cancer. *Cancer Cell* **20**, 79–91 (2011).

82. Yeudall, W. A. *et al.* Gain-of-function mutant p53 upregulates CXC chemokines and enhances cell migration. *Carcinogenesis* **33**, 442–451 (2012).

83. Heidemann, J. *et al.* Angiogenic Effects of Interleukin 8 (CXCL8) in Human Intestinal Microvascular Endothelial Cells Are Mediated by CXCR2. *J. Biol. Chem.* **278**, 8508–8515 (2003).

84. Brown, M. J. *et al.* Chemokine stimulation of human peripheral blood T lymphocytes induces rapid dephosphorylation of ERM proteins, which facilitates loss of microvilli and polarization. *Blood* **102**, 3890–3899 (2003).

85. Linderholm, B. K. *et al.* The Expression of Vascular Endothelial Growth Factor Correlates with Mutant p53 and Poor Prognosis in Human Breast Cancer. *Cancer Res.* **61**, 2256–2260 (2001).

86. Muller, P. A. J. *et al.* Mutant p53 Drives Invasion by Promoting Integrin Recycling. *Cell* **139**, 1327–1341 (2009).

87. Kalluri, R. & Weinberg, R. A. The basics of epithelial-mesenchymal transition. *J. Clin. Invest.* **119**, 1420–1428 (2009).

88. Dowdy, S. F. *et al.* Physical interaction of the retinoblastoma protein with human D cyclins. *Cell* **73**, 499–511 (1993).

89. Helin, K., Harlow, E. & Fattaey, A. Inhibition of E2F-1 transactivation by direct binding of the retinoblastoma protein. *Mol. Cell. Biol.* **13**, 6501–6508 (1993).

90. Flemington, E. K., Speck, S. H. & Kaelin, W. G. E2F-1-mediated transactivation is inhibited by complex formation with the retinoblastoma susceptibility gene product. *Proc. Natl. Acad. Sci.* **90**, 6914–6918 (1993).

91. Giacinti, C. & Giordano, A. RB and cell cycle progression. *Oncogene* **25**, 5220–5227 (2006).

92. Weinberg, R. A. The retinoblastoma protein and cell cycle control. *Cell* **81**, 323–330 (1995).

93. Brehm, A. *et al.* Retinoblastoma protein recruits histone deacetylase to repress transcription. *Nature* **391**, 597–601 (1998).

94. Trouche, D., Le Chalony, C., Muchardt, C., Yaniv, M. & Kouzarides, T. RB and hbrm cooperate to repress the activation functions of E2F1. *Proc. Natl. Acad. Sci.* **94**, 11268–11273 (1997).

95. Jancewicz, I., Siedlecki, J. A., Sarnowski, T. J. & Sarnowska, E. BRM: the core ATPase subunit of SWI/SNF chromatin-remodelling complex—a tumour suppressor or tumour-promoting factor? *Epigenetics Chromatin* **12**, 68–85 (2019).

96. Belchis, D. A. *et al.* Loss of Heterozygosity and Microsatellite Instability at the Retinoblastoma Locus in Osteosarcomas: *Diagn. Mol. Pathol.* **5**, 214–219 (1996).

97. Niederst, M. J. *et al.* RB loss in resistant EGFR mutant lung adenocarcinomas that transform to small-cell lung cancer. *Nat. Commun.* **6**, 6377 (2015).

98. Sharma, A. *et al.* The retinoblastoma tumor suppressor controls androgen signaling and human prostate cancer progression. *J. Clin. Invest.* **120**, 4478–4492 (2010).

99. Ertel, A. *et al.* RB-pathway disruption in breast cancer: Differential association with disease subtypes, disease-specific prognosis and therapeutic response. *Cell Cycle* **9**, 4153–4163 (2010).

100. Knudson, A. G. Mutation and Cancer: Statistical Study of Retinoblastoma. *Proc. Natl. Acad. Sci.* **68**, 820–823 (1971).

101. Moynahan, M. E. & Jasin, M. Loss of heterozygosity induced by a chromosomal double-strand break. *Proc. Natl. Acad. Sci.* **94**, 8988–8993 (1997).

102. Chapman, J. R., Taylor, M. R. G. & Boulton, S. J. Playing the End Game: DNA Double-Strand Break Repair Pathway Choice. *Mol. Cell* **47**, 497–510 (2012).

103. Herschkowitz, J. I., He, X., Fan, C. & Perou, C. M. The functional loss of the retinoblastoma tumour suppressor is a common event in basal-like and luminal B breast carcinomas. *Breast Cancer Res.* **10**, (2008).

104. Graña, X., Garriga, J. & Mayol, X. Role of the retinoblastoma protein family, pRB, p107 and p130 in the negative control of cell growth. *Oncogene* **17**, 3365–3383 (1998).

105. Nevins, J. R. The Rb/E2F pathway and cancer. *Hum. Mol. Genet.* **10**, 699–703 (2001).

106. Knudsen, E. S. & Wang, J. Y. Dual mechanisms for the inhibition of E2F binding to RB by cyclin-dependent kinase-mediated RB phosphorylation. *Mol. Cell. Biol.* **17**, 5771–5783 (1997).

107. Dahiya, A., Gavin, M. R., Luo, R. X. & Dean, D. C. Role of the LXCXE Binding Site in Rb Function. *Mol. Cell. Biol.* **20**, 6799–6805 (2000).

108. Welch, P. A C-terminal protein-binding domain in the retinoblastoma protein regulates nuclear c-Abl tyrosine kinase in the cell cycle. *Cell* **75**, 779–790 (1993).

109. Claudio, P. P., Tonini, T. & Giordano, A. The retinoblastoma family: twins or distant cousins? *Genome Biol.* **3**, (2002).

110. Harbour, J. W., Luo, R. X., Santi, A. D., Postigo, A. A. & Dean, D. C. Cdk Phosphorylation Triggers Sequential Intramolecular Interactions that Progressively Block Rb Functions as Cells Move through G1. *Cell* **98**, 859–869 (1999).

111. Knudsen, E. S. & Wang, J. Y. J. Differential Regulation of Retinoblastoma Protein Function by Specific Cdk Phosphorylation Sites. *J. Biol. Chem.* **271**, 8313–8320 (1996).

112. Knudsen, E. S. *et al.* RB loss contributes to aggressive tumor phenotypes in MYC-driven triple negative breast cancer. *Cell Cycle* **14**, 109–122 (2015).

113. Schaal, C., Pillai, S. & Chellappan, S. P. The Rb–E2F Transcriptional Regulatory Pathway in Tumor Angiogenesis and Metastasis. in *Advances in Cancer Research* vol. 121 147–182 (Elsevier, 2014).

114. Arima, Y. *et al.* Rb Depletion Results in Deregulation of E-Cadherin and Induction of Cellular Phenotypic Changes that Are Characteristic of the Epithelial-to-Mesenchymal Transition. *Cancer Res.* **68**, 5104–5112 (2008).

115. Arima, Y. *et al.* Induction of ZEB Proteins by Inactivation of RB Protein Is Key Determinant of Mesenchymal Phenotype of Breast Cancer. *J. Biol. Chem.* **287**, 7896–7906 (2012).

116. Beischlag, T. V. *et al.* Recruitment of Thyroid Hormone Receptor/Retinoblastoma-interacting Protein 230 by the Aryl Hydrocarbon Receptor Nuclear Translocator Is Required for the Transcriptional Response to Both Dioxin and Hypoxia. *J. Biol. Chem.* **279**, 54620–54628 (2004).

117. Labrecque, M., Prefontaine, G. & Beischlag, T. The Aryl Hydrocarbon Receptor Nuclear Translocator (ARNT) Family of Proteins: Transcriptional Modifiers with Multi-Functional Protein Interfaces. *Curr. Mol. Med.* **13**, 1047–1065 (2013).

118. Labrecque, M. P. *et al.* A TRIP230-Retinoblastoma Protein Complex Regulates Hypoxia-Inducible Factor-1α-Mediated Transcription and Cancer Cell Invasion. *PLoS ONE* **9**, e99214 (2014).

119. Gilkes, D. M. & Semenza, G. L. Role of hypoxia-inducible factors in breast cancer metastasis. *Future Oncol.* **9**, 1623–1636 (2013).

120. Vaupel, P., Schlenger, K., Knoop, C. & Hockel, M. Oxygenation of Human Tumors: Evaluation of Tissue Oxygen Distribution in Breast Cancers by Computerized O2 Tension Measurements. *Cancer Res.* **51**, 3316–3322 (1991).

121. Forsythe, J. A. *et al.* Activation of vascular endothelial growth factor gene transcription by hypoxia-inducible factor 1. *Mol. Cell. Biol.* **16**, 4604–4613 (1996).

122. Vaupel, P., Mayer, A. & Höckel, M. Tumor Hypoxia and Malignant Progression. *Methods Enzymol.* **381**, 335–354 (2004).

123. Yang, C. *et al.* Analysis of Hypoxia-Induced Metabolic Reprogramming. *Methods Enzymol.* **542**, 425–455 (2014).

124. Rankin, E. B., Nam, J.-M. & Giaccia, A. J. Hypoxia: Signaling the Metastatic Cascade. *Trends Cancer* **2**, 295–304 (2016).

125. Lu, X. & Kang, Y. Hypoxia and Hypoxia-Inducible Factors: Master Regulators of Metastasis. *Clin. Cancer Res.* **16**, 5928–5935 (2010).

126. Smith, M. C. P. *et al.* CXCR4 Regulates Growth of Both Primary and Metastatic Breast Cancer. *Cancer Res.* **64**, 8604–8612 (2004).

127. Liang, Z. *et al.* Silencing of *CXCR4* Blocks Breast Cancer Metastasis. *Cancer Res.* **65**, 967–971 (2005).

128. Jin, F., Brockmeier, U., Otterbach, F. & Metzen, E. New Insight into the SDF-1/CXCR4 Axis in a Breast Carcinoma Model: Hypoxia-Induced Endothelial SDF-1 and Tumor Cell CXCR4 Are Required for Tumor Cell Intravasation. *Mol. Cancer Res.* **10**, 1021–1031 (2012).

129. Gilkes, D. M., Bajpai, S., Chaturvedi, P., Wirtz, D. & Semenza, G. L. Hypoxia-inducible Factor 1 (HIF-1) Promotes Extracellular Matrix Remodeling under Hypoxic Conditions by Inducing *P4HA1, P4HA2,* and *PLOD2* Expression in Fibroblasts. *J. Biol. Chem.* **288**, 10819–10829 (2013).

130. Gilkes, D. M. *et al.* Procollagen Lysyl Hydroxylase 2 Is Essential for Hypoxia-Induced Breast Cancer Metastasis. *Mol. Cancer Res.* **11**, 456–466 (2013).

131. Ehrbar, M. *et al.* Elucidating the Role of Matrix Stiffness in 3D Cell Migration and Remodeling. *Biophys. J.* **100**, 284–293 (2011).

132. Padua, D. *et al.* TGFβ Primes Breast Tumors for Lung Metastasis Seeding through Angiopoietin-like 4. *Cell* **133**, 66–77 (2008).

133. Gong, X. *et al.* Interaction of tumor cells and astrocytes promotes breast cancer brain metastases through TGF-β2/ANGPTL4 axes. *Npj Precis. Oncol.* **3**, 24 (2019).

134. Noman, M. Z. *et al.* Hypoxia-Inducible miR-210 Regulates the Susceptibility of Tumor Cells to Lysis by Cytotoxic T Cells. *Cancer Res.* **72**, 4629–4641 (2012).

135. Barsoum, I. B., Smallwood, C. A., Siemens, D. R. & Graham, C. H. A Mechanism of Hypoxia-Mediated Escape from Adaptive Immunity in Cancer Cells. *Cancer Res.* **74**, 665–674 (2014).

136. Chaffer, C. L. & Weinberg, R. A. A Perspective on Cancer Cell Metastasis. *Science* **331**, 1559–1564 (2011).

137. van Zijl, F., Krupitza, G. & Mikulits, W. Initial steps of metastasis: Cell invasion and endothelial transmigration. *Mutat. Res. Mutat. Res.* **728**, 23–34 (2011).

138. Perez-Moreno, M., Jamora, C. & Fuchs, E. Sticky Business. *Cell* **112**, 535–548 (2003).

139. Kim, T. *et al.* p53 regulates epithelial–mesenchymal transition through microRNAs targeting ZEB1 and ZEB2. *J. Exp. Med.* **208**, 875–883 (2011).

140. Hoffmann, C. *et al.* CRP2, a new invadopodia actin bundling factor critically promotes breast cancer cell invasion and metastasis. *Oncotarget* **7**, 13688–13705 (2016).

141. Hoffmann, C. *et al.* CRP2, a new invadopodia actin bundling factor critically promotes breast cancer cell invasion and metastasis. *Oncotarget* **7**, 13688–13705 (2016).

142. Badylak, S., Freytes, D. & Gilbert, T. Extracellular matrix as a biological scaffold material: Structure and function. *Acta Biomater.* **5**, 1–13 (2009).

143. Stamenkovic, I. Matrix metalloproteinases in tumor invasion and metastasis. *Semin. Cancer Biol.* **10**, 415–433 (2000).

144. DeClerck, Y. A. *et al.* Proteases, Extracellular Matrix, and Cancer. *Am. J. Pathol.* **164**, 1131–1139 (2004).

145. Fernandez-Garcia, B. *et al.* Expression and prognostic significance of fibronectin and matrix metalloproteases in breast cancer metastasis. *Histopathology* **64**, 512–522 (2014).

146. Muñoz-Nájar, U. M., Neurath, K. M., Vumbaca, F. & Claffey, K. P. Hypoxia stimulates breast carcinoma cell invasion through MT1-MMP and MMP-2 activation. *Oncogene* **25**, 2379–2392 (2006).

147. Jae Young Choi, Yeon Soo Jang, Sun Young Min, & Jeong Yoon Song. Overexpression of MMP-9 and HIF-1α in Breast Cancer Cells under Hypoxic Conditions. *J. Breast Cancer* **14**, 88–95 (2011).

148. Chakrabarti, S. & Patel, K. D. Matrix Metalloproteinase-2 (MMP-2) and MMP-9 in Pulmonary Pathology. *Exp. Lung Res.* **31**, 599–621 (2005).

149. Lu, P., Takai, K., Weaver, V. M. & Werb, Z. Extracellular Matrix Degradation and Remodeling in Development and Disease. *Cold Spring Harb. Perspect. Biol.* **3**, a005058–a005058 (2011).

150. August Krogh. The number and distribution of capillaries in muscles with calculations of the oxygen pressure head necessary for supplying the tissue. *J. Physiol.* **52**, 409–415 (1919).

151. Labrecque, M. P. *et al.* The retinoblastoma protein regulates hypoxia-inducible genetic programs, tumor cell invasiveness and neuroendocrine differentiation in prostate cancer cells. *Oncotarget* **7**, 24284–24302 (2016).

152. Mark A. Goldberg & Thomas J. Schneider. Similarities between the oxygen-sensing mechanisms regulating the expression of vascular endothelial growth factor and erythropoietin. *Tee J. Biol. Chem.* **269**, 4355–4359 (1994).

153. Oh, H. *et al.* Hypoxia and Vascular Endothelial Growth Factor Selectively Up-regulate Angiopoietin-2 in Bovine Microvascular Endothelial Cells. *J. Biol. Chem.* **274**, 15732–15739 (1999).

154. Mandriota, S. J. *et al.* Hypoxia-Inducible Angiopoietin-2 Expression Is Mimicked by Iodonium Compounds and Occurs in the Rat Brain and Skin in Response to Systemic Hypoxia and Tissue Ischemia. *Am. J. Pathol.* **156**, 2077–2089 (2000).

155. Sottile, J. Regulation of angiogenesis by extracellular matrix. *Biochim. Biophys. Acta BBA - Rev. Cancer* **1654**, 13–22 (2004).

156. Belperio, J. A. *et al.* CXC chemokines in angiogenesis. *J. Leukoc. Biol.* **68**, 1–8 (2000).

157. Mehta, S. A. *et al.* Negative regulation of chemokine receptor CXCR4 by tumor suppressor p53 in breast cancer cells: implications of p53 mutation or isoform expression on breast cancer cell invasion. *Oncogene* **26**, 3329–3337 (2007).

158. Zagzag, D. *et al.* Hypoxia-inducible factor 1 and VEGF upregulate CXCR4 in glioblastoma: implications for angiogenesis and glioma cell invasion. *Lab. Invest.* **86**, 1221–1232 (2006).

159. Hlushchuk, R. *et al.* Tumor Recovery by Angiogenic Switch from Sprouting to Intussusceptive Angiogenesis after Treatment with PTK787/ZK222584 or Ionizing Radiation. *Am. J. Pathol.* **173**, 1173–1185 (2008).

160. Burri, P. H. & Djonov, V. Intussusceptive angiogenesis—the alternative to capillary sprouting. *Mol. Aspects Med.* **23**, 1–27 (2002).

161. Chaturvedi, P., Gilkes, D. M., Takano, N. & Semenza, G. L. Hypoxia-inducible factor-dependent signaling between triple-negative breast cancer cells and mesenchymal stem cells promotes macrophage recruitment. *Proc. Natl. Acad. Sci.* **111**, E2120–E2129 (2014).

162. Nielsen, S. R. & Schmid, M. C. Macrophages as Key Drivers of Cancer Progression and Metastasis. *Mediators Inflamm.* **2017**, 1–11 (2017).

163. Cooks, T. *et al.* Mutant p53 cancers reprogram macrophages to tumor supporting macrophages via exosomal miR-1246. *Nat. Commun.* **9**, 771 (2018).

164. Nguyen, D. X., Bos, P. D. & Massagué, J. Metastasis: from dissemination to organ-specific colonization. *Nat. Rev. Cancer* **9**, 274–284 (2009).

165. Kopp, H.-G., Avecilla, S. T., Hooper, A. T. & Rafii, S. The Bone Marrow Vascular Niche: Home of HSC Differentiation and Mobilization. *Physiology* **20**, 349–356 (2005).

166. Lalor, P. Human hepatic sinusoidal endothelial cells can be distinguished by expression of phenotypic markers related to their specialised functions *in vivo*. *World J. Gastroenterol.* **12**, 5429–5439 (2006).

167. Gupta, G. P. *et al.* Mediators of vascular remodelling co-opted for sequential steps in lung metastasis. *Nature* **446**, 765–770 (2007).

168. Weil, R. J., Palmieri, D. C., Bronder, J. L., Stark, A. M. & Steeg, P. S. Breast Cancer Metastasis to the Central Nervous System. *Am. J. Pathol.* **167**, 913–920 (2005).

169. Minako Murata *et al.* Hypoxia upregulates the expression of angiopoietin-like-4 in human articular chondrocytes: Role of angiopoietin-like-4 in the expression of matrix metalloproteinases and cartilage degradation. *J. Orthop. Res.* **27**, 50–57 (2009).

170. Subbaramaiah, K. *et al.* Inhibition of Cyclooxygenase-2 Gene Expression by p53. *J. Biol. Chem.* **274**, 10911–10915 (1999).

171. Salmaggi, A. *et al.* CXCL12, CXCR4 and CXCR7 expression in brain metastases. *Cancer Biol. Ther.* **8**, 1608–1614 (2009).

172. Fitzgerald, D. P. *et al.* Reactive glia are recruited by highly proliferative brain metastases of breast cancer and promote tumor cell colonization. *Clin. Exp. Metastasis* **25**, 799–810 (2008).

173. Cohen, M. C. & Cohen, S. Cytokine Function: A Study in Biologic Diversity. *Am. J. Clin. Pathol.* **105**, 589–598 (1996).

174. Gril, B. *et al.* Reactive astrocytic S1P3 signaling modulates the blood–tumor barrier in brain metastases. *Nat. Commun.* **9**, 1–18 (2018).

175. Heffernan-Stroud, L. A. *et al.* Defining a role for sphingosine kinase 1 in p53-dependent tumors. *Oncogene* **31**, 1166–1175 (2012).

176. Masters, J. R. W. Human cancer cell lines: fact and fantasy. *Nat. Rev. Mol. Cell Biol.* **1**, 233–236 (2000).

177. Turner, T. Development of the Polio Vaccine: A Historical Perspective of Tuskegee University's Role in Mass Production and Distribution of HeLa Cells. *J. Health Care Poor Underserved* **23**, 5–10 (2012).

178. Longo, D. L. Imatinib Changed Everything. *N. Engl. J. Med.* **376**, 982–983 (2017).

179. Cicconi, L. & Lo-Coco, F. Current management of newly diagnosed acute promyelocytic leukemia. *Ann. Oncol.* **27**, 1474–1481 (2016).

180. Rao, D. D., Vorhies, J. S., Senzer, N. & Nemunaitis, J. siRNA vs. shRNA: Similarities and differences. *Adv. Drug Deliv. Rev.* **61**, 746–759 (2009).

181. Reynolds, A. *et al.* Rational siRNA design for RNA interference. *Nat. Biotechnol.* **22**, 326–330 (2004).

182. Chang, K., Elledge, S. J. & Hannon, G. J. Lessons from Nature: microRNA-based shRNA libraries. *Nat. Methods* **3**, 707–714 (2006).

183. Ran, F. A. *et al.* Genome engineering using the CRISPR-Cas9 system. *Nat. Protoc.* **8**, 2281–2308 (2013).

184. Cailleau, R., Olive, M. & Cruciger, Q. V. Long-term human breast carcinoma cell lines of metastatic origin: preliminary characterization. *In Vitro* **14**, 911–915 (1978).

185. Berglind, H., Pawitan, Y., Kato, S., Ishioka, C. & Soussi, T. Analysis of p53 mutation status in human cancer cell lines: a paradigm for cell line cross-contamination. *Cancer Biol. Ther.* **7**, 699–708 (2008).

186. Labun, K. *et al.* CHOPCHOP v3: expanding the CRISPR web toolbox beyond genome editing. *Nucleic Acids Res.* **47**, W171–W174 (2019).

187. Carter, M. & Shieh, J. Gene Delivery Strategies. in *Guide to Research Techniques in Neuroscience* 239–252 (Elsevier, 2015). doi:10.1016/B978-0-12-800511-8.00011-3.

188. Swinehart, D. F. The Beer-Lambert Law. 3.

189. Clarke, R. *et al.* Enhanced Bacterial Immunity and Mammalian Genome Editing via RNA-Polymerase-Mediated Dislodging of Cas9 from Double-Strand DNA Breaks. *Mol. Cell* **71**, 42-55.e8 (2018).

190. Nguyen, L. T., Atobe, K., Barichello, J. M., Ishida, T. & Kiwada, H. Complex Formation with Plasmid DNA Increases the Cytotoxicity of Cationic Liposomes. *Biol. Pharm. Bull.* **30**, 751–757 (2007).

191. Lin, S.-C., Haga, K., Zeng, X.-L. & Estes, M. K. Generation of CRISPR–Cas9-mediated genetic knockout human intestinal tissue–derived enteroid lines by lentivirus transduction and single-cell cloning. *Nat. Protoc.* **17**, 1004–1027 (2022).

192. Dugina, V. *et al.* Impaired Expression of Cytoplasmic Actins Leads to Chromosomal Instability of MDA-MB-231 Basal-Like Mammary Gland Cancer Cell Line. *Molecules* **26**, 2151 (2021).

193. Baumbusch, L. O. *et al.* Expression of full-length p53 and its isoform Δp53 in breast carcinomas in relation to mutation status and clinical parameters. *Mol. Cancer* **5**, 47 (2006).

194. Avery-Kiejda, K. A., Morten, B., Wong-Brown, M. W., Mathe, A. & Scott, R. J. The relative mRNA expression of p53 isoforms in breast cancer is associated with clinical features and outcome. *Carcinogenesis* **35**, 586–596 (2014).

195. Bourdon, J.-C., Surget, S. & Khoury, M. P. Uncovering the role of p53 splice variants in human malignancy: a clinical perspective. *OncoTargets Ther.* 57 (2013) doi:10.2147/OTT.S53876.

196. Morten, B. C., Wong-Brown, M. W., Scott, R. J. & Avery-Kiejda, K. A. The presence of the intron 3 16 bp duplication polymorphism of *p53* (rs17878362) in breast cancer is associated with a low Δ40p53:p53 ratio and better outcome. *Carcinogenesis* **37**, 81–86 (2016).

197. Bae, Y.-H. *et al.* Gain-of-function mutant p53-R280K mediates survival of breast cancer cells. *Genes Genomics* **36**, 171–178 (2014).

198. Taylor, W. R. & Stark, G. R. Regulation of the G2/M transition by p53. *Oncogene* **20**, 1803–1815 (2001).

199. Koshiji, M. *et al.* HIF-1α induces cell cycle arrest by functionally counteracting Myc. *EMBO J.* **23**, 1949–1956 (2004).

200. Mehta, S. A. *et al.* Negative regulation of chemokine receptor CXCR4 by tumor suppressor p53 in breast cancer cells: implications of p53 mutation or isoform expression on breast cancer cell invasion. *Oncogene* **26**, 3329–3337 (2007).

201. Nobutani, K. *et al.* Downregulation of CXCR4 in Metastasized Breast Cancer Cells and Implication in Their Dormancy. *PLOS ONE* **10**, e0130032 (2015).

202. Park, S.-Y. & Nam, J.-S. The force awakens: metastatic dormant cancer cells. *Exp. Mol. Med.* **52**, 569–581 (2020).

203. Comşa, Ş., Cîmpean, A. M. & Raica, M. The Story of MCF-7 Breast Cancer Cell Line: 40 years of Experience in Research. *ANTICANCER Res.* 8 (2015).

204. Horoszewicz, J. S. *et al.* LNCaP model of human prostatic carcinoma. *Cancer Res.* **43**, 1809–1818 (1983).

205. Luster, A. D., Alon, R. & von Andrian, U. H. Immune cell migration in inflammation: present and future therapeutic targets. *Nat. Immunol.* **6**, 1182–1190 (2005).

206. Hu, M. & Polyak, K. Molecular characterisation of the tumour microenvironment in breast cancer. *Eur. J. Cancer* **44**, 2760–2765 (2008).

207. O'Neil, N. J., Bailey, M. L. & Hieter, P. Synthetic lethality and cancer. *Nat. Rev. Genet.* **18**, 613–623 (2017).

208. Dhanjal, J. K., Radhakrishnan, N. & Sundar, D. Identifying synthetic lethal targets using CRISPR/Cas9 system. *Methods* **131**, 66–73 (2017).

209. Huang, A., Garraway, L. A., Ashworth, A. & Weber, B. Synthetic lethality as an engine for cancer drug target discovery. *Nat. Rev. Drug Discov.* **19**, 23–38 (2020).

210. Jerby-Arnon, L. *et al.* Predicting Cancer-Specific Vulnerability via Data-Driven Detection of Synthetic Lethality. *Cell* **158**, 1199–1209 (2014).

211. Hassler, M. *et al.* Crystal Structure of the Retinoblastoma Protein N Domain Provides Insight into Tumor Suppression, Ligand Interaction, and Holoprotein Architecture. *Mol. Cell* **28**, 371–385 (2007).

Appendix A.

sgRNA sequences used for generating p53-KOs and RB-KOs by Robert Payer

sgRNA	Targeted Gene	Sequence (5' → 3')	Exon	Amino acid preceding the cut site	Protein domain
sgRNA 3	*TP53*	F: caccgGTGCTGTGACTGCTTGTAGA R: aaacTCTACAAGCAGTCACAGCACc	Exon 4	I162	DBD
sgRNA 4	*TP53*	F: caccgTGACTGCTTGTAGATGGCCA R: aaacTGGCCATCTACAAGCAGTCAc	Exon 4	M160	DBD
sgRNA 3	*RB1*	F: caccgTTGGGAGAAAGTTTCATCTG R: aaacCAGATGAAACTTTCTCCCAAc	Exon 2	S82	Cyclin fold A[211]
sgRNA 4	*RB1*	F: caccgAGCATTATCAACTTTGGTAC R: aaacGTACCAAAGTTGATAATGCTc	Exon 4	S141	Cyclin fold A[211]

Note: F = forward, R = reverse. Lowercase sequences indicate specific sequence required for plasmid cloning. Uppercase sequences indicate specific targets on *TP53* or *RB1*. DBD = DNA binding domain.

Appendix B.

Statistical analysis of cell cycle experiments

Table B.1. P-Values of cell cycle experiments under normoxia – G1 phase

	Parental	Vector	p53KO1	p53KO2	RBKO1	RBKO2	DKO1	DKO2
Parental	1.0000	0.9780	0.5670	0.2132	0.0895	0.0424	0.9647	0.2208
Vector	0.9780	1.0000	0.6516	0.2822	0.1572	0.0856	1.0000	0.3361
p53-KO1	0.5670	0.6516	1.0000	0.0836	0.0282	0.0140	0.4487	0.4855
p53-KO2	0.2132	0.2822	0.0836	1.0000	0.6082	0.2292	0.0829	0.0190
RB-KO1	0.0895	0.1572	0.0282	0.6082	1.0000	0.1908	0.0059	0.0024
RB-KO2	0.0424	0.0856	0.0140	0.2292	0.1908	1.0000	0.0019	0.0011
DKO1	0.9647	1.0000	0.4487	0.0829	0.0059	0.0019	1.0000	0.0492
DKO2	0.2208	0.3361	0.4855	0.0190	0.0024	0.0011	0.0492	1.0000

Table B.2. P-Values of cell cycle experiments under normoxia – S phase

	Parental	Vector	p53KO1	p53KO2	RBKO1	RBKO2	DKO1	DKO2
Parental	1.0000	0.2361	0.1348	0.3264	0.8351	0.9796	0.2060	0.6689
Vector	0.2361	1.0000	0.0097	0.9934	0.1054	0.1067	0.9949	0.0778
p53KO1	0.1348	0.0097	1.0000	0.0386	0.0760	0.0280	0.0044	0.1235
p53KO2	0.3264	0.9934	0.0386	1.0000	0.2092	0.2348	0.9895	0.1643
RBKO1	0.8351	0.1054	0.0760	0.2092	1.0000	0.7780	0.0732	0.7661
RBKO2	0.9796	0.1067	0.0280	0.2348	0.7780	1.0000	0.0651	0.5451
DKO1	0.2060	0.9949	0.0044	0.9895	0.0732	0.0651	1.0000	0.0530
DKO2	0.6689	0.0778	0.1235	0.1643	0.7661	0.5451	0.0530	1.0000

Table B.3. P-Values of cell cycle experiments under normoxia – G2 phase

	Parental	Vector	p53KO1	p53KO2	RBKO1	RBKO2	DKO1	DKO2
Parental	1.0000	0.0220	0.0327	0.0290	0.1135	0.0147	0.4316	0.0900
Vector	0.0220	1.0000	0.0091	0.4882	0.5095	0.2145	0.0124	0.0291
p53KO1	0.0327	0.0091	1.0000	0.0111	0.0169	0.0114	0.0407	0.9010
p53KO2	0.0290	0.4882	0.0111	1.0000	0.8861	0.5283	0.0137	0.0362
RBKO1	0.1135	0.5095	0.0169	0.8861	1.0000	0.8097	0.0682	0.0444
RBKO2	0.0147	0.2145	0.0114	0.5283	0.8097	1.0000	0.0040	0.0402
DKO1	0.4316	0.0124	0.0407	0.0137	0.0682	0.0040	1.0000	0.1074
DKO2	0.0900	0.0291	0.9010	0.0362	0.0444	0.0402	0.1074	1.0000

Table B.4. P-Values of cell cycle experiments under hypoxia – G1 phase

	Parental	Vector	p53KO1	p53KO2	RBKO1	RBKO2	DKO1	DKO2
Parental	1.0000	0.4957	0.5846	0.1539	0.0213	0.0099	0.2238	0.9031
Vector	0.4957	1.0000	0.3079	0.6347	0.2627	0.1460	0.7052	0.5278
p53KO1	0.5846	0.3079	1.0000	0.0537	0.0016	0.0006	0.1026	0.8691
p53KO2	0.1539	0.6347	0.0537	1.0000	0.3407	0.1387	0.9321	0.2601
RBKO1	0.0213	0.2627	0.0016	0.3407	1.0000	0.2198	0.3716	0.0964
RBKO2	0.0099	0.1460	0.0006	0.1387	0.2198	1.0000	0.1780	0.0574
DKO1	0.2238	0.7052	0.1026	0.9321	0.3716	0.1780	1.0000	0.3115
DKO2	0.9031	0.5278	0.8691	0.2601	0.0964	0.0574	0.3115	1.0000

Table B.5. P-Values of cell cycle experiments under hypoxia – S phase

	Parental	Vector	p53KO1	p53KO2	RBKO1	RBKO2	DKO1	DKO2
Parental	1.0000	0.1048	0.1418	0.2737	0.8954	0.4137	0.5270	0.5167
Vector	0.1048	1.0000	0.0723	0.3420	0.1263	0.0852	0.1894	0.0897
p53KO1	0.1418	0.0723	1.0000	0.1489	0.6514	0.6394	0.2448	0.5238
p53KO2	0.2737	0.3420	0.1489	1.0000	0.3393	0.1956	0.5845	0.2128
RBKO1	0.8954	0.1263	0.6514	0.3393	1.0000	0.8163	0.5882	0.8779
RBKO2	0.4137	0.0852	0.6394	0.1956	0.8163	1.0000	0.3455	0.8767
DKO1	0.5270	0.1894	0.2448	0.5845	0.5882	0.3455	1.0000	0.3835
DKO2	0.5167	0.0897	0.5238	0.2128	0.8779	0.8767	0.3835	1.0000

Table B.6. P-Values of cell cycle experiments under hypoxia – G2 phase

	Parental	Vector	p53KO1	p53KO2	RBKO1	RBKO2	DKO1	DKO2
Parental	1.0000	0.0751	0.0827	0.1925	0.1499	0.3170	0.6752	0.0008
Vector	0.0751	1.0000	0.0285	0.3081	0.3163	0.1656	0.0796	0.0048
p53KO1	0.0827	0.0285	1.0000	0.0469	0.0403	0.0575	0.1870	0.0929
p53KO2	0.1925	0.3081	0.0469	1.0000	0.9517	0.5777	0.2034	0.0033
RBKO1	0.1499	0.3163	0.0403	0.9517	1.0000	0.5157	0.1734	0.0025
RBKO2	0.3170	0.1656	0.0575	0.5777	0.5157	1.0000	0.3231	0.0021
DKO1	0.6752	0.0796	0.1870	0.2034	0.1734	0.3231	1.0000	0.0079
DKO2	0.0008	0.0048	0.0929	0.0033	0.0025	0.0021	0.0079	1.0000

Table B.7. P-Values of cell cycle experiments under normoxia vs. hypoxia

	G1 Phase	S Phase	G2 Phase
Parental	0.8698	0.0681	0.0416
Vector	0.6047	0.9437	0.8339
p53KO1	0.9506	0.0548	0.9868
p53KO2	0.8864	0.2275	0.3162
RBKO1	0.1718	0.1277	0.4337
RBKO2	0.1136	0.0087	0.0884
DKO1	0.1948	0.0374	0.2506
DKO2	0.5494	0.0378	0.2646

Appendix C.

Statistical analysis of gene expression experiments

Table C.1. P-Values of gene expression experiments under normoxia – *CXCR4*

	Parental	Vector	p53KO1	p53KO2	RBKO1	RBKO2	DKO1	DKO2
Parental	1.0000	0.2799	0.1731	0.1767	0.1296	0.0795	0.0655	0.0803
Vector	0.2799	1.0000	0.2557	0.5962	0.6804	0.2432	0.2400	0.2429
p53KO1	0.1731	0.2557	1.0000	0.1439	0.1191	0.0612	0.0272	0.0752
p53KO2	0.1767	0.5962	0.1439	1.0000	0.2958	0.1295	0.1260	0.1292
RBKO1	0.1296	0.6804	0.1191	0.2958	1.0000	0.1138	0.1124	0.1136
RBKO2	0.0795	0.2432	0.0612	0.1295	0.1138	1.0000	0.2295	0.9185
DKO1	0.0655	0.2400	0.0272	0.1260	0.1124	0.2295	1.0000	0.3928
DKO2	0.0803	0.2429	0.0752	0.1292	0.1136	0.9185	0.3928	1.0000

Table C.2. P-Values of gene expression experiments under hypoxia – *CXCR4*

	Parental	Vector	p53KO1	p53KO2	RBKO1	RBKO2	DKO1	DKO2
Parental	1.0000	0.3312	0.0020	0.0459	0.0547	0.0025	0.0002	0.0268
Vector	0.3312	1.0000	0.3169	0.7002	0.4989	0.3071	0.3046	0.3095
p53KO1	0.0020	0.3169	1.0000	0.0411	0.0449	0.0172	0.0028	0.1734
p53KO2	0.0459	0.7002	0.0411	1.0000	0.2221	0.0381	0.0373	0.0389
RBKO1	0.0547	0.4989	0.0449	0.2221	1.0000	0.0394	0.0381	0.0412
RBKO2	0.0025	0.3071	0.0172	0.0381	0.0394	1.0000	0.1616	0.5814
DKO1	0.0002	0.3046	0.0028	0.0373	0.0381	0.1616	1.0000	0.2903
DKO2	0.0268	0.3095	0.1734	0.0389	0.0412	0.5814	0.2903	1.0000

Table C.3. P-Values of normoxia to hypoxia fold change in gene expression experiments – *CXCR4*

	Parental	Vector	p53KO1	p53KO2	RBKO1	RBKO2	DKO1	DKO2
Parental	1.0000	0.5193	0.8446	0.2182	0.1845	0.9188	0.3573	0.0869
Vector	0.5193	1.0000	0.5965	0.3998	0.1104	0.4710	0.1991	0.1652
p53KO1	0.8446	0.5965	1.0000	0.2335	0.1185	0.8707	0.2691	0.0850
p53KO2	0.2182	0.3998	0.2335	1.0000	0.0734	0.1830	0.1119	0.5624
RBKO1	0.1845	0.1104	0.1185	0.0734	1.0000	0.0435	0.7006	0.0231
RBKO2	0.9188	0.4710	0.8707	0.1830	0.0435	1.0000	0.2262	0.0524
DKO1	0.3573	0.1991	0.2691	0.1119	0.7006	0.2262	1.0000	0.0468
DKO2	0.0869	0.1652	0.0850	0.5624	0.0231	0.0524	0.0468	1.0000

Table C.4. P-Values of gene expression experiments under normoxia – *PLOD2*

	Parental	Vector	p53KO1	p53KO2	RBKO1	RBKO2	DKO1	DKO2
Parental	1.0000	0.5831	0.9596	0.9434	0.1381	0.6730	0.5445	0.7556
Vector	0.5831	1.0000	0.8180	0.5183	0.1852	0.9428	0.7875	0.3079
p53KO1	0.9596	0.8180	1.0000	0.9285	0.2584	0.8518	0.7153	0.8370
p53KO2	0.9434	0.5183	0.9285	1.0000	0.1278	0.6155	0.5066	0.8098
RBKO1	0.1381	0.1852	0.2584	0.1278	1.0000	0.1923	0.3150	0.0984
RBKO2	0.6730	0.9428	0.8518	0.6155	0.1923	1.0000	0.7658	0.4318
DKO1	0.5445	0.7875	0.7153	0.5066	0.3150	0.7658	1.0000	0.3939
DKO2	0.7556	0.3079	0.8370	0.8098	0.0984	0.4318	0.3939	1.0000

Table C.5. P-Values of gene expression experiments under hypoxia – *PLOD2*

	Parental	Vector	p53KO1	p53KO2	RBKO1	RBKO2	DKO1	DKO2
Parental	1.0000	0.3282	0.6537	0.2125	0.2836	0.1550	0.3518	0.3635
Vector	0.3282	1.0000	0.4484	0.9474	0.6145	0.9659	0.7340	0.5292
p53KO1	0.6537	0.4484	1.0000	0.3293	0.5973	0.2769	0.4161	0.7468
p53KO2	0.2125	0.9474	0.3293	1.0000	0.4891	0.9739	0.7542	0.3991
RBKO1	0.2836	0.6145	0.5973	0.4891	1.0000	0.4418	0.5056	0.7955
RBKO2	0.1550	0.9659	0.2769	0.9739	0.4418	1.0000	0.7338	0.3418
DKO1	0.3518	0.7340	0.4161	0.7542	0.5056	0.7338	1.0000	0.4621
DKO2	0.3635	0.5292	0.7468	0.3991	0.7955	0.3418	0.4621	1.0000

Table C.6. P-Values of normoxia to hypoxia fold change in gene expression experiments – *PLOD2*

	Parental	Vector	p53KO1	p53KO2	RBKO1	RBKO2	DKO1	DKO2
Parental	1.0000	0.3432	0.3766	0.0788	0.2121	0.1770	0.3793	0.3095
Vector	0.3432	1.0000	0.5216	0.2777	0.1664	0.6888	0.7139	0.6948
p53KO1	0.3766	0.5216	1.0000	0.8591	0.3033	0.6103	0.6736	0.6526
p53KO2	0.0788	0.2777	0.8591	1.0000	0.0499	0.4289	0.6345	0.5695
RBKO1	0.2121	0.1664	0.3033	0.0499	1.0000	0.0929	0.2494	0.1883
RBKO2	0.1770	0.6888	0.6103	0.4289	0.0929	1.0000	0.9138	0.9275
DKO1	0.3793	0.7139	0.6736	0.6345	0.2494	0.9138	1.0000	0.9790
DKO2	0.3095	0.6948	0.6526	0.5695	0.1883	0.9275	0.9790	1.0000

Table C.7. P-Values of gene expression experiments under normoxia – *ANGPTL4*

	Parental	Vector	p53KO1	p53KO2	RBKO1	RBKO2	DKO1	DKO2
Parental	1.0000	0.1733	0.3949	0.8811	0.7034	0.7912	0.2387	0.6018
Vector	0.1733	1.0000	0.0968	0.1757	0.3022	0.1598	0.0783	0.1225
p53KO1	0.3949	0.0968	1.0000	0.6010	0.3523	0.6792	0.7197	0.7602
p53KO2	0.8811	0.1757	0.6010	1.0000	0.6515	0.9220	0.4485	0.7819
RBKO1	0.7034	0.3022	0.3523	0.6515	1.0000	0.5907	0.2655	0.4676
RBKO2	0.7912	0.1598	0.6792	0.9220	0.5907	1.0000	0.5143	0.8673
DKO1	0.2387	0.0783	0.7197	0.4485	0.2655	0.5143	1.0000	0.5290
DKO2	0.6018	0.1225	0.7602	0.7819	0.4676	0.8673	0.5290	1.0000

Table C.8. P-Values of gene expression experiments under hypoxia – *ANGPTL4*

	Parental	Vector	p53KO1	p53KO2	RBKO1	RBKO2	DKO1	DKO2
Parental	1.0000	0.2288	0.6610	0.4084	0.5073	0.3821	0.7741	0.1708
Vector	0.2288	1.0000	0.1848	0.9984	0.5080	0.8427	0.3773	0.1094
p53KO1	0.6610	0.1848	1.0000	0.3489	0.3835	0.3354	0.5943	0.4773
p53KO2	0.4084	0.9984	0.3489	1.0000	0.6329	0.8609	0.5182	0.2600
RBKO1	0.5073	0.5080	0.3835	0.6329	1.0000	0.5500	0.7656	0.1953
RBKO2	0.3821	0.8427	0.3354	0.8609	0.5500	1.0000	0.4631	0.2660
DKO1	0.7741	0.3773	0.5943	0.5182	0.7656	0.4631	1.0000	0.3322
DKO2	0.1708	0.1094	0.4773	0.2600	0.1953	0.2660	0.3322	1.0000

Table C.9. P-Values of normoxia to hypoxia fold change in gene expression experiments – *ANGPTL4*

	Parental	Vector	p53KO1	p53KO2	RBKO1	RBKO2	DKO1	DKO2
Parental	1.0000	0.8517	0.2648	0.0045	0.5797	0.0326	0.0189	0.7808
Vector	0.8517	1.0000	0.3618	0.0346	0.6532	0.0412	0.0473	0.7349
p53KO1	0.2648	0.3618	1.0000	0.0620	0.3882	0.0669	0.0936	0.8744
p53KO2	0.0045	0.0346	0.0620	1.0000	0.0048	0.2149	0.7813	0.3240
RBKO1	0.5797	0.6532	0.3882	0.0048	1.0000	0.0373	0.0230	0.8759
RBKO2	0.0326	0.0412	0.0669	0.2149	0.0373	1.0000	0.2846	0.1397
DKO1	0.0189	0.0473	0.0936	0.7813	0.0230	0.2846	1.0000	0.3012
DKO2	0.7808	0.7349	0.8744	0.3240	0.8759	0.1397	0.3012	1.0000

Table C.10. P-Values of gene expression experiments under normoxia vs. hypoxia

	CXCR4	PLOD2	ANPTL4
Parental	0.0185	0.1171	0.0210
Vector	0.4011	0.1890	0.0636
p53KO1	0.0092	0.2313	0.0874
p53KO2	0.0625	0.0896	0.1691
RBKO1	0.5293	0.3847	0.0808
RBKO2	0.2403	0.0657	0.1882
DKO1	0.5426	0.2762	0.1273
DKO2	0.3296	0.0403	0.0324

Appendix D.

Statistical analysis of cell migration experiments

Table D.1. P-Values of cell migration experiments under normoxia

	Parental	Vector	p53KO1	p53KO2	RBKO1	RBKO2	DKO1	DKO2
Parental	1.0000	0.2948	0.4531	0.4171	0.1108	0.1839	0.3407	0.0728
Vector	0.2948	1.0000	0.6993	0.6471	0.5708	0.6234	0.7816	0.9776
p53KO1	0.4531	0.6993	1.0000	0.9635	0.3451	0.9856	0.5883	0.5588
p53KO2	0.4171	0.6471	0.9635	1.0000	0.2886	0.9264	0.5575	0.4482
RBKO1	0.1108	0.5708	0.3451	0.2886	1.0000	0.2037	0.9168	0.3929
RBKO2	0.1839	0.6234	0.9856	0.9264	0.2037	1.0000	0.5508	0.0842
DKO1	0.3407	0.7816	0.5883	0.5575	0.9168	0.5508	1.0000	0.7605
DKO2	0.0728	0.9776	0.5588	0.4482	0.3929	0.0842	0.7605	1.0000

Table D.2. P-Values of cell migration experiments under hypoxia

	Parental	Vector	p53KO1	p53KO2	RBKO1	RBKO2	DKO1	DKO2
Parental	1.0000	0.2263	0.7762	0.2929	0.2181	0.2965	0.4923	0.2787
Vector	0.2263	1.0000	0.4191	0.4314	0.4922	0.3652	0.9462	0.6154
p53KO1	0.7762	0.4191	1.0000	0.7050	0.2875	0.7633	0.5963	0.5884
p53KO2	0.2929	0.4314	0.7050	1.0000	0.3035	0.7448	0.6824	0.7002
RBKO1	0.2181	0.4922	0.2875	0.3035	1.0000	0.2843	0.6514	0.3571
RBKO2	0.2965	0.3652	0.7633	0.7448	0.2843	1.0000	0.6503	0.5574
DKO1	0.4923	0.9462	0.5963	0.6824	0.6514	0.6503	1.0000	0.7656
DKO2	0.2787	0.6154	0.5884	0.7002	0.3571	0.5574	0.7656	1.0000

Table D.3. P-Values of normoxia to hypoxia fold change of cell migration experiments

	Parental	Vector	p53KO1	p53KO2	RBKO1	RBKO2	DKO1	DKO2
Parental	1.0000	0.6054	0.2155	0.7114	0.8327	0.1073	0.2967	0.3191
Vector	0.6054	1.0000	0.2563	0.9106	0.8657	0.3179	0.3608	0.4066
p53KO1	0.2155	0.2563	1.0000	0.3172	0.2490	0.3492	0.7531	0.5987
p53KO2	0.7114	0.9106	0.3172	1.0000	0.8322	0.6610	0.4426	0.5165
RBKO1	0.8327	0.8657	0.2490	0.8322	1.0000	0.3448	0.3460	0.3875
RBKO2	0.1073	0.3179	0.3492	0.6610	0.3448	1.0000	0.5170	0.6267
DKO1	0.2967	0.3608	0.7531	0.4426	0.3460	0.5170	1.0000	0.8327
DKO2	0.3191	0.4066	0.5987	0.5165	0.3875	0.6267	0.8327	1.0000

Table D.4. P-Values of cell migration experiments under normoxia normalized to Vector

	Parental	Vector	p53KO1	p53KO2	RBKO1	RBKO2	DKO1	DKO2
Parental	1.0000	0.0047	0.4604	0.0146	0.3038	0.3241	0.4089	0.2416
Vector	0.0047	#DIV/0!	0.9152	0.0011	0.5319	0.9326	0.6131	0.7003
p53KO1	0.4604	0.9152	1.0000	0.6938	0.6592	0.8934	0.6919	0.9001
p53KO2	0.0146	0.0011	0.6938	1.0000	0.4173	0.6676	0.5162	0.4396
RBKO1	0.3038	0.5319	0.6592	0.4173	1.0000	0.5447	0.9651	0.6896
RBKO2	0.3241	0.9326	0.8934	0.6676	0.5447	1.0000	0.6125	0.7287
DKO1	0.4089	0.6131	0.6919	0.5162	0.9651	0.6125	1.0000	0.7254
DKO2	0.2416	0.7003	0.9001	0.4396	0.6896	0.7287	0.7254	1.0000

Table D.5. P-Values of cell migration experiments under hypoxia normalized to Vector

	Parental	Vector	p53KO1	p53KO2	RBKO1	RBKO2	DKO1	DKO2
Parental	1.0000	0.0125	0.6292	0.1197	0.3285	0.2949	0.4761	0.0355
Vector	0.0125	#DIV/0!	0.6491	0.1358	0.5161	0.3637	0.7572	0.0451
p53KO1	0.6292	0.6491	1.0000	0.9677	0.4499	0.9718	0.6398	0.8723
p53KO2	0.1197	0.1358	0.9677	1.0000	0.4232	0.9950	0.6211	0.5886
RBKO1	0.3285	0.5161	0.4499	0.4232	1.0000	0.4279	0.7825	0.4464
RBKO2	0.2949	0.3637	0.9718	0.9950	0.4279	1.0000	0.6249	0.7737
DKO1	0.4761	0.7572	0.6398	0.6211	0.7825	0.6249	1.0000	0.6566
DKO2	0.0355	0.0451	0.8723	0.5886	0.4464	0.7737	0.6566	1.0000